

Dielectric relaxation, electrostrictive properties and Raman light scattering in PbZrO3 and PbHfO3 single crystals pure and doped with small amount of PbTiO3

Irena Jankowska-Sumara

▶ **To cite this version:**

Irena Jankowska-Sumara. Dielectric relaxation, electrostrictive properties and Raman light scattering in PbZrO3 and PbHfO3 single crystals pure and doped with small amount of PbTiO3. Physics [physics]. UPVM - Université Paul Verlaine - Metz, 1997. English. NNT : 1997METZ051S . tel-02002099

HAL Id: tel-02002099

https://hal.univ-lorraine.fr/tel-02002099

Submitted on 7 Feb 2019

HAL is a multi-disciplinary open access archive for the deposit and dissemination of scientific research documents, whether they are published or not. The documents may come from teaching and research institutions in France or abroad, or from public or private research centers.

L'archive ouverte pluridisciplinaire **HAL**, est destinée au dépôt et à la diffusion de documents scientifiques de niveau recherche, publiés ou non, émanant des établissements d'enseignement et de recherche français ou étrangers, des laboratoires publics ou privés.

AVERTISSEMENT

Ce document est le fruit d'un long travail approuvé par le jury de soutenance et mis à disposition de l'ensemble de la communauté universitaire élargie.

Il est soumis à la propriété intellectuelle de l'auteur. Ceci implique une obligation de citation et de référencement lors de l'utilisation de ce document.

D'autre part, toute contrefaçon, plagiat, reproduction illicite encourt une poursuite pénale.

Contact : ddoc-theses-contact@univ-lorraine.fr

LIENS

Code de la Propriété Intellectuelle. articles L 122. 4
Code de la Propriété Intellectuelle. articles L 335.2- L 335.10
http://www.cfcopies.com/V2/leg/leg_droi.php
http://www.culture.gouv.fr/culture/infos-pratiques/droits/protection.htm

DB 122370

Uniwersytet Śląski w Katowicach

Instytut Fizyki

Université de Metz

Centre Lorrain d'Optique et Electronique des Solides

UNIVERSITE DE METZ
TECHNOPOLE
BIBLIOTHEQUE

Irena Jankowska-Sumara

DIELECTRIC RELAXATION, ELECTROSTRICTIVE PROPERTIES AND RAMAN LIGHT SCATTERING IN $PbZrO_3$ AND $PbHfO_3$ SINGLE CRYSTALS PURE AND DOPED WITH SMALL AMOUNT OF $PbTiO_3$

A Thesis in Solid State Science

for the Degree of

Doctor of Physics

BIBLIOTHEQUE UNIVERSITAIRE - METZ
N° inv. 19971065
Cote S/Mz 97/51
Loc Magasin

Thesis Advisors

Dr hab. prof. US Krystian Roleder - University of Silesia (POLAND)

Prof. Godefroy E. Kugel - University of Metz (FRANCE)

Katowice, Metz 1997

Errata

page	it is	it should be
12[6]	application	the application
87[7]	predict	predicts
104[9]		and this relaxation has been observed „Roleder et al. (1996)
106[9]	The line a (Figure 4.23a) is of particulair importance...	The line a (Figure 4.23a) which is of particulair .....
120[13]	Maglione and Belkaoumi (1992)	Maglione M., M. Belkaoumi, Phys. Rev. B, **45**, 2029 (1992)

This Thesis has been performed under the
„CONVENTION DE CO-TUTELLE
DE THESE N° 95/007"
signed by the University of Metz
and University of Silesia

ACKNOWLEDGEMENTS

I would like to express my gratitude to Prof. Krystian Roleder for being my thesis advisor and for training my mind to think in a more logical and precise way. I wish to thank Prof. Godefroy Kugel for being my co-advisor of this thesis, for giving me the privilege to be his Ph. D. student and for all he did for me during my stay in his laboratory.

I would like to thank the authority of the Institute of Physics of the University of Silesia for giving me the possibility of making the majority of my experiments in the Experimental Physics Division and especially to Prof. Jan Hańderek for a kind hospitality in his Division. To all my colleagues from this Institute for helpful and stimulating discussions during the preparation of this thesis. Special thanks I address to Prof. Jan Dec for growing of the crystals for my experiments and Dr Seweryn Miga for informatic help.

I would like to acknowledge the hospitality of the Laboratoire Matériaux Optiques à Propriétés Spécifiques and his head Prof. Marc Fontana at the Centre Lorrain d'Optique et Electronique des Solides in the University of Metz in France where the Raman scattering investigations were made. Financial support of French Government under French-Polish scientific agreement is also kindly acknowledged. I express my gratitude to all the people from the CLOES Laboratory for many enlightening discussions and also for the friendship and smile they have offered to me since I arrived in Metz.

STRESZCZENIE

Przedmiotem pracy są badania relaksacji dielektrycznej, własności elektrostrykcyjnych oraz Ramanowskie rozpraszanie światła w kryształach:

- $PbZrO_3$ czystym oraz domieszkowanych niewielką ilością $PbTiO_3$.
- $PbHfO_3$ czystym oraz domieszkowanych niewielką ilością $PbTiO_3$.

gdzie; $PbZrO_3$ jest przykładem antyferroelektryka z jednym przejsciem fazowym podczas gdy $PbHfO_3$ jest antyferroelekrykiem z dwoma przejściami fazowymi.

Badania te miały na celu przybliżyć rozwiązanie problemu mechanizmów odpowiedzialnych za strukturalne przejścia fazowe w antyferroelektrycznych związkach ABO_3 typu perowskitu oraz określić wkład procesów relaksacyjnych oraz drgań sieci krystalicznej do niskoczęstotliwościowej zależności przenikalności dielektrycznej $\varepsilon(T)$ obserwowanej w pobliżu przejść fazowych. Zbadano wpływ jaki na wymienione procesy wywiera zastąpienie jonów Zr i Hf w sieci $PbZrO_3$ oraz $PbHfO_3$ jonami Ti. Badania zostały przeprowadzone w szerokim zakresie temperatur 300 - 700 K i częstotliwości 10 Hz - 10 MHz oraz w zakresie częstotliwości optycznych.

Dysertacja obejmuje obszerną dokumentację wyników eksperymentalnych i ich opracowanie numeryczne opierające się na wybranych modelach teoretycznych. W przypadku cyrkonianu ołowiawego znaleziono silny związek deformacji elektrostrykcyjnej z nikoczęstotliwościową relaksacją dipolową. W poszukiwaniu miękkich fononów przeprowadzono eksperymentalne badania ramanowskiego rozpraszania światła w przedziale częstotliwości 10 - 800 cm^{-1} i w zakresie temperatur 10 - 700 K. Numeryczne opracowanie widm, dokonywane przy uwzględnieniu symetrii faz, pokazało wyraźną zależność częstotliwości drgań optycznych od temperatury i potwierdziło występowanie w badanych materiałach przejść fazowych typu przesunięcia.

Praca składa się z czterech rozdziałów z których pierwszy jest teoretycznym wstępem opisującym znane z literatury własności dielektryczne i stukturalne badanych materiałów.

W drugiej części pracy opisano badania dyspersji dielektrycznej. W trzech podrozdziałach opisano następujące wyniki badań eksperymentalnych:

- procesy dyspersji dielektrycznej w $PbZrO_3$ w zakresie częstości do 10 MHz
- procesy relaksacyjne w stałych roztworach $PbZr_{1-x}Ti_xO_3$

- własności dielektryczne dla $PbHfO_3$ oraz $PbHf_{1-x}Ti_xO_3$ ze szczególnym uwzględnieniem fazy antyferroelektrycznej.

Wykonane pomiary ujawniły istnienie kilku występujących po sobie procesów relaksacji dielektrycznej, bądź to wspólnych dla wszystkich badanych kryształów bądź to zależnych od ich indywidualnych właściwości. Najsilniejszy efekt relaksacyjny, występujący w zakresie najniżych badanych częstotliwości (<100Hz) związano z procesami elektrochemicznymi w warstwach przyelektrodowych kryształu. Kolejny wspólny dla wszystkich badanych próbek efekt relaksacji dipolowej, mający znaczny wpływ na zależność $\varepsilon(T)$, zaobserwowano w zakresie do 1kHz. Relaxację tę powiązano ze zdefektowaniem oraz nieuporządkowaniem podsieci atomów tlenu. W zakresie kilku kHz dla kryształów $PbZr_{1-x}Ti_xO_3$ znaleziono słabą relaksację dielektryczną będącą bezpośrednim efektem wprowadzenia do sieci badanych kryształów jonów Ti i związaną z dynamiką granic fazowych. W przypadku materiałów $PbHfO_3$ i $PbHf_{1-x}Ti_xO_3$ podobna relaksacja w zakresie kilku MHz została związana z przebudową struktury domenowej w pobliżu przejścia fazowego między stanami antyferroelektrycznymi.

Trzecia część pracy opisuje badania właściwości elektromechanicznych. Badania te jak i poprzednio, wykonano dla następującego zestawu kryształów:

- $PbZrO_3$ czystego
- stałych roztworów $PbZr_{1-x}Ti_xO_3$
- oraz $PbHfO_3$ i $PbHf_{1-x}Ti_xO_3$,

W zakresie częstotliwości, w którym w fazie paraelektrycznej obserwowano dipolową relaksaję dielektryczną, występuje dyspersja odkształcenia elektrostrykcyjnego. Zjawisko dyspersji elektrostrykcyjnej potraktowano jako modyfikację właściwości elastycznych kryształu wynikającą z istnienia dynamiki dipoli elektrycznych w zmiennym polu elektrycznym.

Czwarta, ostatnia cześć pracy dotyczy badań Ramanowskiego rozpraszania światła w pobliżu przejść fazowych oraz w szerokim zakresie temperatur fazy paraelektrycznej. We wstępie, korzystając z teorii grup przeprowadzono analizę drgań dla kryształów $PbZrO_3$ oraz $PbHfO_3$ w poszczególnych fazach występujących w tych kryształach t.j.

Paraelektrycznej (PE)→Ferroelektrycznej(FE)→Antyferroelektrycznej (AFE) dla $PbZrO_3$ oraz $PbZr_{1-x}Ti_xO_3$,

Paraelektrycznej (PE)→Antyferroelektrycznej(AFE1)→Antyferroelektrycznej (AFE2) dla $PbHfO_3$ oraz $PbHf_{1-x}Ti_xO_3$.

Celem badań rozpraszania Ramanowskiego było poszukiwanie miękkiego drgania. Z przeprowadzonych eksperymentów wysunięto następujące wnioski:

- dla $PbZr_{0,99}Ti_{0,01}O_3$ zachowanie tego miękkiego drgania obserwowano we wszystkich fazach występujących w tym krysztale. Szczególną uwagę zwrócono na fazę paraelektryczną, w której możliwość wystąpienia linii ramanowskich I-rzędu jest wykluczona ze względu na reguły wyboru. Złamanie tych reguł jest tu związane bądź z wprowadzeniem defektów do podsieci Pb lub O, bądź z pojawianiem się dynamicznych obszarów polarnych indukowanych wprowadzeniem do sieci krystalicznej jonów Ti.
- w $PbHfO_3$ oraz $PbHf_{0,96}Ti_{0,04}O_3$ zachowanie typu miękkiego drgania zaobserwowano w okolicy przejścia fazowego pomiędzy dwoma fazami antyferroelektrycznymi. Wystąpienie miękkiego drgania w tym przejściu fazowym świadczy o tym, że jest ono po części typu przesunięcia.

Podobnie jak w $PbZr_{0,99}Ti_{0,01}O_3$ tak i w $PbHfO_3$ oraz $PbHf_{0,96}Ti_{0,04}O_3$ obserwowano w fazie parelektrycznej zabronione prawami symetrii linie ramanowskie I-rzędu. Żadna z tych linii w przypadku tych kryształów nie wykazywała jednak cech miękkiego drgania.

Po dyskusjach wyników przeprowadzanych oddzielnie po zakończeniu każdego z rozdziałów oraz ustosunkowaniu się do zamierzonych celów , pracę kończą wnioski.

RESUME DE LA THESE

L'object du travail de recherche est une étude de la relaxation diélectrique, des propriétés électrostrictives et de la diffusion de la lumiere Raman dans les deux systemes perovskites a base de plomb:

- $PbZrO_3$ pur ou faiblement dopé par des ions Ti
- $PbHfO_3$ pur ou faiblement dopé par des ions Ti

Les deux systemes ont la charactéristique commune, en étant meme des substances prototypes, de présenter une (pour $PbZrO_3$) voire deux (pour $PbHfO_3$) transitions de phase structurales vers de phases antiferroélectriques (AFE).

Le but des travaux faits dans la these est d'étuder expérimentalement et théoriquement les transitions de phase structurales exhibées par les deux systemens, et notamment celles menant a des phases AFE, et d'en comprendre les méchanismes. Afin d'arriver a ces objectifs, nous avons mis en oeuvre des mesures de relaxation diélectrique, des propriétés électrostrictives et de diffusion de lumiere Raman, cela dans des intervalles de températures allant a 10 K a 700 K et dans des gammes des fréquences de 10 Hz a 10 MHz pour les mésures diélectriques et élecrostrictives. Les différences mesures dont été réalisées sur des monocristaux purs $PbZrO_3$ et de $PbHfO_3$ et sur des monocristaux présentant de faible dopage (de l'ordre 4%) en ions Ti.

Le mémoire de these comporte quatre chapitres détaillant, de façon progressive, les différentes phases du travail.

Le premier chapitre est consacré a un rappel des propriétés diélectriques et structurales des deux systémes étudiés. Il pose ainsi clairement l'object scientifique de l'étude envisagée en la situant dans le champ des connaissances déja acquises et en posant les problémes non résolus et abordés dans les trois chapitres qui suivent.

Le second chapitre du mémoire est plus spécifiquement aux propriétés diélectriques des cristaux étudiés. Ce chapitre commence par rappeler les éléments théoriques essentiels concernant les fonctions de susceptibilités diélectriques de matériaux isolants telles que par exemple la fonction de Debye, la fonction de Cole-Cole, la fonction de Cole-Davidson. Puis sont données les conditions et les dispositifs expérimentaux mis en oeuvre ainsi que quelques informations essentielles sur la croissance et la nature des cristaux étudiés.

La seconde partie de ce chapitre donne un aperçu systématique des résultats expérimentaux obtenus, cela en les présentant sous trois sous-sections:

- les résultats de dispersion dielectrique de $PbZrO_3$ en dessous de 10 MHz;
- les processus de relaxation diélectrique dans des monocristaux de solutions solides de $PbZr_{1-x}Ti_xO_3$
- les anomalies diélectriques de $PbHfO_3$ et $PbHf_{1-x}Ti_xO_3$ a proximité de la transition de phase antiferroélectrique

Les mesures ont mis en évidence plusieurs sortes de relaxations diélectriques, qui sont soientt communes a tous les énchantillons, ou soientt spécifiques a chaque composition cristalline. Une forte relaxation a été mise en évidence au base fréquence et est attributée a des processus de type électro-chimique. Les énchantillons étudiés présentent également la propriété commune d'une dispersion diélectrique significative dans le domaine du kHz attributée aux impuretés et a des désorderes dans le sous-réseau des ions oxygene. D'autres contributions diélectriques d'intensitiés moins importantes ont étés observées et analysées comme étant spécifiques a chaque échantillon.

Le troisieme chapitre du mémoire décrit les études électromécaniques enterpris sur les systemes cristallins analysés. Aprés avoir rappelé les aspects théoretiques et précisé les montages en expérimentaux utilisés, nous détaillons l'ensemble des réultats de mesures obtenus:

- sur le cristal $PbZrO_3$
- sur la solution solide $PbZr_{1-x}Ti_xO_3$
- sur le cristal $PbHfO_3$ et la solution solide $PbHf_{1-x}Ti_xO_3$ dans la phase paraélectrique.

Les résultants mettent en évidence l'apparition, simultanément aux relaxations dipolaires, de dispersions de la déformation électrostrictive. Cet effect a été interprété comme un „modulateur" des propriétés élastiques des cristaux consécutives a l'existence de dynamiques dipolaires.

Le quatrieme chapitre de la thése concerne une étude expérimentale systématique de la diffusion de lumiére Raman sur les cristaux perovskite a base de plomb et son interprétation.

Le premiere section de chapitre 4, rappelle les éléments essentiels et indispensables a la bonne compréhension du mémoire sur la spectroscopie Raman et la dynamique cristalline. Puis est donnée l'analyse en terme de théorie de groupes, des symétries des vibrations des cristaux de $PbZrO_3$ et $PbHfO_3$ dans les différentes séquences de transitions de phase:

Paraélectrique (PE) → Ferroélectrique (FE) → Antiferroélectrique pour $PbZrO_3$

Paraélectrique (PE) → Antiferroélectrique 2 (AFE2) → Antiferroélectrique 1 (AFE1) pour $PbHfO_3$

Suite a ces considérations sur les symétries de vibrations, nous donnons les principaux résultats obtenus par specroscopie Raman :

- sur $PbZrO_3$ et $PbZr_{1-x}Ti_xO_3$ dans de phase AFE1
- l'évolution du spectre a la transition de phase AFE1→PE
- sur le secteur de $PbHfO_3$ at $PbHf_{1-x}Ti_xO_3$ lors de la séquence AFE1 - AFE2 oaz z PE.

Dans la derniére section 4, nous analysons le spectre Raman en relation avec les résultats obtenus dans les chapitres 2 et 3. Les points essentiels mis en évidence sont les suivants:

- la phase paraélectrique, par symétrie inactive en spectre Raman du 1er ordre, développe en spectre Raman significatif interprété comme étant du, soit a l'existence ou l'introduction de défaux dans le sous-réseau Pb/O, soit a l'existence d'amas dipolaires dynamiques consécutif a l'introduction d'ions Ti au centre de la cellule perovskite de thése.
- la transition de phase PE - AFE2 -AFE1 a été analysée du point de vue diélectrique a partir des résultats de dynamique cristalline déduits du spectre Raman et a permis d'analyser les contributions respectives des dynamiques phononiques et relaxationnelles dans les transitions. Les dynamiques relaxationelles ont été reliées aux observations du chapitre 2 et a la diffusion quasi-élastique de lumiere.
- l'activation d'un spectre Raman assez intense dans $PbZrO_3$ et $PbZr_{1-x}Ti_xO_3$ a été analysée en terme d'occurrence d'un mode ferroélectrique mou qui pourrait participer en tant que mécanisme moteur lors de la transition de phase PE→FE.

Dans la conclusion, nous présentons une synthése de résultats noveaux obtenus par notre étude en les discutant de façon comparative et en les analysant criquement par rapport aux données connues présentées dans le chapitre 1.

CONTENS

1. INTRODUCTION 1

1.1 DIELECTRIC DIVERGENCE AT PHASE TRANSITION POINT OF PEROVSKITE OXIDES 1

1.2. ANTIFERROELECTRIC PEROVSKITES - LITERATURE DATA 5

1.2.1. Structural properties of Lead zirconate 5

1.2.2. Substitution of Zr by Ti ions in $PbZrO_3$ - solid solution $PbZr_{1-x}Ti_xO_3$ (PZT) 8

1.2.3. Phase transformations in Lead hafnate - $PbHfO_3$ 10

2. DIELECTRIC DISPERSIONS 12

2.1. THEORETICAL INTRODUCTION 12

2.2. DIELECTRIC MEASUREMENTS 15

2.2.1. Crystal growth and composition determination 17

2.2.2. Experimental conditions 18

2.3. EXPERIMENTAL RESULTS 19

2.3.1. Dielectric dispersion in Lead zirconate below 10 MHz 19

2.3.2. Relaxation processes in single crystals of $PbZr_{1-x}Ti_xO_3$ solid solutions 30

2.3.3. Dielectric permittivity anomalies at antiferroelectric phase transitions in $PbHfO_3$ and $PbHf_{1-x}Ti_xO_3$ 37

2.4. DISCUSSION - POSSIBLE SOURCES OF RELAXATIONS BELOW 10 MHz 46

3. ELECTROSTRICTION 53

3.1. THEORETICAL BACKGROUND 53

3.2. EXPERIMENTAL SETUP 55

3.3. EXPERIMENTAL RESULTS 57

3.3.1. Electrostriction in $PbZrO_3$ 57

3.3.2. Strain dispersion in the $PbZr_{1-x}Ti_xO_3$ single crystal 62

3.3.3. Electrostriction in $PbHfO_3$ and PHT 65

3.4. DISCUSSION - ELECTROSTRICTION AND LOW-FREQUENCY DIELECTRIC RELAXATIONS 68

4. RAMAN SPECTROSCOPY 72

4.1. THEORETICAL ASPECTS OF RAMAN LIGHT SCATTERING 72

4.1.1. Scattering of light by material media 72

4.1.2. Inelastic Raman light scattering 72

4.1.3. Symmetry analysis 75

4.1.4. Selection rules for Raman scattering 77

4.1.5. Selection rules from a quantum-mechanical point of viev 77

4.1.6. The temperature dependence od Raman intensities 78

4.2. THE LYDDANE-SACHS-TELLER RELATION 79

4.3. CLASSICAL OSCILLATOR MODEL OF SPECTRAL FUNCTION 80

4.4. THE EXPERIMENTAL CONDITIONS 81

4.5. SYMMETRY ANALYSIS AND CALCULATIONS OF VIBRATIONAL MODES 83

4.5.1. Vibrational modes in $PbZrO_3$ pure and $PbZr_{1-x}Ti_xO_3$ ($x<0.6$) 83

4.5.2. Vibrational modes in $PbHfO_3$ and $PbHf_{1-x}Ti_xO_3$ solid solutions 85

4.6. RAMAN SCATTERING LITERATURE DATA IN PURE $PbZrO_3$ 86

4.6.1. Raman spectra for two kinds of $PbZrO_3$ single crystals 87

4.7. EXPERIMENTAL RESULTS 90

4.7.1. Raman spectrum of $PbZr_{0.99}Ti_{0.01}O_3$ in the antiferroelectric phase 90

4.7.2. The evolution of Raman spectra near the A-F phase transition 91

4.7.3. Raman spectra at the F-P phase transition 92

4.7.4. Raman spectra around antiferroelectric phase transition in $PbHfO_3$ and $PbHf_{1-x}Ti_xO_3$ 93

4.8. ANALYSIS OF THE RAMAN RESULTS 97

4.8.1. Introduction 97

4.8.2. Calculations of the Raman spectra intensities and frequencies in the A and F phases for $PbZr_{0.99}Ti_{0.01}O_3$ 98

4.8.3. Raman scattering in the P phase of $PbZr_{0.99}Ti_{0.01}O_3$ - modes share in dielectric response 101

4.8.4. $A_1 \rightarrow A_2$ and $A_2 \rightarrow P$ phase transitions in $PbHfO_3$ and $PbHf_{1-x}Ti_xO_3$ 104

4.8.5. Influence of low frequency Raman lines on low frequency dielectric response in the vicinity of the A_1 and A_2 phases for $PbHfO_3$ and PHT 108

4.8.6. Study of the A_2-P transition and Raman light scattering in P phase 110

4.9. DISCUSSION - HIGH FREQUENCY DIELECTRIC RESONSE ABOVE 10^{11} Hz 112

5. CONCLUSIONS **116**

REFERENCES **118**

1. INTRODUCTION

1.1. DIELECTRIC DIVERGENCE AT PHASE TRANSITION POINT OF PEROVSKITE OXIDES

Ferroelectrics and antiferroelectrics represent a special class of materials in which structural phase transitions from high to low symmetry phase are accompanied by the appearance of spontaneous polarization (Forsbergh, 1956; Megaw, 1957; Känzig, 1957; Jona & Shirane, 1962; Fatuzzo & Merz, 1967; Smolenskii et al., 1971; Mitsui et al., 1973). The appearance of long range polar or anti-polar order in coordinate space is thus characteristic for ferroelectric (F) and antiferroelectric (A) phase transitions.

Among large number of ferroelectric and antiferroelectric materials, double oxides of perovskite type have been for many years of great interest in the investigations of both nature and mechanism of phase transitions. The perfect perovskite structure is extremely simple with general formula ABO_3, where A is a monovalent or divalent metal and B is a tetra- or pentavalent one (see Fig 1.1). It is a cube with A atoms at the cubic corners, B atoms at the body centres and O at the face centred positions.

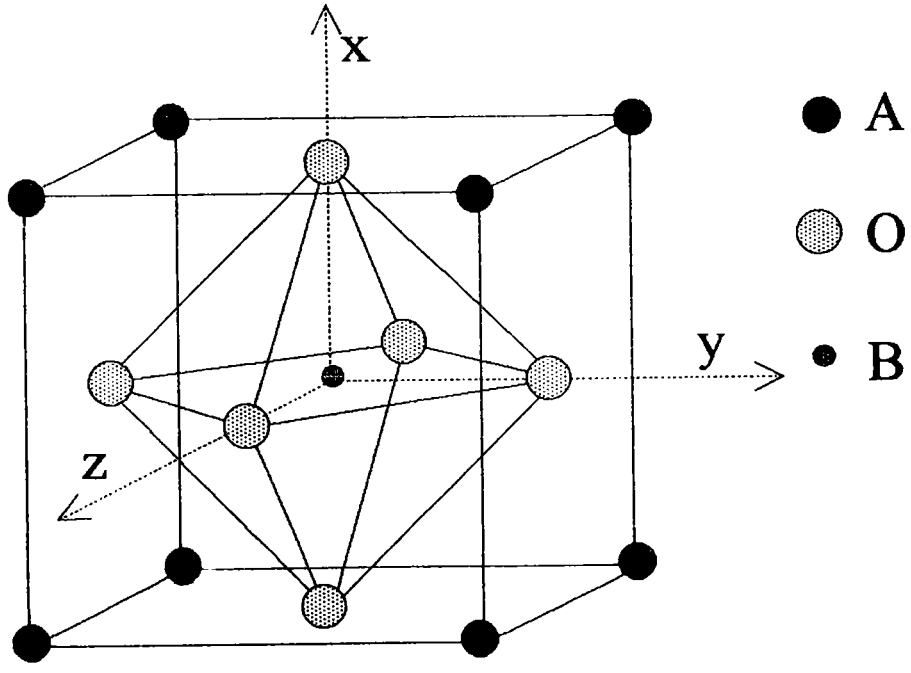


Figure 1.1. Cubic perovskite-type structure ABO_3.

Taking the origin at the position of the A atom, the coordinates of the atoms are then:

A at (0,0,0)

B at $\left(\frac{1}{2},\frac{1}{2},\frac{1}{2}\right)$

O at $\left(\frac{1}{2},\frac{1}{2},0\right),\left(\frac{1}{2},0,\frac{1}{2}\right),\left(0,\frac{1}{2},\frac{1}{2}\right)$

The structure can be also regarded as a set of BO_6 octahedra arranged in a simple cubic pattern and linked together by shared oxygen atoms, with A atoms occupying the spaces in between. Many of these compounds are characterised by very drastic anomalies in dielectric permittivity at certain temperatures. These anomalies indicate corresponding phase transitions.

A crystal is said to be *ferroelectric* when it has two or more orientational states in the absence of an electric field and can be shifted from one to another of these states by an electric field. Any two of the orientation states are identical (or enantiomorphous) in crystal structure and differ only in electric polarization vector at null field. A ferroelectric phase change represents a special class of structural phase transition denoted by the appearance of a spontaneous polarization and large divergence of the dielectric permittivity at a Curie point T_c. Above T_c (in a paraelectric phase) the dielectric permittivity ε, varies with temperature in an approximate Curie-Weiss manner $\varepsilon=C/(T-T_o)$, where T_o is the Curie-Weiss temperature.

The first ferroelectric perovskite to be discovered was $BaTiO_3$. It was an event of particular significance as prior to the discovery only complex hydrogen-bonded crystals had been known to exhibit ferroelectricity and the presence of hydrogen had been considered essential for the phenomenon. Other leading representatives of this class of crystals are $PbTiO_3$ and $KNbO_3$.

Materials are called *antiferroelectrics*, in the sense given by Kittel (1951), when the system exhibits large dielectric anomalies near the Curie temperature (T_c), but no net spontaneous polarization can be observed in the lower phase, where the crystal's structure is characterised by antiparallel displacements of certain atoms. The system can be transformed to an induced ferroelectric phase by application of an electric field. The most important representatives of ABO_3-type class of antiferroelectric crystals are $PbZrO_3$, $NaNbO_3$ and $PbHfO_3$.

According to Lyddane-Sachs-Teller relation (Lyddane et al., 1941) the large dielectric permittivity divergence observed near the ferroelectric phase transition should be associated with the condensation of soft phonon at the Brillouin zone centre ($\vec{q} = 0$). In antiferroelectrics the phase transitions (where the size of unit cell increases at the phase transition) are due to condensation of soft phonon at the Brillouin zone boundary ($\vec{q} \neq 0$). The order parameter of the transition is in both cases related to the static part of the normal coordinate of the corresponding soft phonon. In ferroelectrics the order parameter is thus the static homogeneous polarization or, which is the same, the Fourier component of the polarization with a wave vector zero, $\vec{q} = 0$. In antiferroelectrics, on the other hand, the important quantity is the Fourier component of the polarization with a non-zero wave vector, $\vec{q} \neq 0$. It means that the antiferroelectric crystal is composed of two collinear sublattices with opposite polarization and thus cannot be described by a single order parameter. In such a case the transition corresponds to simultaneous condensation of more than one soft phonon.

In perovskite $BaTiO_3$ and $KNbO_3$ crystals the soft mode concept was connected with the phonon like motion of central ions (Ti or Nb) with respect to their oxygen octahedra (Lines & Glass, 1977). However it was shown recently that for these materials the concept did not fully explain the $\varepsilon(T)$ behaviour and the relaxational process was found to be mainly responsible for the dielectric response measured in the audio-frequency region (Fontana et al., 1984; Maglione et al. 1989). In both cases the relaxation process was associated with hopping of off-center Ti/Nb ions between symmetry-related potential wells. In $BaTiO_3$ a Debye-like relaxation peak occurred in the 10^8 Hz range, with the slowest relaxation time at the transition temperature (413 K) between the paraelectric (cubic) and ferroelectric (tetragonal) phases. According to Maglione et al. (1989), the susceptibility maximum at T_c comes directly from the relaxational mode. In the $KNbO_3$ crystal a model of coupled resonator and relaxation mode proposed by Fontana et al. (1984) well describes the $\varepsilon(T)$ dependence throughout the whole temperature range. In ferroelectric $PbTiO_3$ the large discrepancy at T_c between the clamped susceptibility and the one - calculated from the Lydden-Sachs-Teller relation was explained as due to the relaxing motion of lead (or oxygen) ions around displaced sites (Fontana et al. 1990). The existence of the relaxation mode was linked to the order-disorder nature of the phase transitions in these ferroelectric materials. The soft phonon observed experimentally in

both barium titanate and potassium niobate, were strongly overdamped presumably because of the relaxation mentioned above.

Investigations of antiferroelectric materials making use of dielectric and optical spectroscopy are rather poorly represented in the literature (Perry & McCarthy 1965). For lead zirconate $PbZrO_3$ crystal which is the best known antiferroelectric material among perovskites, most papers on dielectric and structural properties deal with the problem of a transient phase appearing below T_c (Scott & Burns, 1972; Ujma & Hańderek, 1975; Whatmore & Glazer, 1979, Fuishita & Hoshino, 1984; Roleder & Dec, 1989; Dec & Kwapuliński, 1989). Papers on Raman scattering in $PbZrO_3$ crystals of this type were focused on searching of soft mode (Pasto & Condrate, 1973; Roleder et al. ,1988). Using this method phase transitions in pure lead zirconate were quite satisfactorily recorded, though clear soft mode ($\vec{q} = 0$) behaviour was not found. Only a 130 cm^{-1} line was detected at room temperature in Raman spectra, which shifted very slowly towards lower frequencies with increasing of temperature. It might be considered as a soft mode but this mode was strongly overdamped when approaching transition to the intermediate and then to the cubic phase (Roleder et al. 1988). Some investigations concerning the dielectric relaxation were reported by Lanagan et al. (1988) but only at room temperature and in ceramic lead zirconate and also without final identification of loss mechanisms. In the system of $Pb(ZrTiNb)O_3$ a strong Debye-like dielectric dispersion at GHz region in the para- and ferroelectric phases was found, but also for ceramics of these compounds (Arlt et al., 1994: Hassan et al., 1995). The relaxation found was attributed either to the sound emission by ferroelectric domain walls (Arlt et al., 1994) or to the presence of clusters of micro- or nanometer size (Hassan et al., 1995). Some experiments on dielectric dispersion at the above mentioned frequency region were performed recently by Roleder et al. (1996) for $PbZrO_3$ single crystal. The investigations revealed the existence of a relaxational polar mode in the antiferroelectric and paraelectric states.

To some extent a similar situation occurs in $PbHfO_3$ for which earlier investigations made on ceramics indicated two temperature-induced phase transitions (Goulpeau, 1966; Samara, 1966; Shirane & Pepinski, 1953; Forker et al., 1973). However in literature there is virtually no reported information on lattice dynamics or dielectric relaxations in lead hafnate single crystals except some investigations of Raman scattering made in high pressure (Jayaraman et al. ,1994).

Hence in the present study was decided to undertake a systematic dielectric relaxation and Raman spectroscopy investigations of these two antiferroelectric crystals: $PbZrO_3$ with one phase transition and $PbHfO_3$ with two phase transitions. For these crystals, like in the case of several ferroelectric crystals the dielectric dispersions can be expected in a very wide frequency range from few hertz's up to GHzs. The central problem here is the origin and physical mechanisms of particular relaxations. Solving this problem could be of considerable importance for the description of the nature of phase transitions (order-disorder or displacive) existing in those crystals and the mechanisms responsible for the real part of the dielectric permittivity $\varepsilon'(T)$ dependence, especially in the vicinity of the phase transition point. The similar investigations were undertaken for the crystals doped with small amount of $PbTiO_3$ i.e. $PbZr_{1-x}Ti_xO_3$ (PZT) and $PbHf_{1-x}Ti_xO_3$ (PHT). It is well known that introduction of foreign component leads radically to changes of the properties of basic compounds. In solid solutions PZT, Ti substitution induces the formation of polar regions even in the paraelectric phase. Thus the introduction of the substituted component was designed to help to elucidate the nature and origin of the observed dielectric relaxations and Raman scattering spectra. In fact some experimental data in case of PZT are known in literature however numerical elaboration of spectra were not presented.

The measurement of electrostrictive deformation as a function of frequency at different temperatures in paraelectric phase have been also designed to find possible correlation to dielectric dispersion especially at lower frequency region. Although the lead zirconate is the best known antiferroelectric crystal, there is still little knowledge on its electromechanical properties. Some electrostrictive measurements were performed for ceramic samples (Cieminski & Roleder, 1989) but the investigations for single crystals are still unheard. On the other hand no measurements on electromechanical properties of $PbHfO_3$ are reported in literature.

1.2. ANTIFERROELECTRIC PEROVSKITES - LITERATURE DATA

1.2.1. Structural properties of Lead zirconate

The best known and most frequently studied case of antiferroelectricity in perovskites is $PbZrO_3$. At high temperatures it possesses the prototype cubic perovskite structure but with temperature decrease it exhibits a marked dielectric anomaly at about 503 K. The high

temperature phase is paraelectric with the dielectric constant following the Curie-Weiss law with Curie constant $C \approx 1.6 \cdot 10^{+5}$K and Curie-Weiss temperature $T_o \propto 463$ K. Although the general character of this dielectric anomaly appears similar to the one observed in typical first-order ferroelectric perovskite like $BaTiO_3$, dielectric hystheresis is not generally observed in the low temperature phase and early X-ray and neutron diffraction experiments (Sawaguchi et al., 1951; Jona et al., 1957) proved that the room-temperature structure is antiferroelectric.

Early experiments on ceramic samples of $PbZrO_3$ indicated that the phase transition at 503 K was the only structural transition to occur as a function of temperature in zero field (Jona et al., 1957). However the application of an external electric field below T_c induces a transition to an intermediate rhombohedral ferroelectric phase. This implies that the antiferroelectric and ferroelectric phases are very closely equal as to the free energy value. Nevetherless it is possible that the rhombohedral ferroelectric phase may be stable in zero field within a narrow intermediate temperature range between the antiferroelectric and paraelectric phases. The intermediate ferroelectric phase was observed to be stable over a

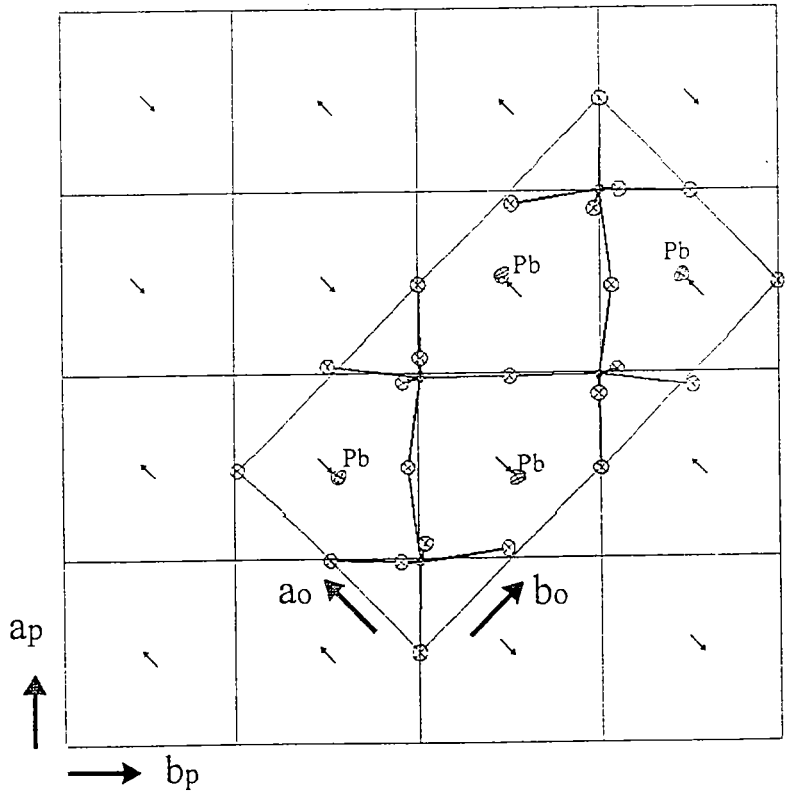


Figure 1.2. A schematic representation of the basic antipolar arrangement in $PbZrO_3$. The unit cell of the AFE phase is outlined.

temperature range of the order 10 - 25 deg below, but the range of stability depends very sensitively upon stoichiometry and growth conditions of the samples (Scott & Burns, 1972; Benguigi et al., 1971; Ujma & Handerek, 1975; Whatmore & Glazer, 1979; Fuishita & Hoshino, 1984).

In spite of uncertainty concerning the form of the transition or transitions, the antiferroelectric structure at room temperature seems to be well established with the accuracy at the level 1 pm (Jona et al, 1957). The crystal structure - first proposed by Sawaguchi et al. (1951) - is orthorhombic with a pseudocubic perovskite unit cell given by $4a_p \times 4b_p \times 2c_p$ with $a_p=b_p$. The quadrupoling of the pseudocubic a_p and b_p axes could be explained by Pb displacements from their prototypic perovskite sites as shown in Figure 1.2. Sawaguchi et al. (1951) determined that the displacements were approximately 0.2 Å and that true space group was either Pbam or Pba2. More recently the structure of $PbZrO_3$ was examined thoroughly by Sawaguchi et al. (1980), Fuishita & Sawaguchi (1981), Tanaka et al. (1982). Following these studies the space group was determined to be Pbam.

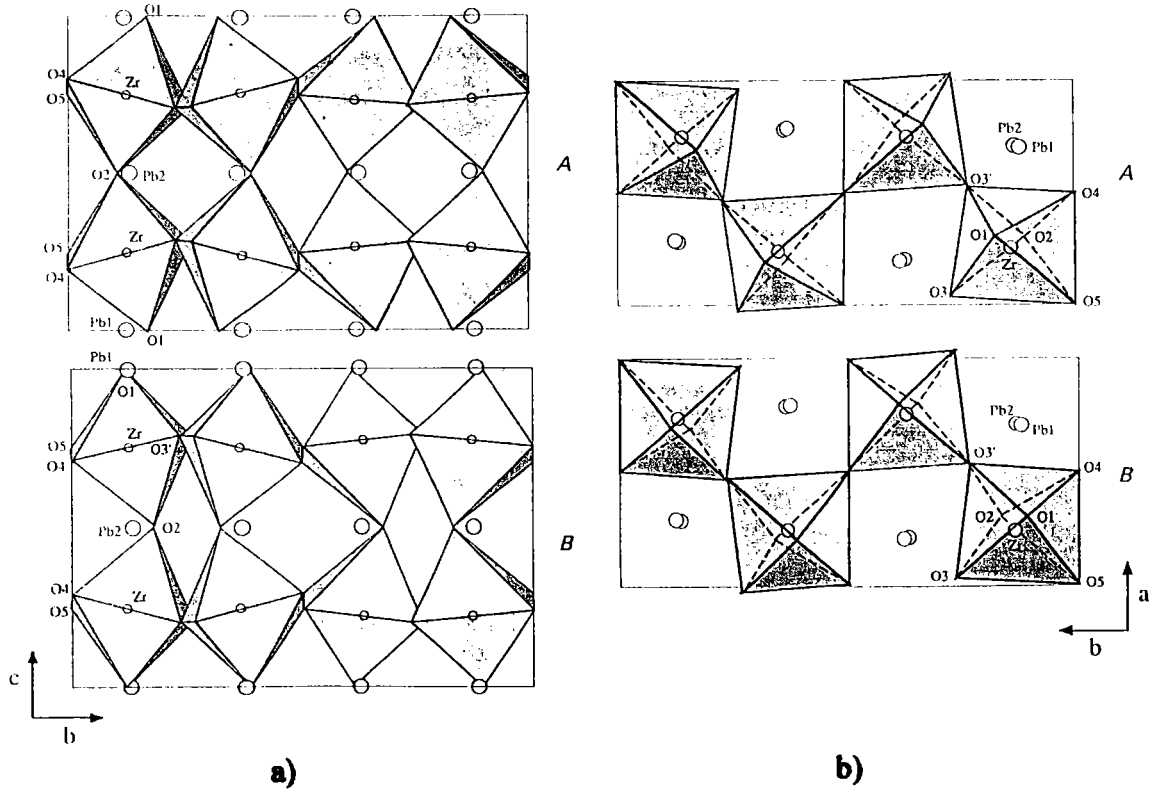


Figure 1.3. The structure of $PbZrO_3$ on (100) (a) and (001) (b) divided into its two constituent substructures **A** and **B**.

In all these structural studies it was assumed that the structure was fully ordered. However Whatmore (1967) and later Glazer et al. (1993) described the large octahedral distortions in $PbZrO_3$ structure. Moreover they showed that the structure of $PbZrO_3$ could be considered to be a superposition of two substructures **A** and **B** as shown in Figure 1.3.

The relationship between the substructures almost exactly corresponds to displacement through $(0,0,\frac{1}{2})$ thus:

$$x_A, y_A, z_A \rightarrow x_B, y_B, \frac{1}{2} + z_B$$

With reference to pseudocubic axes the tilting of the octahedra in Figure 1.3 in each substructure is well described by the tilt scheme $a^-a^-c^0$ (Glazer, 1972; 1975).

1.2.2. Substitution of Zr by Ti ions in $PbZrO_3$ - solid solution $PbZr_{1-x}Ti_xO_3$ (PZT)

A very large amount of work was performed on solid solutions based on $PbZrO_3$. Of particular interest are $Pb(ZrTi)O_3$ both ceramics and single crystals which exhibit strong electromechanical activity and are of some technical importance accordingly. The properties of solid solutions of the antiferroelectric $PbZrO_3$ with ferroelectric $PbTiO_3$ are described by a very complex diagram (Jaffe et al., 1971; Sawaguchi, 1952; Morozov et al., 1978; Roleder, 1980). This refers in particular to PZT solid solution with Ti concentration of a few molar percent (<5% mol). When Ti ions are added to the system, X-ray investigations show the existence of an intermediate phase below T_c. On the basis of X-ray, dielectric, pyroelectric, piezoelectric and DTA measurements, many authors have tried to relate the width of the transient phase with the concentration of Ti in PZT (the more Ti ions in the system, the broader is the transient phase). This concept was fairly successfully verified in the case of ceramic materials but seemed to fail when single crystals were considered. The phase diagram for the PZT ceramic system is presented in Figure 1.4.

For solid solution with Ti content above x=0.5, a unique phase transition exists, often considered as purely displacive nature, between the cubic paraelectric (P) phase (Pm3m - O_h^1) and the ferroelectric tetragonal (F) phase of P4mmm (C_{4v}^1) symmetry. For PZT with Ti content less than 0.5, the sequence of transitions is more complex. In the PZT with small Ti concentration up to 0.06, the phase transition from cubic structure (P) to an antiferroelectric (A) phase of orthorhombic symmetry (Pbam) is realised via an

intermediate I phase. For $0<x<0.03$ in the I phase coexistence of phases P and A with the rhombohedral ferroelectric (F) phase was ascertained (only for ceramic samples) (Hańderek et al., 1985). The pure F phase of R3m (C_{3v}^5) symmetry (usually called F_R^{ht}) is clearly present only in solutions for which $x \geq 0.03$. For a slightly higher concentration (above 0.06) the A phase vanishes and a low temperature ferroelectric phase F_R^{lt} appears implying, contrary to the F_R^{ht} phase, rotations of oxygen octahedra and rhombohedral symmetry (R3c - C_{3v}^6)

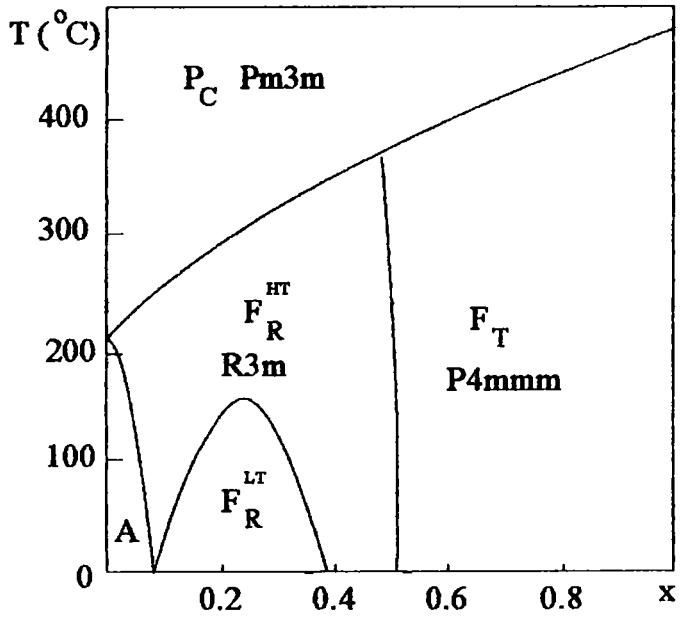


Figure 1.4. Phase diagram of the $PbZr_{1-x}Ti_xO_3$ solid solution (Jaffe et al., 1971)

Numerous investigations established that the non-stoichiometry in the Pb and/or O sublattices strongly influenced the properties of both $PbZrO_3$ and PZT compounds. The problem is caused by the concentration of point defects in the Pb and/or O sublattices, which are so easily produced in the technological process. For this reason it is possible to obtain two kinds of $PbZrO_3$ single crystals in the growth process. The first one exhibiting only one phase transition directly from the paraelectric to antiferroelectric phase and the second one in which a sufficiently high concentration of point defects can provoke a ferroelectric transient phase below T_c (Roleder & Dec, 1989; Dec & Kwapuliński, 1989a). X-ray examinations showed that crystals with one phase transition were structurally more perfect than those with two transitions which exhibited structural nonhomogeneity i.e.

superposition of two different cubic systems in the antiferroelectric and paraelectric phase respectively (Dec & Kwapuliński, 1989b). Similarly it is well known that Ti ions introduced to the lead zirconate also radically change the properties of solid solutions obtained from this compound. Ti substitution induces the formation of polar regions even in paraelectric phase (Roleder, 1989) and also significantly extends the temperature range of the occurrence of the intermediate phase towards lower temperatures (Roleder, 1980). As a consequence, both causes i.e. point defects and introduction of Ti ions, can influence the range and the nature (ferroelectric or mixture of paraelectric, ferroelectric and antiferroelectric phases) of the intermediate phase in PZT. Thus it may be expected that for a $PbZrO_3$ single crystal with some Ti concentration the temperature range of the transient phase may also vary and could differ considerably from the one reported in the literature.

1.2.3. Phase transformations in Lead hafnate $PbHfO_3$.

Lead hafnate ($PbHfO_3$) is an antiferroelectric of the perovskite-type structure. It was described for the first time by Shirane & Pepinski (1953) as the material analogous to lead zirconate ($PbZrO_3$). Earlier investigations made on ceramics under air pressure indicated two temperature-induced phase transitions: the first from paraelectric (P) to the intermediate antiferroelectric (A_2) state and the second to the low-temperature antiferroelectric (A_1) phase (Goulpeau, 1966; Samara, 1966; Shirane & Pepinski, 1953; Forker et al., 1973). While the temperature of the A_2-P transition reported in those papers varied from 477 K to 488 K, the A_2-A_1 transition was fairly well established at 433-436 K. The P phase exhibits a classical cubic perovskite structure and the symmetries of A_1 and A_2 phases appears to be both orthorhombic. The A_1 phase was considered as isomorphous with that of $PbZrO_3$ at room temperature (Fesenko & Balyunis, 1980).

The investigations of two antiferroelectric phases A_1 and A_2 did not finally determine the structure of these two phases. Although they seem to be well described in the recent literature (Zaitsev et al., 1979; Leontiev et al., 1984; Topolov at al 1990a & b). The possible symmetries of the A_1 and A_2 phases according to Zaitsev et al. (1979), Leontiev et al. (1984) belong to the space group Pba2 or Pbam for A_1 and one of the symmetries $P222_1$, Pmm2, Pmmm or P222 for A_2 all of the orthorhombic symmetry.

Concerning the paraelectric phase, Kwapulinski et al. (1994) reported the existence of disorder in high temperature Pm3m phase of $PbHfO_3$. On the basis of X-ray measurements, they reported that Pb ions were randomly displaced in the Pb/O sublattice.

Up till now however rather little work of different relevance (except the structural aspects previously mentioned) to antiferroelectricity is published especially on the mechanism of the two phase transitions in $PbHfO_3$.

To the best of our knowledge there is no literature data on the materials $PbHf_{1-x}Ti_xO_3$.

2. DIELECTRIC DISPERSIONS

2.1. THEORETICAL INTRODUCTION

Debye process

In order to acquire a physical picture of the dynamic mechanism of phase transitions we have to study first the response of the dielectric susceptibility of the dielectric crystal to application of time-dependent electric field. In that case a dipole moment of the crystal which is activated by external electric field is going to be oriented in the direction of the applied field. Than if the electric field alternates its orientation, the orientation of the dipole moments will depend on time too. Thus, the phase difference can appear between the dipole moments orientation and the electric field direction. It causes the dielectric susceptibility to become a complex value. The behaviour of the complex susceptibility or dielectric permittivity was firstly derived by Debye (Debye et al., 1934).

Under the assumption that the dipole moments in the crystal do not interact between each other the dielectric susceptibility $\chi=\chi'-j\chi''$ in fuction of frequency behaves in a manner described by the equation 2.1 which is the complex relation:

$$\chi(\omega) = \chi_\infty + \frac{\chi_s - \chi_\infty}{1 + j\omega\tau} \qquad 2.1$$

where χ_s and χ_∞ are the static susceptibility and the susceptibility measured above the dispersion region, respectively, τ is the mean relaxation time and ω is the angular frequency ($\omega=2\pi f$, f - frequency). The relation 2.1 can be divided into two: real and imaginary parts:

$$\chi' = \chi_\infty + \frac{\chi_s - \chi_\infty}{1+\omega^2\tau^2} \qquad 2.2$$

$$\chi'' = \frac{\chi_s - \chi_\infty}{1+\omega^2\tau^2}\omega\tau \qquad 2.3$$

Regarding connections between χ and dielectric permittivity $\varepsilon=\varepsilon'-j\varepsilon''$:

$$\chi'=\varepsilon'-1$$

$$\chi''=\varepsilon'' \qquad 2.4$$

Equations 2.2 and 2.3 can be rewritten in the following way:

$$\varepsilon' = \varepsilon_\infty + \frac{\varepsilon_s - \varepsilon_\infty}{1+\omega^2\tau^2} \qquad 2.5$$

$$\varepsilon'' = \frac{\varepsilon_s - \varepsilon_\infty}{1+\omega^2\tau^2}\omega\tau \qquad 2.6$$

and loss tangent: $$tg\delta = \frac{\varepsilon''}{\varepsilon'} = \frac{(\varepsilon_s - \varepsilon_\infty)\omega\tau}{\varepsilon_s + \varepsilon_\infty\omega^2\tau^2} \qquad 2.7$$

Equations 2.5-2.7 are called Debye equations and describe changes of the real and imaginary parts of dielectric permittivity (ε' and ε'') in function of frequency ω with constant relaxation time τ. ε_s is the static permittiviy and ε_∞ - permittivity at high frequencies (see figure below). τ is the relaxation time of the Debye process. Maximum of ε'' will appear for $\omega=\omega_{max}$, obeying relation $\omega_{max}\tau=1$ (τ=cons). Both ω_{max} and τ values depend on temperature.

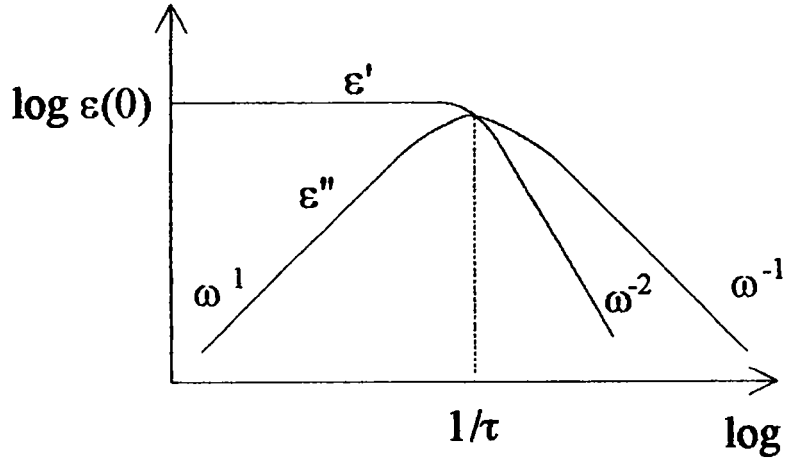


Figure 2.1. Illustration of Debye process (dependence of ε' and ε'' in function of frequency) (Jonscher, 1983). For a pure Debye process the functions log ε' and log ε'' versus log ω (for ωτ<<1) have linear parts with slopes equal -2 and -1 respectively.

Cole - Cole equation

It is evident that the behaviour of most dielectric materials diverges to varying degree from the „ideal" Debye response and it became necessary to modify the Debye expression. One such modification was proposed by Cole & Cole (1941) and is given by the empirical equation:

$$\varepsilon(\omega) = \varepsilon_\infty + \frac{\varepsilon_s - \varepsilon_\infty}{1+(j\omega\tau)^{1-\alpha}} \qquad 2.8$$

where parameter α belongs to the range $0 \leq \alpha \leq 1$ and equation 2.8 becomes Debye equation when $\alpha=0$. Thus α describes the degree of deviation of the given process from the ideal but it must be clear that it is a purely empirical factor and has no real physical significance.

The frequency dependence of real and imaginary parts of dielectric constant ε corresponding to the Cole-Cole expression 2.8 are presented in Figure 2.2.

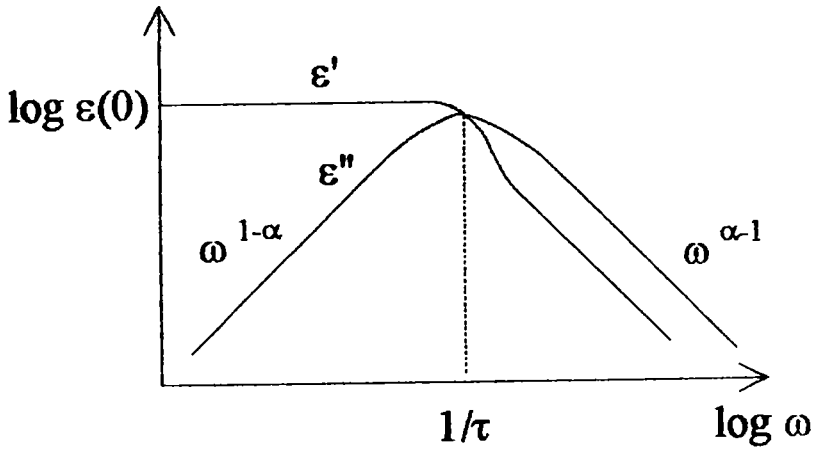


Figure 2.2. Illustration of the Cole-Cole process.

Cole - Davidson equation

While the Cole-Cole expression correctly maps small departures from the ideal Debye response, it is not adequate to represent more severe forms of non-Debye behaviour and this led Davidson & Cole (1951) to propose the following modification:

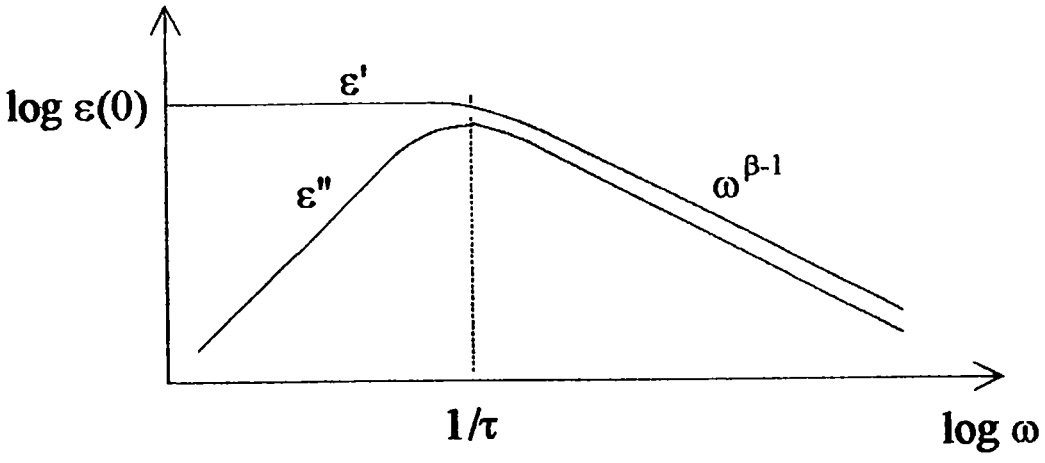


Figure 2.3. Illustration of the Cole-Davidson equation

$$\varepsilon(\omega) = \varepsilon_\infty + \frac{\varepsilon_s - \varepsilon_\infty}{(1 + j\omega\tau)^{1-\beta}} \qquad 2.9$$

This formula corresponds reasonably well to a number of actually observed dielectric responses. Once again, the parameter β has no direct physical significance.

The other functions

There are many examples of dielectric behaviour which cannot be mapped by either of these last two expressions, both of which contain only one adjustable parameter to describe the shape of the complex plot. For this reason, a further generalisation was introduced by Havriliak & Negami (1996), consisting of both Cole-Cole and Cole-Davidson expressions:

$$\varepsilon(\omega) = \varepsilon_\infty + \frac{\varepsilon_s - \varepsilon_\infty}{\{1 + (j\omega\tau)^{1-\alpha}\}^{1-\beta}} \qquad 2.10$$

Many of the observed results fit this two-parameters formula.

Several other empirical expressions have been proposed to represent the dielectric relaxation function, either in its entirely or the imaginary component only. Among these may be mentioned the Fuoss-Kirkwood (1941), Williams-Watts (1970), Jonscher (1975) and Hill (1978), but only those having the parameters α and/or β can represent the majority of experimentally determined functions.

2.2. DIELECTRIC MEASUREMENTS

The usefulness of dielectric measurements for characterisation of ferroelectrics and antiferroelectrics comes clearly from an examination of the low-frequency measurements of the dielectric constant ε'. Extremely large increase of the dielectric constant of ferroelectric and also antiferroelectric materials is observed at their paraelectric - antiferro/ferroelectric first or second order phase transitions. The dielectric loss ε'' generally follows similar temperature behaviour of the dielectric constant ε', although measurements of ε'' are often masked by the d.c. conductivity σ of crystals at low frequencies. If the phase transition is sharp, ε' and ε'' peak at the same temperature and both follow Curie-Weiss behaviour as expected from the Kramers-Krönig relations. If the phase transition is not well defined then ε' and ε'' peak at different temperatures, the

separation of the maxima depends on the degree of broadening of the transition and the temperature dependence of the dielectric relaxation.

The rate at which the dielectric polarization responds to a change of applied electric field is determined by the dielectric relaxation times τ of the various contributions (subscript i) to the polarization which can be described by the Debye equation:

$$\varepsilon(\omega) = \sum_{1}\left(\varepsilon_{\infty_i} + \frac{\varepsilon_s^i - \varepsilon_{\infty_i}}{1 + j\omega\tau_i}\right) \qquad 2.11$$

Figure 2.4 illustrates schematically the manner in which real and imaginary parts of dielectric permittivity behaves in function of frequency. Three processes are shown in this Figure denoted by the subscripts i=1,2,3 (the last one is the resonance process) and they are assumed to be reasonably well separated in frequency. The real part of the dielectric permittivity $\varepsilon'(\omega)$ of every process adds to the sum of the contributions of all higher processes which define the "high frequency" permittivity $\varepsilon_{\infty i}$ for that process. Note that the real part of the permittivity remains flat in regions where losses are negligible.

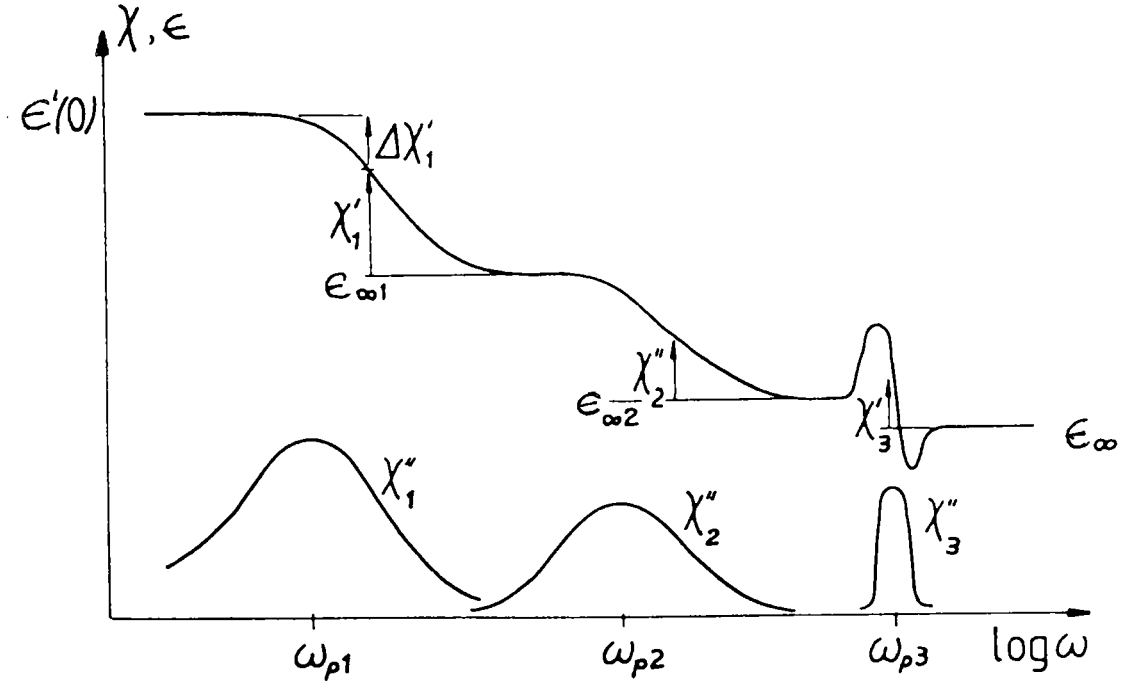


Figure 2.4. The behaviour of dielectric permittivity in function of frequency.

For a symmetrical bistable system of non-interacting dipoles with barrier energy E the relaxation time of each process (except the last resonance process) is given by the Arrhenius equation:

$$\tau_i = \tau_\infty \exp\frac{E_i}{kT} \qquad 2.12$$

In ferroelectrics and antiferroelectrics the relaxation effects can be due to many mechanisms e.g. motion of ions (point defects), polarisation fluctuation in the crystal lattice or domain walls motion in multi-domain crystals. Studies of the dielectric constant ε' and the dielectric loss ε'' as function of frequency near the phase transitions are thus of great interest in the context of the phase transitions mechanisms.

The dielectric constant and dielectric loss are obtained from a measuring of real and complex admittance of a crystal in conventional ways i.e.:

$$I/E = \sigma_o + j\omega\varepsilon = (\sigma_o + \omega\varepsilon'') + j(\omega\varepsilon') \qquad 2.13$$

where I is the current density and E - electric field. $\varepsilon = \varepsilon' - j\varepsilon''$ is separated into real and imaginary parts. These measurements are particularly straightforward with impedance bridges which separate conductance and capacitance of crystals. For this reason, as well as the fact that qualitative information may be obtained from unpoled crystals, ceramics and powders dielectric measurements are most commonly used for identification of phase transitions and the recording of transition temperature. At frequencies of the range from 100 MHz to optical frequencies, the crystal must be part of a transmission line, waveguide or resonant cavity, and the impedance is measured by conventional RF or microwave techniques (see e.g. Lines & Glass (1977)). Studies at optical frequencies will be discussed in Chapter 4. The most commonly used method of measuring the dielectric properties in the range of acoustic frequencies is the bridge method which is analogous to the Wheatstone bridge. However, measurements below 100 MHz usually involve electroding crystals. In this case the results may be strongly affected by the space-charge fields just below the contacts. Problem of this kind can become serious close to phase transition where the bulk impedance of crystal becomes very low. These effects can sometimes be identified and understood by using different contact electrodes or crystal geometries.

2.2.1. Crystal growth and composition determination

Investigations were performed on the crystals produced by the flux-method. All the crystals were made in the Institute of Physics of the University of Silesia by Prof. J. Dec. A mixture of $PbZrO_3$ (and $PbTiO_3$ in the case of PZT), PbO and B_2O_3 was used and the soaking process was carried out in a Pt crucible at the temperature of 1350 K for 4 hours.

Then the melt was cooled at the rate of 9 K/h to 1200 K and the solvent was poured off. Constant temperature gradient of 8 K/cm was maintained along the crucible axis. Transparent light-grey crystals in the form of thin plates were obtained and used in further investigations. For the PZT samples the exact concentration of Ti ions - x, was established for each sample by X-ray microanalysis investigations by dr. K Stróż from the Institute of Physics and Chemistry of metals at the University of Silesia.

Similar procedure was applied in the case of growing $PbHfO_3$ and $PbHf_{1-x}Ti_xO_3$ crystals. The growing process here was carried out in the temperatures from 1473 K to 1223 K with the cooling rate 12 K/h. Transparent yellow crystals in the form of rectangulars or thin plates and polydomain structure were obtained and used in the investigations. The exact Ti concentration in PHT was established like in PZT by X-ray microanalysis.

2.2.2. Experimental conditions.

Only experiments performed in the frequency range below 10 MHz will be considered in further considerations. Crystals in the form of thin plates were used for these measurements. The opposite faces of the crystal were electroded using cold silver paste and the dielectric permittivity (ε' and ε'') was determined by means of a Hewlett-Packard 4192 Impedance Analyser. In this layout the sample was considered to be a lossy capacitor with lumped-circuit capacitance C and resistance R. Investigations were performed in the frequency range 10 Hz < f < 10 MHz and temperature range 300 K<T<630 K. Sample temperature was controlled by a thermocouple with an accuracy of 0.05 K. The real and imaginary parts of dielectric permittivity were calculated from the relations $\varepsilon' C_o = C$ and $\varepsilon'' = \varepsilon' \mathrm{tg}\delta$ and where C_o is empty cell capacitance. C and tgδ were recorded directly from the analyser. In some cases due to high losses of the sample the measurements of conductivity G were more convenient than tgδ. In that case ε' and ε'' were calculated from the relations $\varepsilon' = C/C_o$ and $\varepsilon'' = G/\omega C_o$.

Experiments of dielectric dispersion were made on crystals of pure $PbZrO_3$ and several compositions of $PbZr_{1-x}Ti_xO_3$ (where x=0.0015, 0.018 and 0.03). In the case of lead hafnate pure crystal of $PbHfO_3$ was also chosen together with composition of $PbHf_{1-x}Ti_xO_3$ (x=0.04). Together with the dielectric dispersion measurements the variations with temperature of the dielectric permittivity were performed in order to detect the phase transitions sequence for each sample.

2.3. EXPERIMENTAL RESULTS

2.3.1. Dielectric dispersion in Lead zirconate below 10 MHz.

The experimental data presented below, concern the dielectric properties of two kinds of $PbZrO_3$ crystals (without and with transient phase). In both instances in the begining the $\varepsilon'(T)$ dependences are presented in order to show the anomalies of the ε' near the phase transitions observed in these crystals.

$PbZrO_3$ with one phase transition

Experiments were carried out on a $PbZrO_3$ sample of dimensions 3 x 3.1 x 0.05 mm^3. Electrodes were deposited on the opposite faces using cold silver paste. Temperature and frequency measurements of dielectric susceptibility were made in the frequency range 20 Hz - 300 kHz and electric field strength 70 V/m. Prior to measurements the sample was maintained at 600 K for half an hour in order to relieve any strains at the electrode/crystal interface.

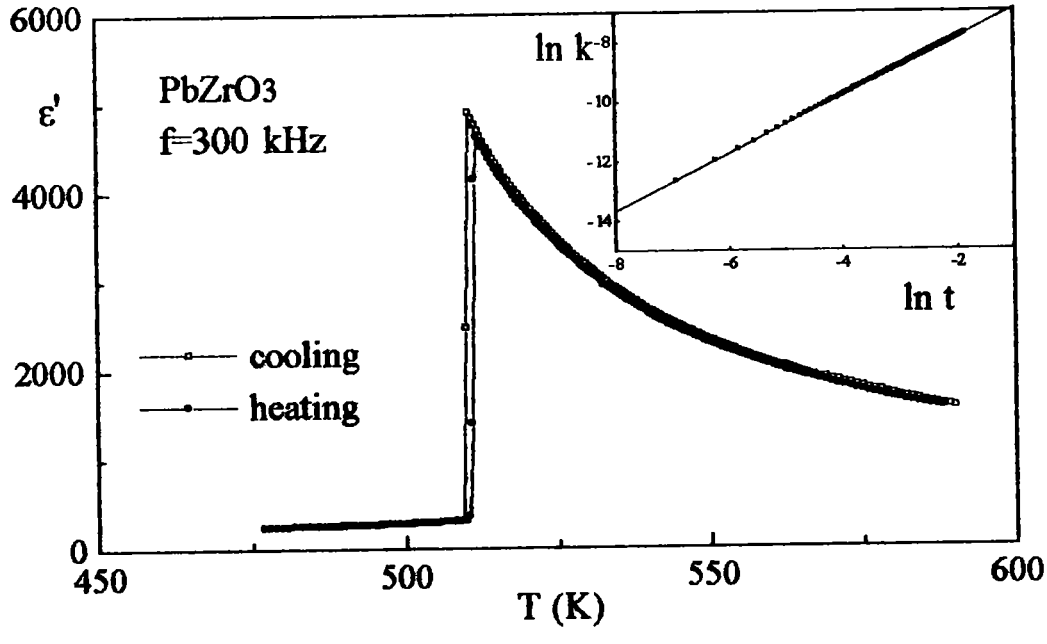


Figure 2.5. Temperature dependence of real part ε' on cooling and on heating for $PbZrO_3$ crystal measured at $3 \cdot 10^5$ Hz. An inset shows the Curie-Weiss-like law obeyed ($k=1/\varepsilon-1/\varepsilon_{max}$, $t=(T-T_c)/T_c$, with $\varepsilon_{max}=5000$ and $T_c=510$ K).

In Figure 2.5, temperature dependence of ε' measured at frequency 300 kHz both on heating (511 K) and cooling (510 K), shows a sharp transition at T_c between the paraelectric and antiferroelectric phase. Above T_c the Curie-Weiss-like law $\varepsilon=C/(T-T_0)^{\gamma}$ is obeyed with $\gamma=0.97$, $C=1.55 \times 10^5$ K and $T_0=472.5$ K.

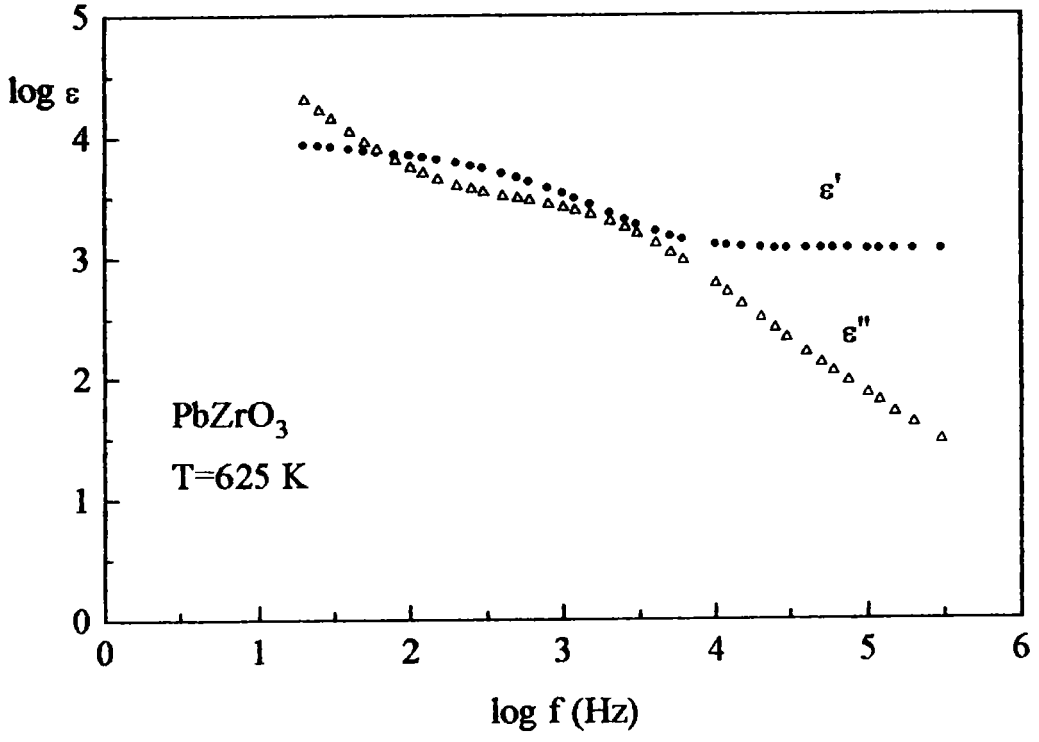


Figure 2.6. Frequency dependence of ε' and ε'' at 625 K (paraelectric phase)

Figure 2.6 represents the frequency dependence of the real and imaginary parts of dielectric susceptibility at 625 K in the paraelectric phase plotted in the log-log plane. The shape of these curves resembles the classical Debye relaxation described by the equation 2.5 and 2.6 except the low frequency region for ε''. Marked increase in this value towards low frequencies is associated with the presence of d.c. conductivity represented by σ_o which gives a contribution to ε'' as in the equation:

$$\varepsilon(\omega)=\varepsilon'-j(\varepsilon''+\sigma_o/\omega) \qquad 2.13$$

while leaving the real part independent of frequency (Jonsher, 1983). Assuming the absence of d.c. influence in the high frequency region (log f > 3.5) and generating low frequency dependence of the imaginary part of the susceptibility, it was checked that $\varepsilon''\sim 1/\omega$ in the frequency range below 100 Hz. The d.c. conductivity effect is considered

here as that caused by departure from stoichiometry of the crystal, introduced during the technological process and most probably connected with defects in the Pb and O sublattices. The plots obtained are thus characteristic for the behaviour observed in many dipolar systems at high temperatures with d.c. influence in the low frequency region (Jonscher, 1983).

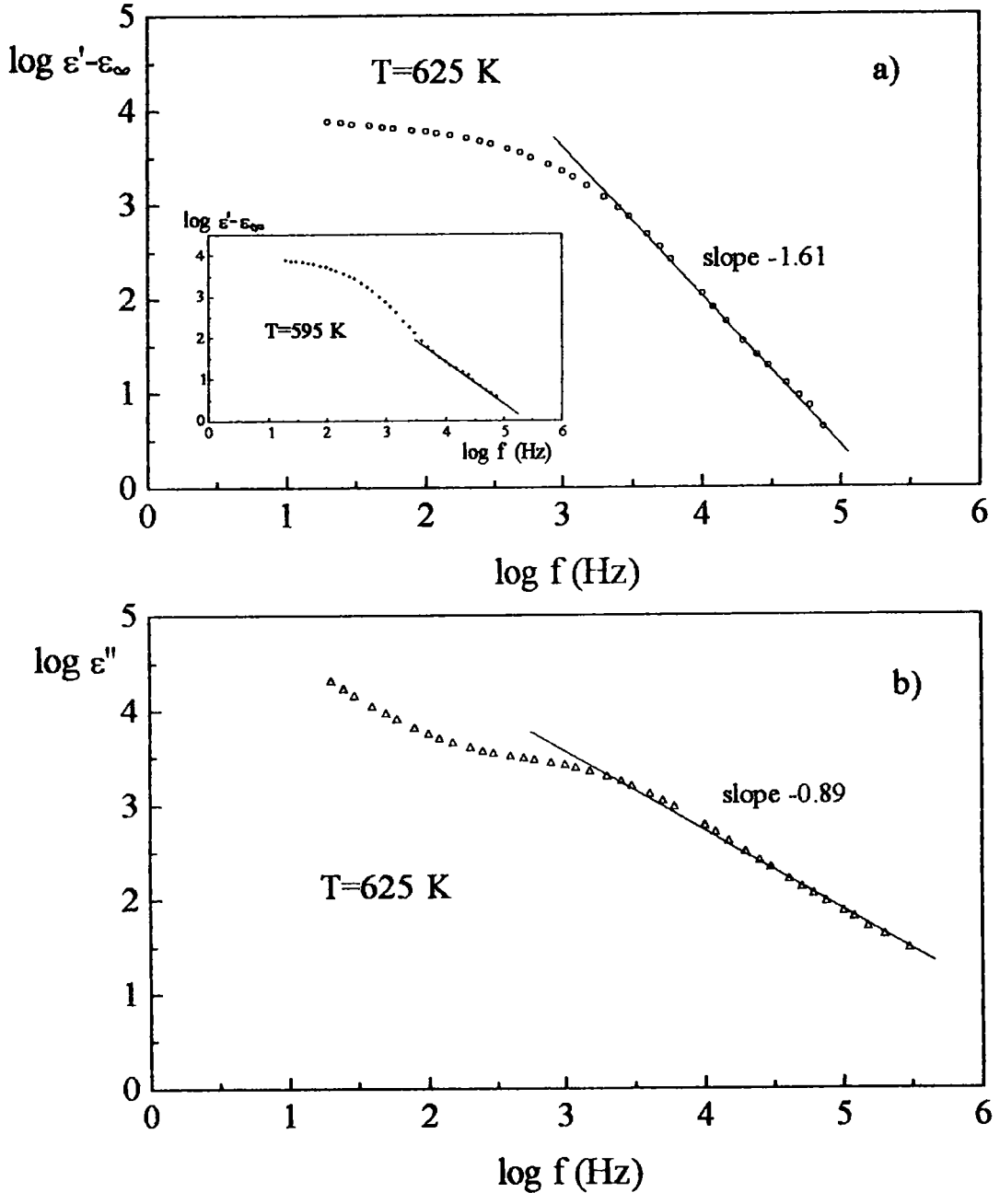


Figure 2.7. Linear fits to the high frequency part of ε' (a) and ε'' (b) for the data from Figure 2.6. An inset in (a) shows run of log (ε'-ε) v.s. log f in lower temperature which is quite similar to that theoretical run of the Cole-Cole function presented in figure 2.2

It is very convenient to find the parameters of dielectric relaxation, using the log-log representation. For a pure Debye process, it can be shown from equations 2.5 and 2.6 that functions $\log(\varepsilon'-\varepsilon_\infty)$ and $\log \varepsilon''$ versus log f will have linear parts (for $\omega\tau>>1$) with slopes equal to -2 and -1 respectively. Knowing the slopes, value of relaxation time τ can be easily determined after finding ε_s by extrapolation of $\log(\varepsilon'-\varepsilon_\infty)$ vs. log f to very low frequencies. In our case ε_∞ is given directly from the experiments. Such a procedure enables avoiding the influence of d.c. conductivity in the low frequency region.

In Figures 2.7a and 2.7b the functions mentioned above were plotted for the same data as in Figure 2.6. Linear fit to the high frequency parts of dielectric response indicates clear deviations from the predicted slopes. Better results were obtained by fitting these data to the well-known Cole-Cole expression (eq. 2.8) and using the same log-log procedure with α=0.11, ε_s=8150, ε_∞=1152, $\tau=2.66 \times 10^{-4}$ s. In this case the only convenient function allowing these parameters to be determined is $\log\varepsilon''(\log f)$. It is noteworthy that with the temperature lowering, the logarithmic representations of ε'' and $(\varepsilon'-\varepsilon_\infty)$ versus f observed experimentally gradually resemble the theoretical runs of formula 2.8 with two characteristic slopes on $\log(\varepsilon'-\varepsilon_\infty)$ vs. log f (Jonscher, 1983). Since parameter α in eq 2.8 takes values between 0 and 1 and determines the distribution of relaxation times at given temperature, the value α=0.11 obtained indicates a certain departure from the monodispersive relaxation.

Frequency dependence of complex permittivity for chosen temperatures is shown in Figure 2.8. In the paraelectric phase, with decreasing temperature the dielectric dispersion shifts towards lower frequencies with increasing value of ε_∞ (Figure 2.8a). The lower the temperature, the smaller the participation of the d.c. effect in the value of ε'' (Figure 2.8b). Below T_c the dispersion is still present but already 20 K from the phase transition its main changes lie below the experimental frequency range, i.e. below 20 Hz.

Calculations made by the logarithmic procedure described above showed that in the paraelectric phase the relaxation process can be described by eq. 2.8 in which parameter α was equal to 0.11 and independent of temperature (linear parts of function in Figure 2.8b are parallel). Defining the loss peak frequency as:

$$f_p = f_\infty \exp(-E_a / kT) \qquad 2.14$$

where f_∞ describes the typical lattice vibrations frequency (10^{12} Hz), the numerical values of the activation energy ΔE change from 0.3 eV - 1 eV for experimental conditions applied here.

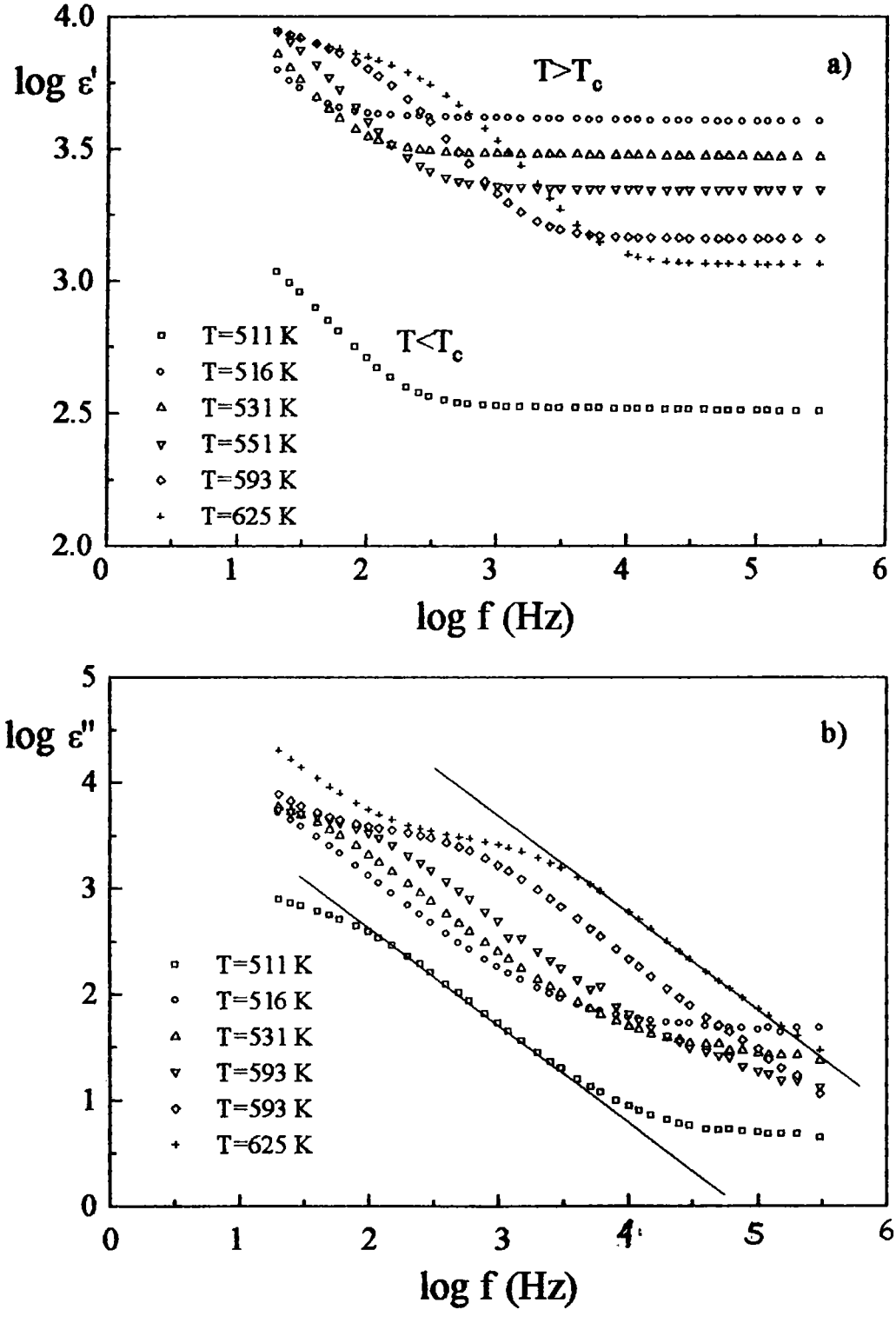


Figure 2.8. Temperature/frequency evolution of ε' (a) and ε'' (b). Note the parallel shift of log ε''(log f) toward lower frequency (α=const)

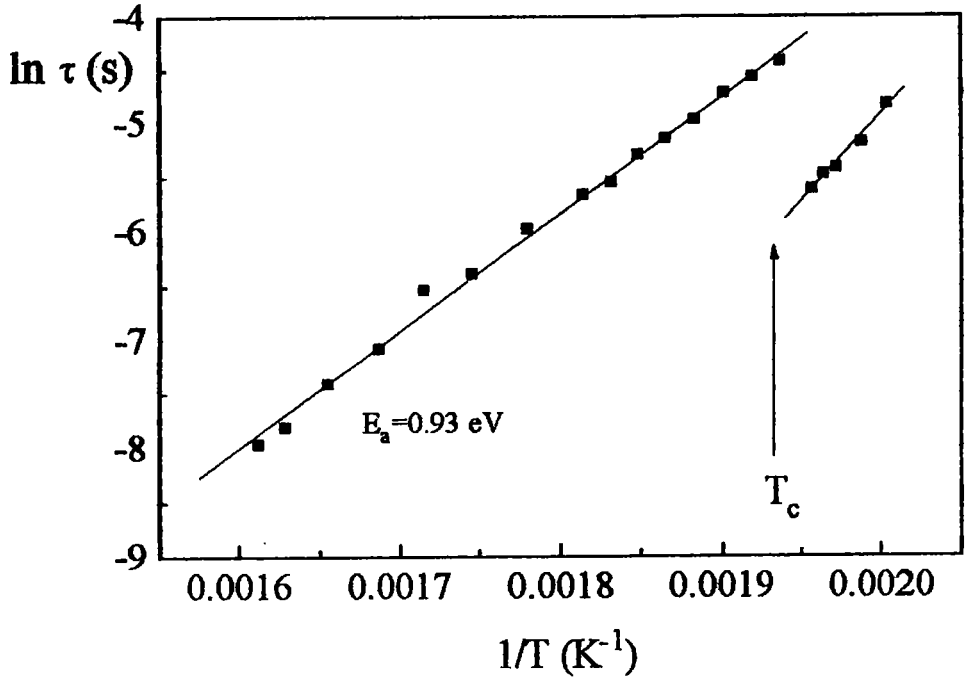


Figure 2.9. Arhenius plot of the relaxation times.

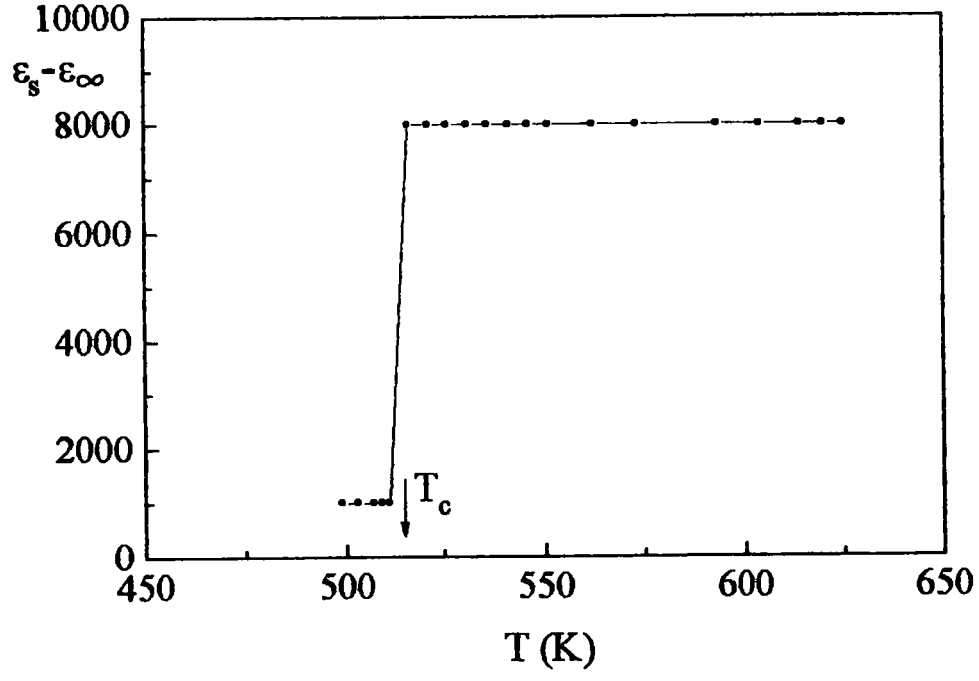


Figure 2.10. Dispersion step (ε_s-ε_∞) versus temperature above and slightly below phase transition

The obtained relaxation times well obey this Arrhenius function with E_a=0.93 eV but with pre-exponential factor equal to 1.6 x 10^{10} Hz which is lower than lattice vibrations (Figure 2.9). At T_c value of τ reaches 1.5 x 10^{-2} s (f=11 Hz) and then exhibits a distinct jump to smaller values. From the data obtained the dispersion step (ε_s-ε_∞) may be found which is independent from temperature and has high discontinuity at the phase transition point (Figure 2.10).

$PbZrO_3$ with a transient phase

Some additional measurements were made for the $PbZrO_3$ single crystals in which the transient phase was detected. As mentioned in chapter 1.2.2 the investigations of $PbZrO_3$ single crystals showed that the non-stoichiometry in the Pb and/or O sublattices can provoke the existence of transient phase below T_c in $PbZrO_3$ single crystal. For this reason a crystal with transient phase was also chosen for the measurement and the experimental results were compared to those for $PbZrO_3$ without transient phase.

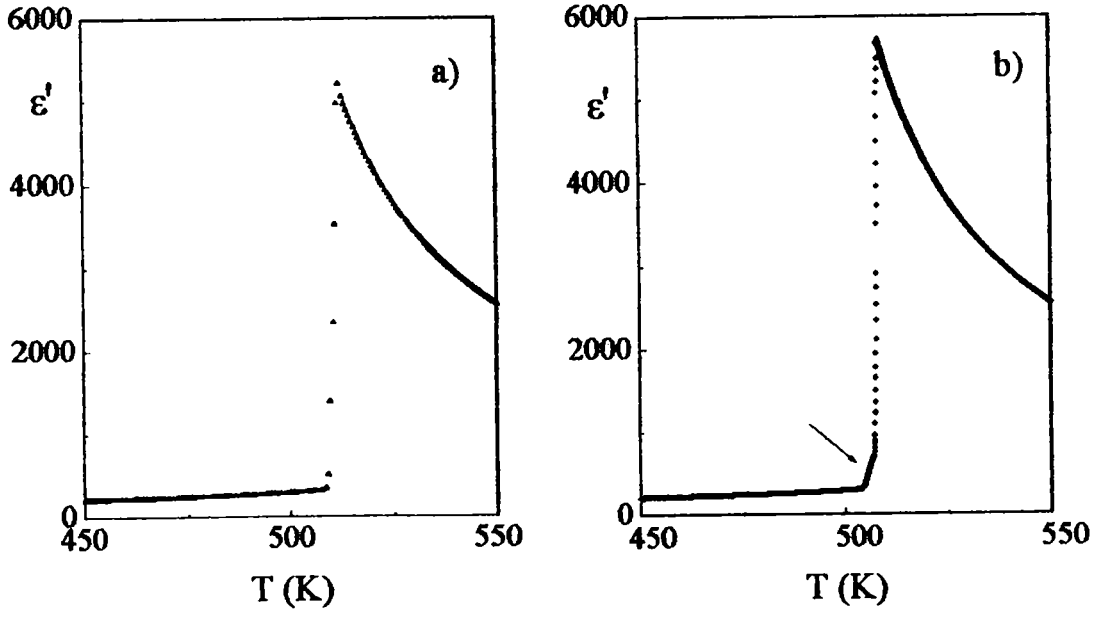


Figure 2.11. Temperature dependence of ε' measured on heating (a) and on cooling (b) for the $PbZrO_3$ single crystal with transient phase.

In Figure 2.11, temperature dependence of ε' at frequency 1 MHz both on cooling and heating is presented. On heating a sharp transition between antiferroelectric and paraelectric phases can be observed, but on cooling a small anomaly occurs of about 2 deg

just below T_c (see arrow). For this sample the Curie-Weiss-like law $\varepsilon = C/(T-T_o)^\gamma$ is obeyed with parameters γ=0.96, T_o=475 K and C=1.93 x 10^5 K.

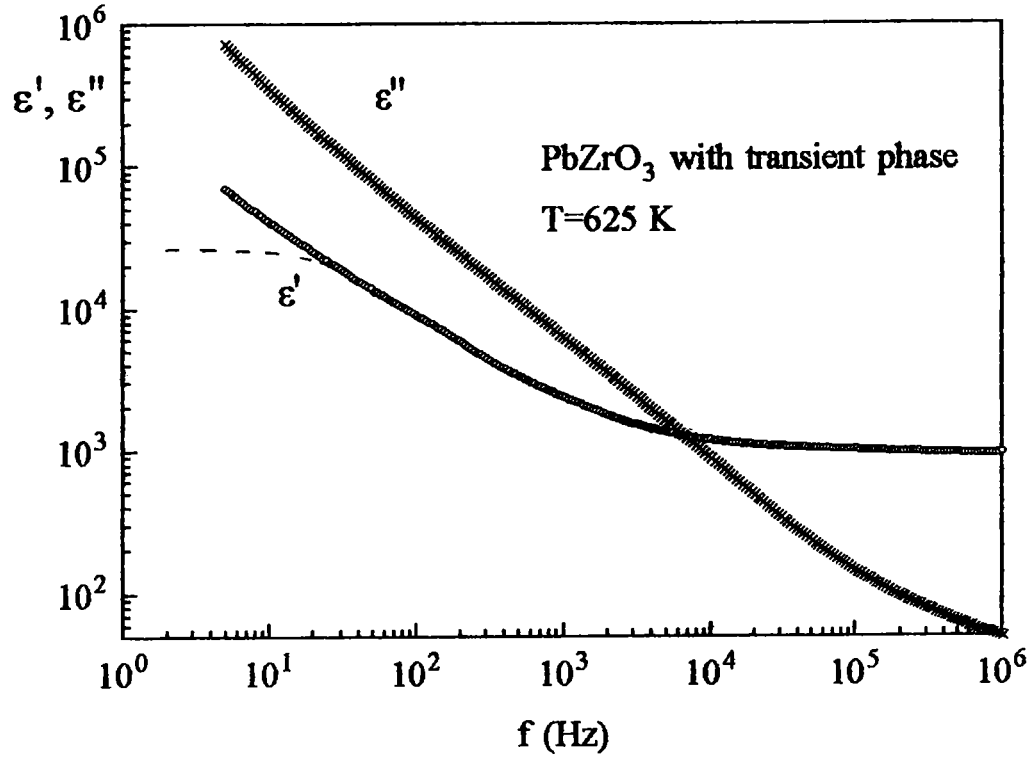


Figure 2.12. Frequency dependence of the ε' and ε'' at 625 K in log-log scale.

Figure 2.12 represents real and imaginary parts of dielectric dispersion at 625 K in paraelectric phase versus frequency. Contrary to the sample without transient phase the obtained plots do not resemble now the classical Debye relaxation. A very fast increase of ε' and ε'' in the region of low frequencies can be observed. It can indicate high concentration of point defects giving a space charge contribution to ε' and high d.c. conductivity adding to ε'' response. For this reason the evaluation of dielectric relaxation parameters becomes very difficult. Comparing to the $PbZrO_3$ without transient phase (Fig. 2.6) the conjectural relaxation seems to lie in considerably lower frequencies. The estimated relaxation times basing on the Cole-Cole function (eq. 2.8) are presented in Figure 2.13 as the Arrhenius plot. The activation energy E_a=0.77 eV and pre-exponential factor τ_o=1.2 $*10^9$ s are smaller than the adequate values for $PbZrO_3$ without transient phase described above. The calculations showed, that the dispersion step (ε_s-ε_∞) is high

and slightly temperature dependent (Figure 2.14) contrary to the sample with one phase transition where $\Delta\varepsilon$ was temperature independent, in the same temperature range.

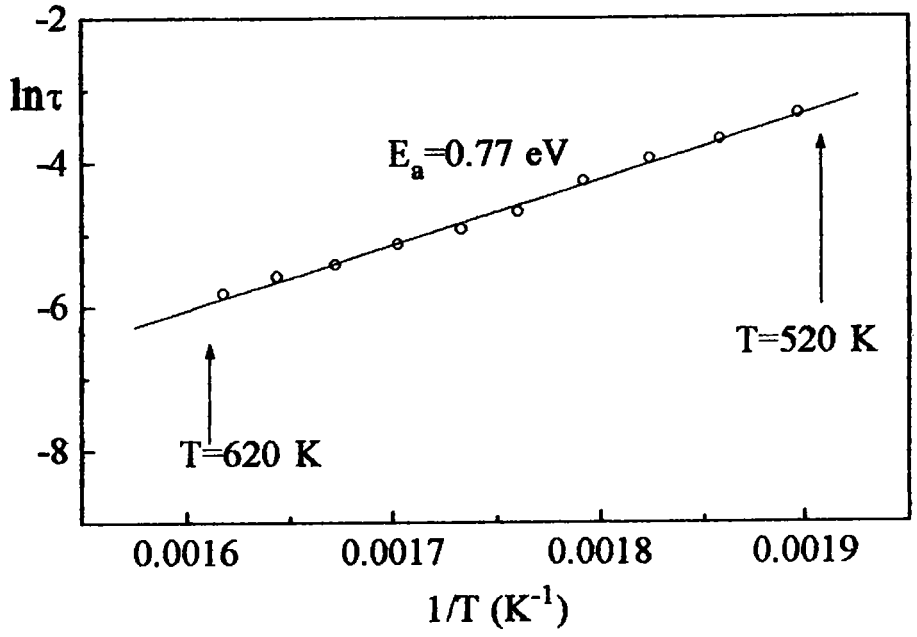


Figure 2.13. Arhenius plot of the relaxation times for $PbZrO_3$ with transient phase.

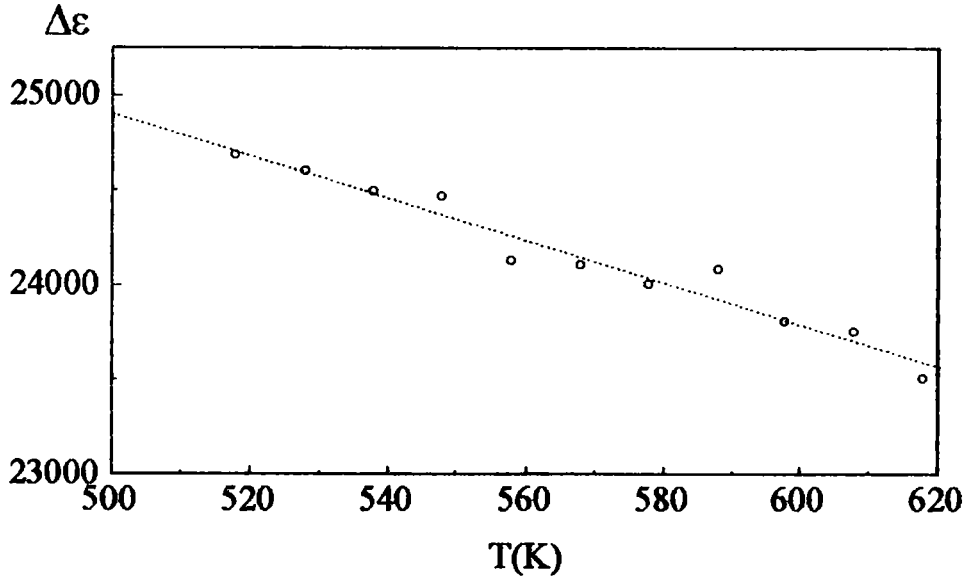


Figure 2.14. Dispersion step $\Delta\varepsilon$ versus temperature in paraelectric phase.

The other interesting phenomenon which can be observed in this sample is appearance near T_o of very weak but clearly visible new independent relaxation existing in higher frequencies (f_r~70 kHz) (Figure 2.15 & 2.16) and of strongly polydispersive character ($\alpha \approx$ 0.47 - 0.56).

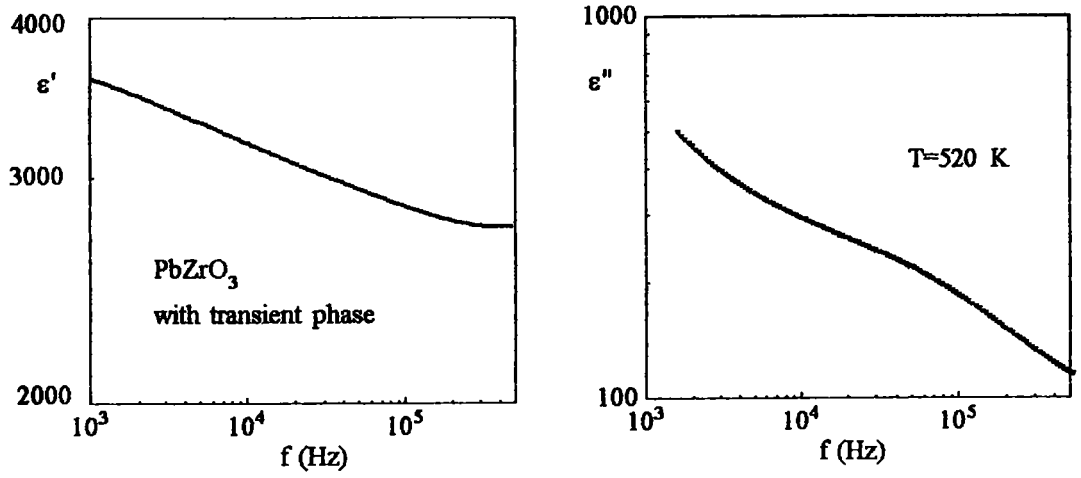


Figure 2.15. Frequency dependence of the ε' and ε'' at 520 K

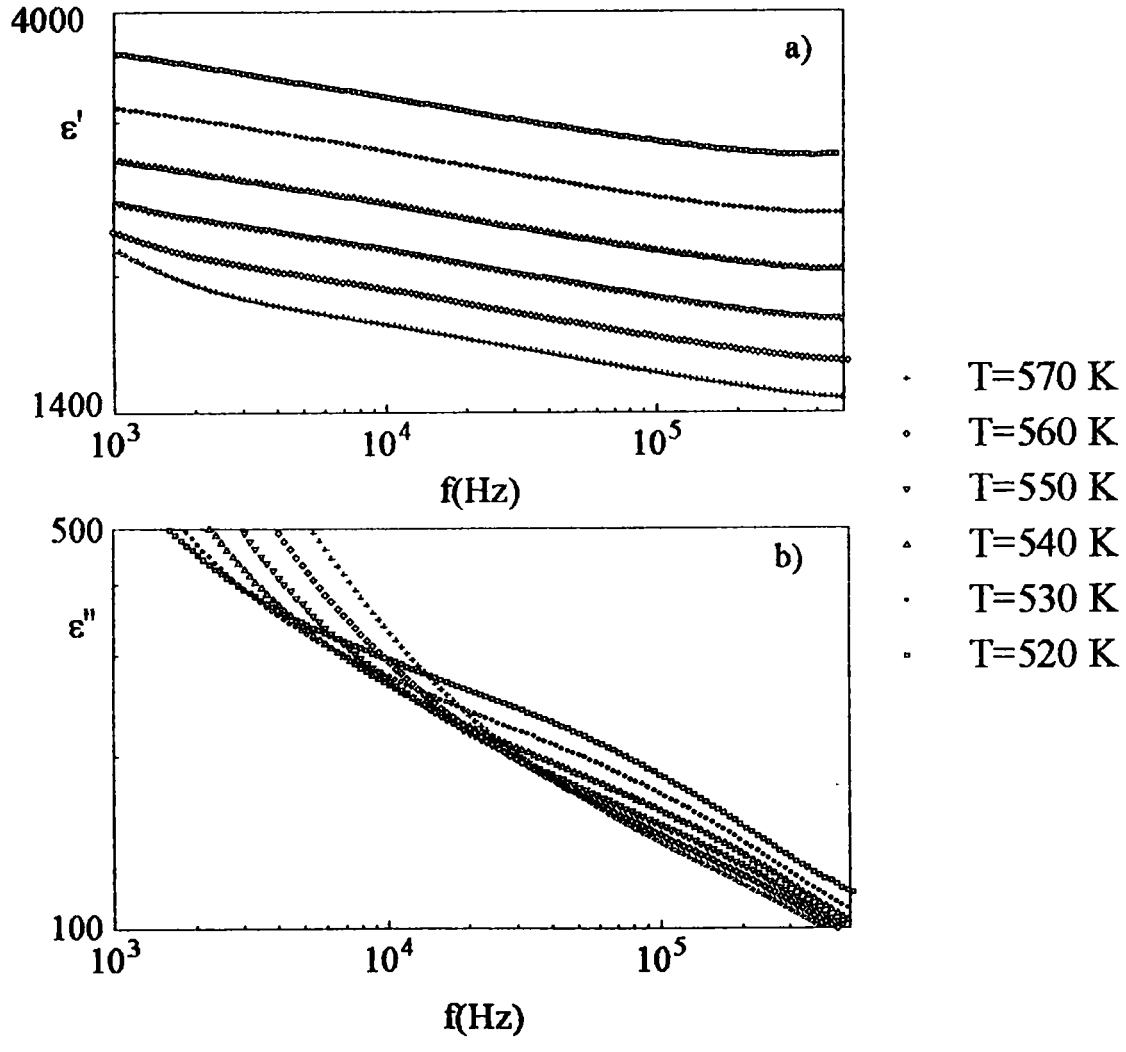


Figure 2.16. Temperature/frequency evolution of ε' (a) and ε'' (b) for $PbZrO_3$ with transient phase.

The real and imaginary parts of this relaxation process in the paraelectric phase up to 570 K are presented in Figures 2.16a and b respectively. Using the Cole-Cole equations for fits, the parameters τ and $\Delta\varepsilon$ of the process were calculated and presented in the Figure 2.17. It is easy to notice the temperature dependencies of the calculated parameters, especially $\Delta\varepsilon$ which grows over two times between 570 K and T_c.

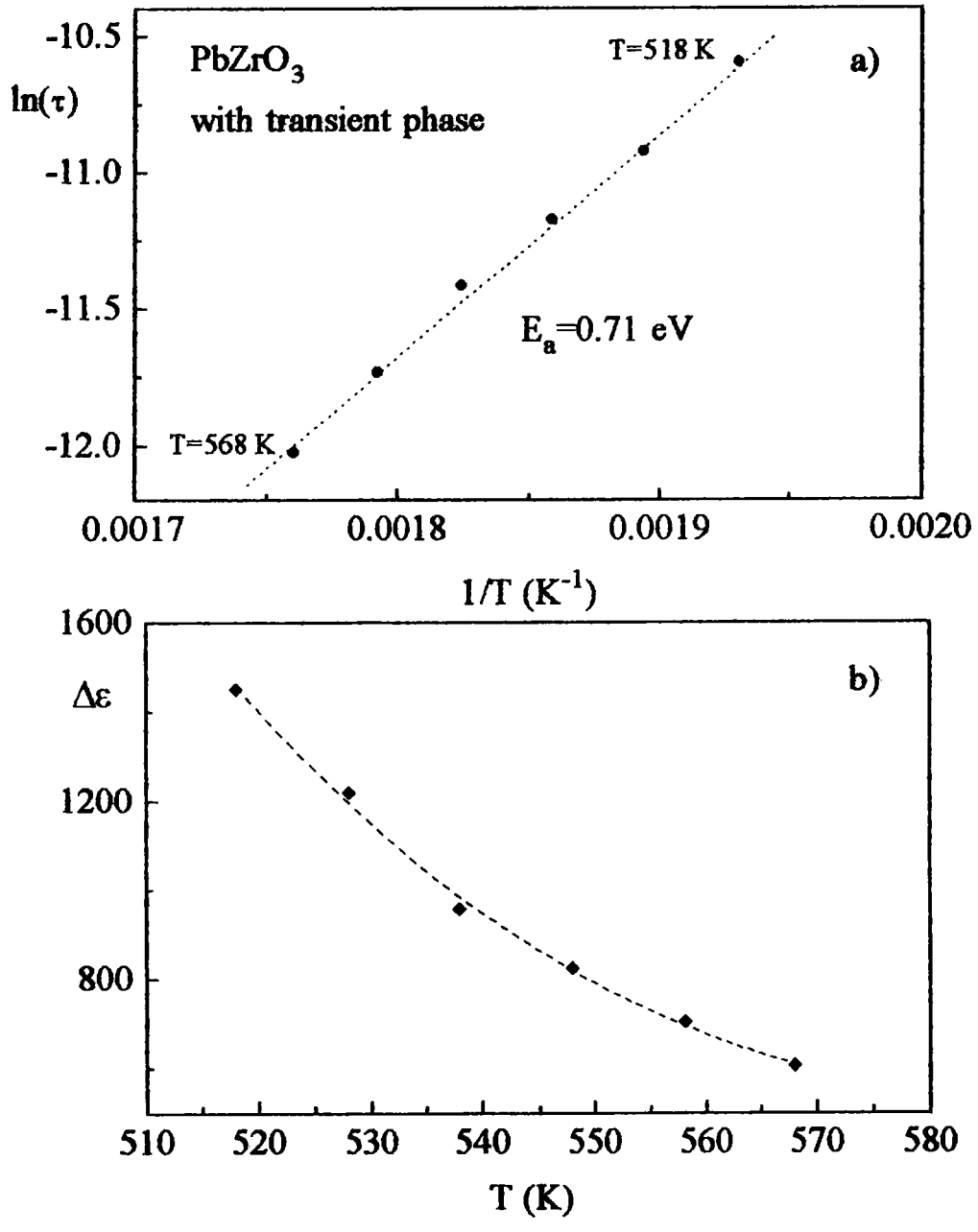


Figure 2.17. Calculated parameters (a) τ and (b) $\Delta\varepsilon$ of the higher frequency relaxation process presented as a function of temperature in paraelectric phase close to the phase transition.

2.3.2. Relaxation processes in single crystal of $PbZr_{1-x}Ti_xO_3$ solid solutions.

Investigations were performed on the crystals produced by the method described in the paragraph 2.2.1. Transparent light-grey crystals in the form of thin plates were obtained and used in the investigations. Three compositions of $PbZr_{1-x}Ti_xO_3$ were chosen in which x had a real concentration: 0.0015, 0.018, 0.03.

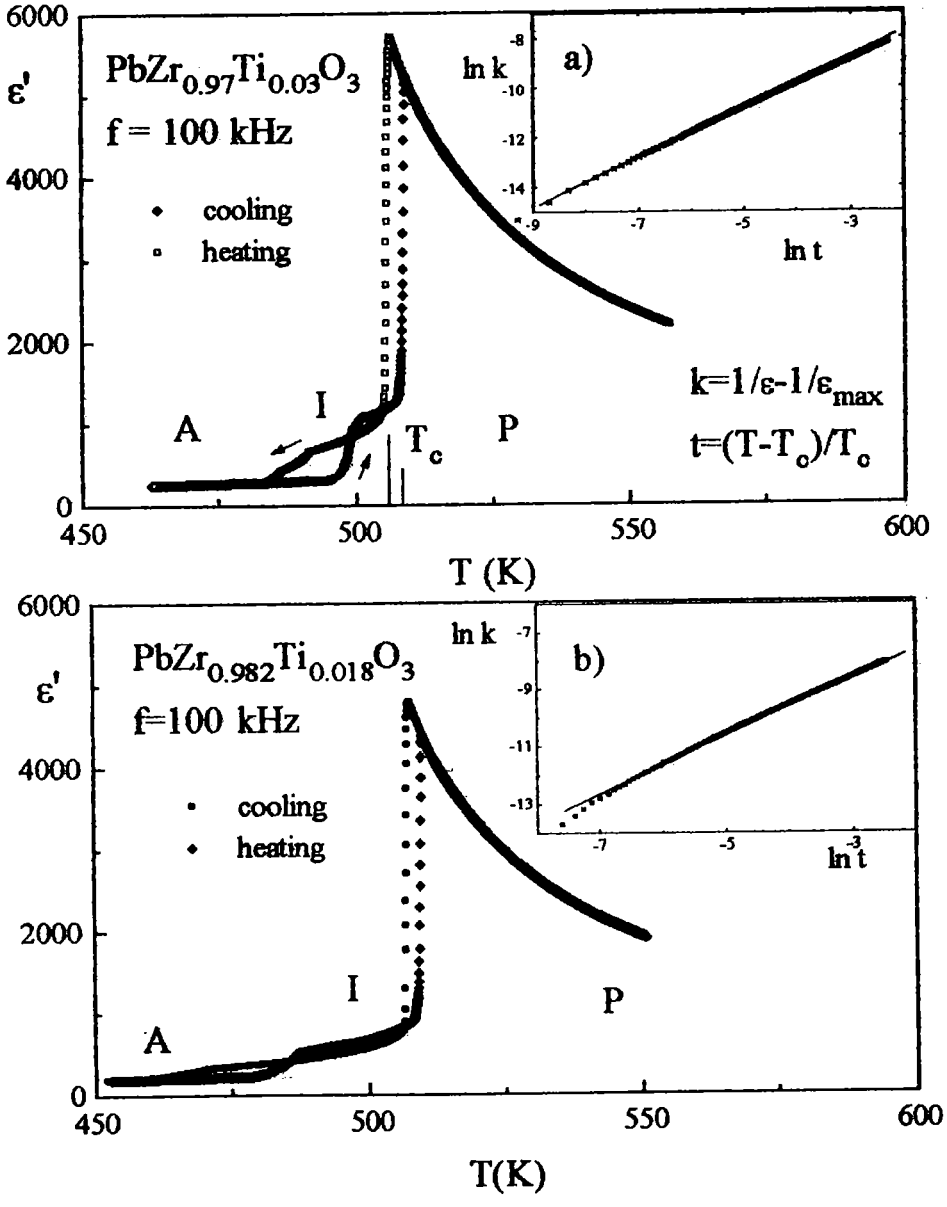


Figure 2.18. Temperature dependence of the real part of ε' on heating and on cooling for $PbZr_{0.97}Ti_{0.03}O_3$ and $PbZr_{0.982}Ti_{0.018}O_3$ single crystals. The insets show the Curie-Weiss like law $\varepsilon=C/(T-T_o)^\gamma$ generaly obeyed in paraelectric phase (a small deviation from this law can be observed for $PbZr_{0.982}Ti_{0.018}O_3$ single crystal)

Transition between A and I phase is characterised by hump-like anomalies with temeperature hystheresis much greater than this for I-P phase transition. According to the discussion presented in par. 1.2.2. the range of I phase is not proportional to the Ti content.

Relaxation in the paraelectric phase (10 Hz - 20 kHz)

In Figure 2.19 the frequency dependencies of real (a) and imaginary (b) parts of ε(f) for the $PbZr_{0.97}Ti_{0.03}O_3$ sample were presented for chosen temperatures from 620 K to 510 K i.e. to the P-I phase transition. Similar plots were also obtained for $PbZr_{0.982}Ti_{0.018}O_3$ and $PbZr_{0.0985}Ti_{0.0015}O_3$.

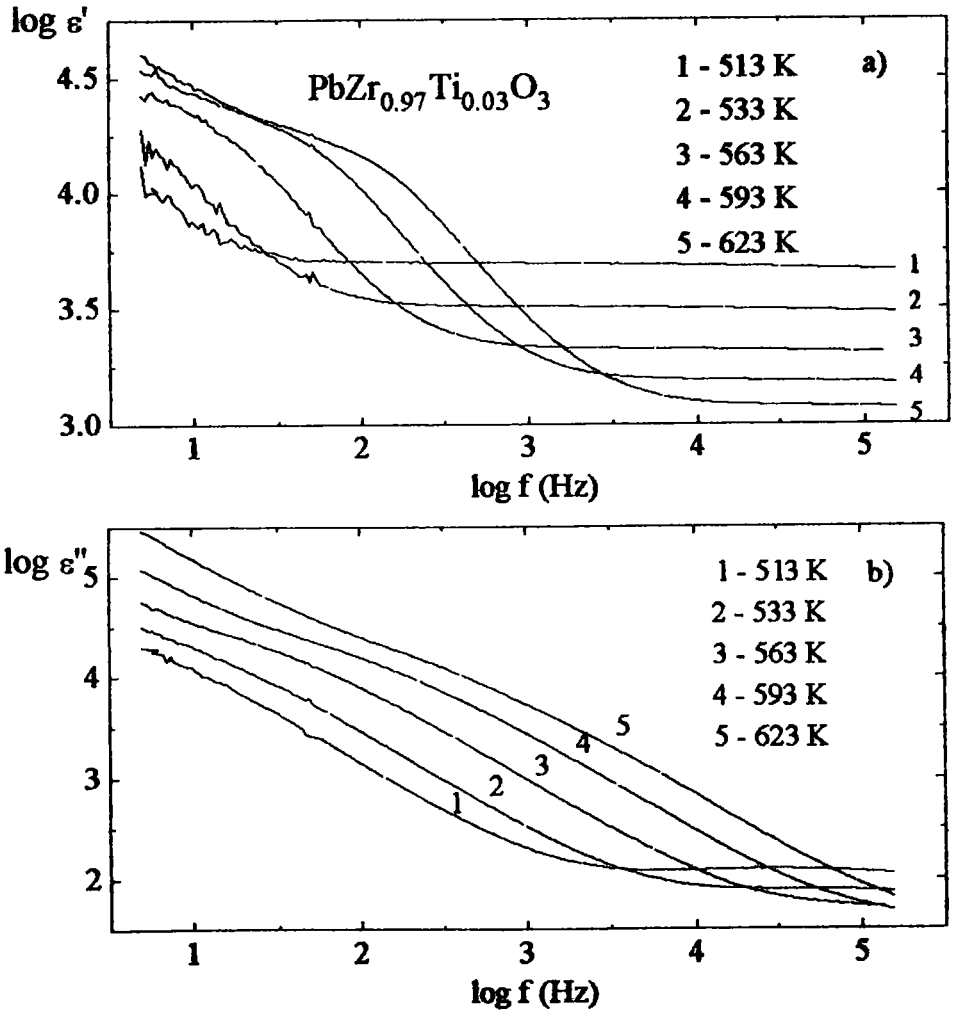


Figure 2.19. Temperature/frequency functions of (a) ε' and (b) ε'' for the $PbZr_{0.97}Ti_{0.03}O_3$ sample in paraelectric phase

The data obtained for each temperature were systematically fitted to the Cole-Cole expression (2.8). In all samples the calculated values of α are less than 0.16.

It may be seen that the imaginary part of dielectric response consists of two components:
1) frequency-independent conductivity response of free charges represented by σ_o which gives a contribution to ε'' (see eq. 2.13) and,
2) frequency-dependent polarization loss response of dipoles.

With this assumption both parts of ε^* were fitted simultaneously and the relaxation parameters were calculated. A typical example of fit for a chosen temperature is presented in Figure 2.20. The calculated relaxation times τ obey an Arrhenius-type function

$$\tau = \tau_o \exp\left(\frac{E_a}{kT}\right) \qquad 2.15$$

as shown in Figure 2.21 for different samples. The values of the activation energy are given in the Figure for each Ti concentration and compared with that for pure $PbZrO_3$.

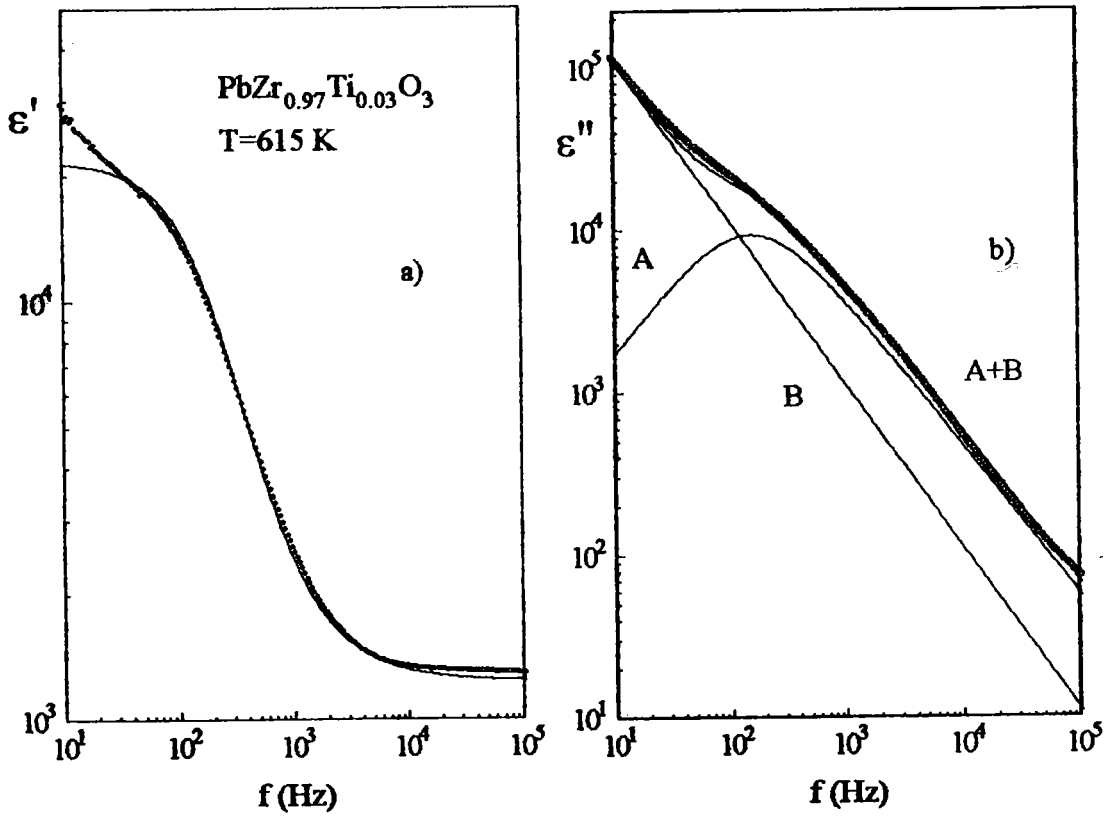


Figure 2.20. An example of fitting procedure using the Cole-Cole formula for $\varepsilon'(f)$ and $\varepsilon''(f)$. The curve $\varepsilon''(f)$ was separated into „pure" $\varepsilon''(f)$ (A) and that from σ_o contribution (B).

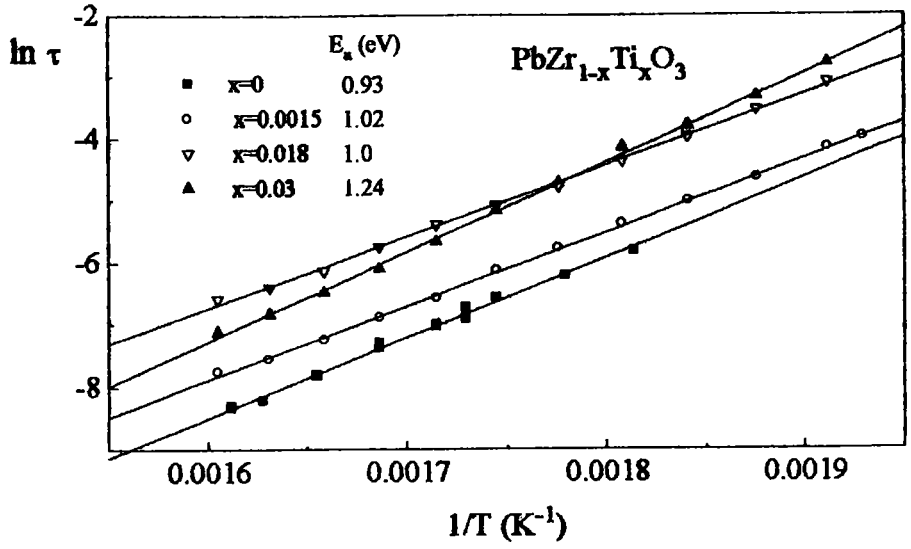


Figure 2.21. Arhenius plots of the relaxation times for various concentrations of Ti. E_a values were calculated with an error of ±0.02 eV.

By fitting the lowest-frequency data of ε'', values of thermally stimulated σ_o conductivity were obtained and presented in Figure 2.22 in form $\ln\sigma_o(1/T)$. The values of activation energy W were calculated using a simple linear regression method and then added to the Figure 2.22. The value of σ_o in pure $PbZrO_3$ varies between ~10^{-6}-10^{-5} $\Omega^{-1}m^{-1}$. The contribution of Ti to PZT is shown as increase in value of d.c. electric conductivity σ_o up to ~$10^{-4}\Omega^{-1}m^{-1}$

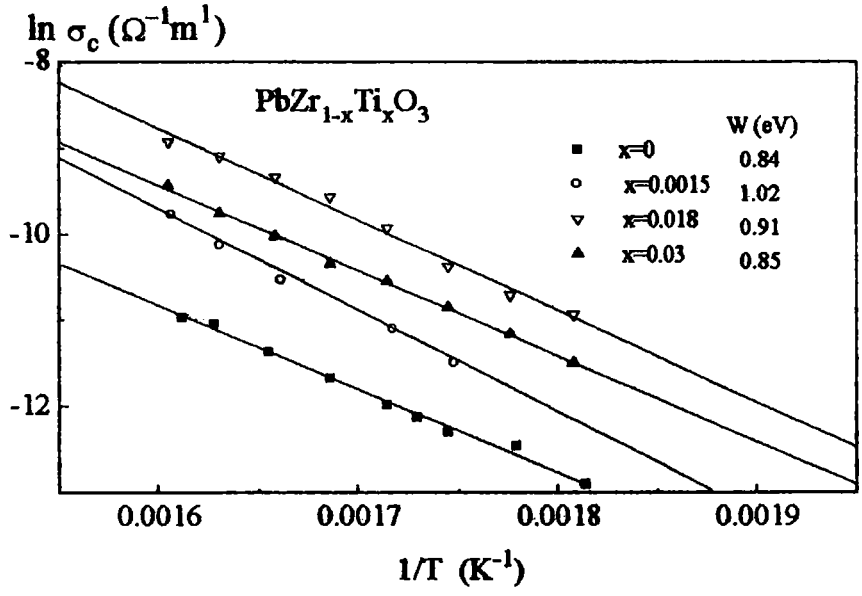


Figure 2.22. Plots of the thermally stimulated conductivity σ_o versus reciprocal temperature.

Unlike pure $PbZrO_3$ with one phase transition, in the paraelectric phase the dispersion step (ε_s - ε_∞) becomes temperature dependent (Figure 2.23). The preexponential factor τ_o ~10^{-12} s in 2.15 is lower the one corresponding to the usual ionic reorientational frequencies 10^{13} Hz (τ~10^{-15} s) and thus indicates that this is not a single-ion process

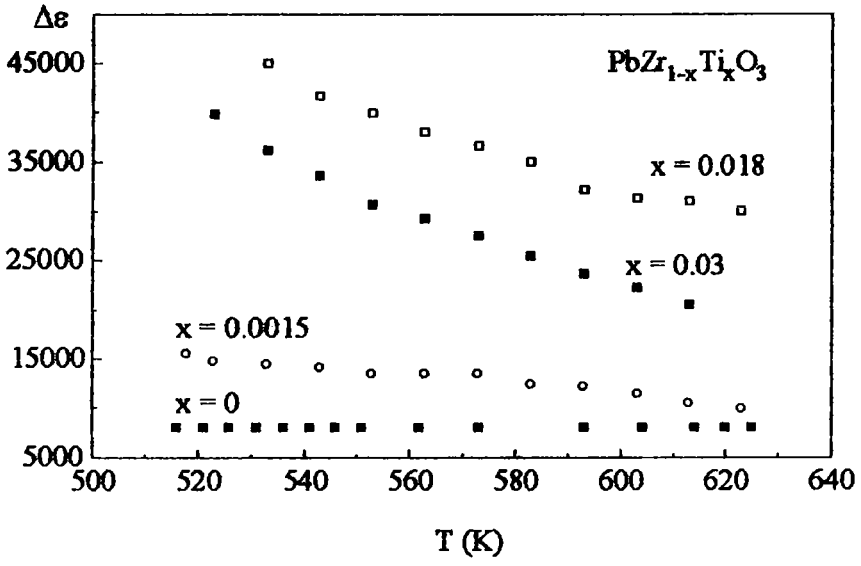


Figure 2.23. Dispersion step $\Delta\varepsilon=(\varepsilon_s-\varepsilon_\infty)$ versus temperature in the paraelectric phase for various Ti concentrations in PZT (compared with pure $PbZrO_3$).

Relaxations inside the transient phase (1kHz - 1MHz)

As mentioned in the paragraph 1.2.2, when Ti ions are substituted for the central Zr ions, a new phase called an intermediate phase is creates below T_c. In this phase and up to a little above T_c (T_c+30 K) a new independent relaxation process may be observed in a frequency range 1 kHz - 1 MHz. The real and imaginary parts of this relaxation process for $PbZr_{0.97}Ti_{0.03}O_3$ in the intermediate and paraelectric phase up to 533 K are presented in Figures 2.24a and b.

Basing on the assumption that the left side of the observed "new" relaxation corresponds to the right side of the low-frequency part of relaxation, the overall dielectric response has been fitted to the superposition the two Cole-Cole equations (eq.2.8). The sample fit is presented in Figure 2.25 for the imaginary part of $\varepsilon(f)$.

While the low-frequency relaxation process was weakly polydispersive (α~ 0.11- 0.16), the second process on higher frequencies appears to be strongly polydispersive (α~0.4 for x_{Ti}=0.03).

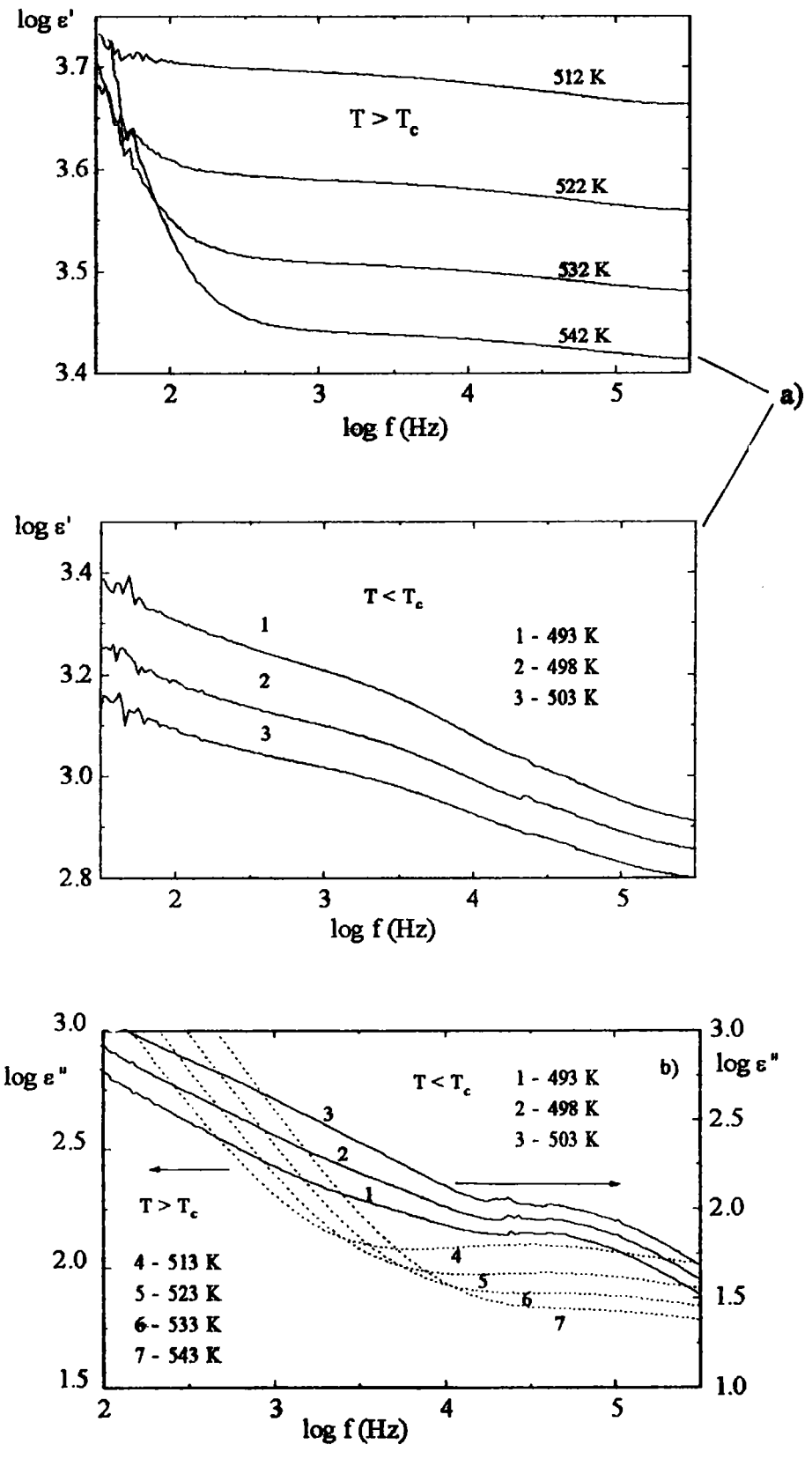


Figure 2.24. The real (a) and imaginary (b) parts of the higher-frequency relaxation process for $PbZr_{0.97}Ti_{0.03}O_3$ in paraelectric and intermediate phases

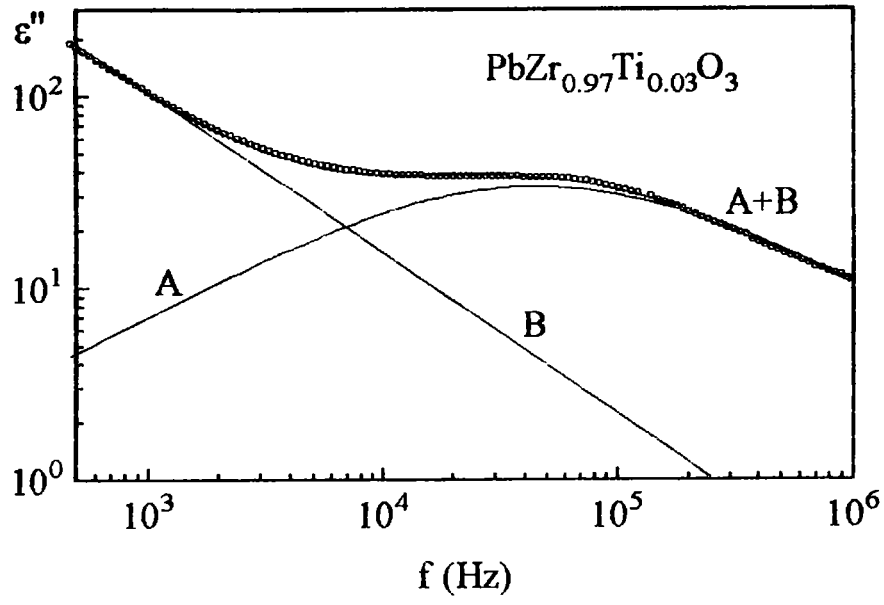


Figure 2.25. An example of fitting procedure using the Cole-Cole formula (α=0.4) for the $\varepsilon''(f)$ at 503 K separated into the relaxation **A** of the higher-frequency and high-frequency part of the low relaxation **B**.

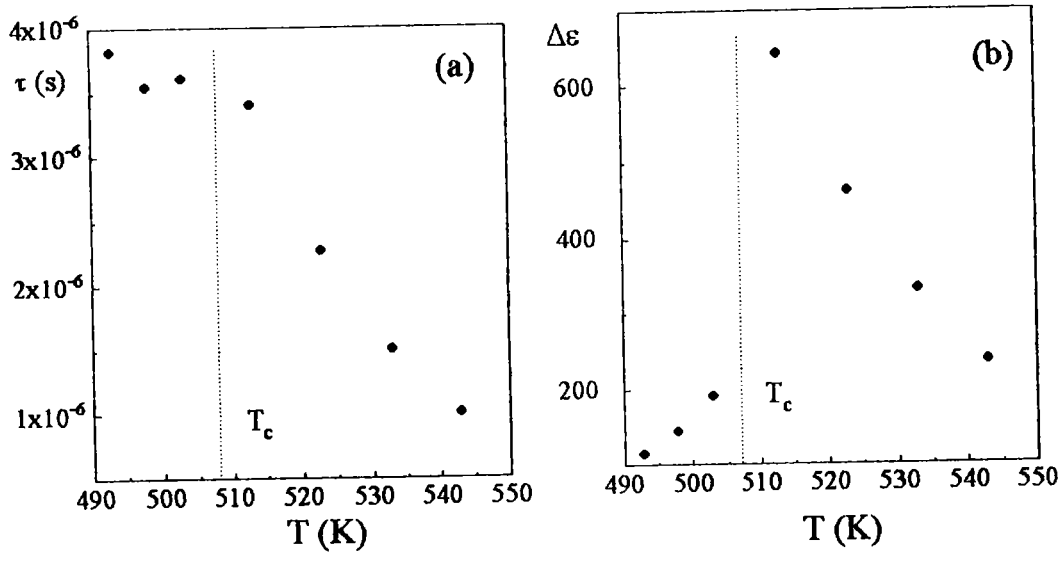


Figure 2.26. Calculated parameters (a) τ and (b) $\Delta\varepsilon$ of the higher frequency process presented as a function of temperature slightly above and below the phase transition

The parameters τ and $\Delta\varepsilon = \varepsilon_s - \varepsilon_\infty$ of the second relaxation process calculated from fits are given in Figure 2.26.

In the paraelectric phase the mean relaxation time τ of the second process is temperature dependent. Near T_c , τ reaches the value $3.4 \cdot 10^{-6}$ s and below T_c becomes virtually constant. The $\Delta\varepsilon$ originating from this relaxation also exhibits a distinct anomaly at T_c and follows the shape of $\varepsilon'(T)$ presented in Figure 2.18, showing clearly that this relaxation is closely related to the phase transition (it was also the case in pure $PbZrO_3$ with two phase transitions but with higher values.)

2.3.3. Dielectric permittivity anomalies of antiferroelectric phase transitions of $PbHfO_3$ and $PbHf_{1-x}Ti_xO_3$.

The investigations of dielectric dispersion were performed on two kinds of crystals: pure $PbHfO_3$ and solid solution $PbHf_{0.96}Ti_{0.04}O_3$.

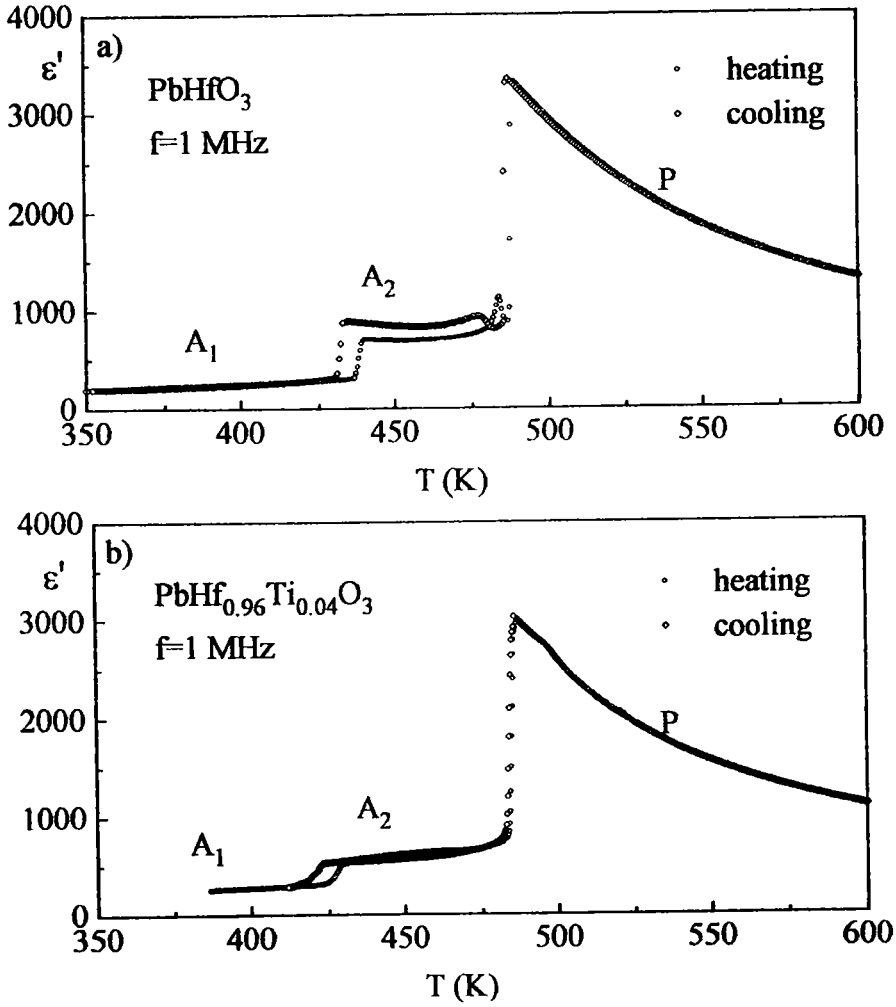


Figure 2.27. Temperature dependencies of the ε' on cooling and on heating for pure $PbHfO_3$ and for $PbHf_{0.96}Ti_{0.04}O_3$ single crystals.

First the variations of the dielectric permittivity with temperature crystals were measured for both crystals at the frequency 1 MHz on cooling and heating. Results are presented in Figure 2.27. The obtained plots are basically similar to those quoted for $PbHfO_3$ in the literature (Forker, 1973; Goulpeau, 1966; Samara, 1966; Shirane 1953) (Fig. 2.27a). ε_{max} corresponds to the transition from paraelectric to the intermediate A_2 phase and next anomaly indicates the transition between two antiferroelectric phases $A_2 \leftrightarrow A_1$. A small but clear anomaly close to $P \leftrightarrow A_2$ phase transition was found (its origin is not yet known and will not be discussed here). For the $PbHf_{0.96}Ti_{0.04}O_3$ sample dielectric measurements gives evidence of a shift in the transient A_2 phase towards lower temperatures and smoother form of the $\varepsilon'(T)$ curve through the $A_2 \leftrightarrow A_1$ transition in comparison with pure $PbHfO_3$. The $P \leftrightarrow A_2$ phase transition seems to be independent from Ti doping and takes place at 486 K with a sharp divergence in ε' and only very small thermal hystheresis (about 1 K). A small anomaly (of the origin unknown for the moment) a few degree above T_c can be observed also for this sample.

Dielectric dispersion in $PbHfO_3$ up to 10 MHz.

In Figure 2.28 the temperature evolution of the frequency dependencies of complex permittivity are presented in all three P, A_2 and A_1 phases and in frequency ranges where the dielectric dispersions were observed.

The frequency dependence of the real and imaginary parts of $\varepsilon(f)$ at the temperature T=715 K in the paraelectric phase is presented in Figure 2.29. The obtained plots are quite different than the one observed for $PbZrO_3$ and PZT crystals. In the figure one can easily distinguish two broad contributions A and B to $\varepsilon(f)$, therefore the dielectric response was fitted to the superposition of the two Cole-Cole expressions (eq. 2.8). The large linear response of ε'' found at very low frequencies was treated as a d.c. conductivity represented by σ_o and giving contribution in the form $\sigma_o/\varepsilon_o\omega$ like in the case of PZT samples. The way of fitting of these two independent processes was presented in the inset of Figure 2.29.

Concerning the two relaxation processes A and B the adjustable parameters were the relaxation times τ_A and τ_B and dispersion steps $\Delta\varepsilon_A$ and $\Delta\varepsilon_B$. While the polydispersive

character of the B relaxation was very small (α~0.04) the low frequency process A appears to be significantly polydispersive (α~0.2).

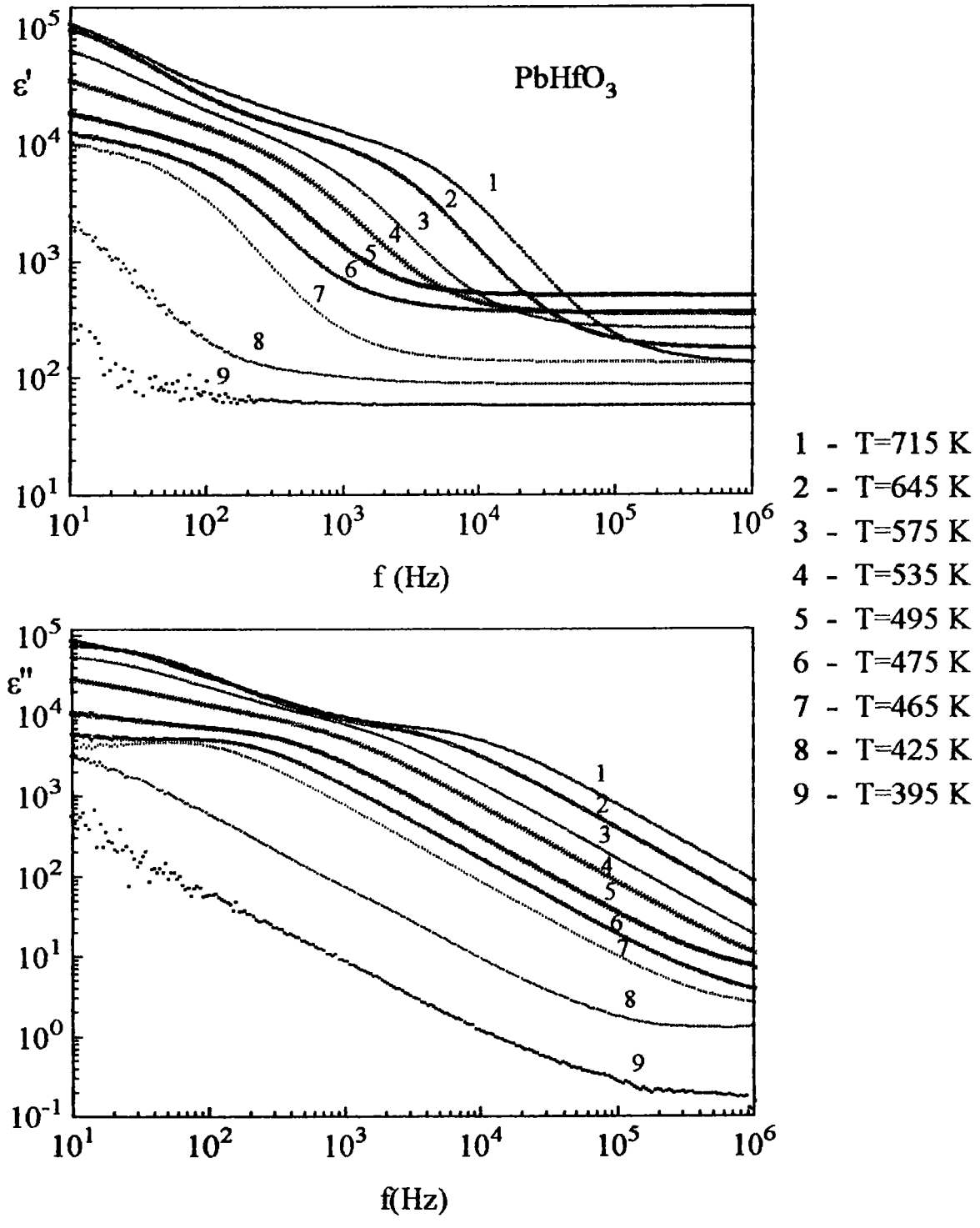


Figure 2.28. Temperature/frequency evolution of the ε' and ε'' for $PbHfO_3$ in all three phases (A_1, A_2 and P)

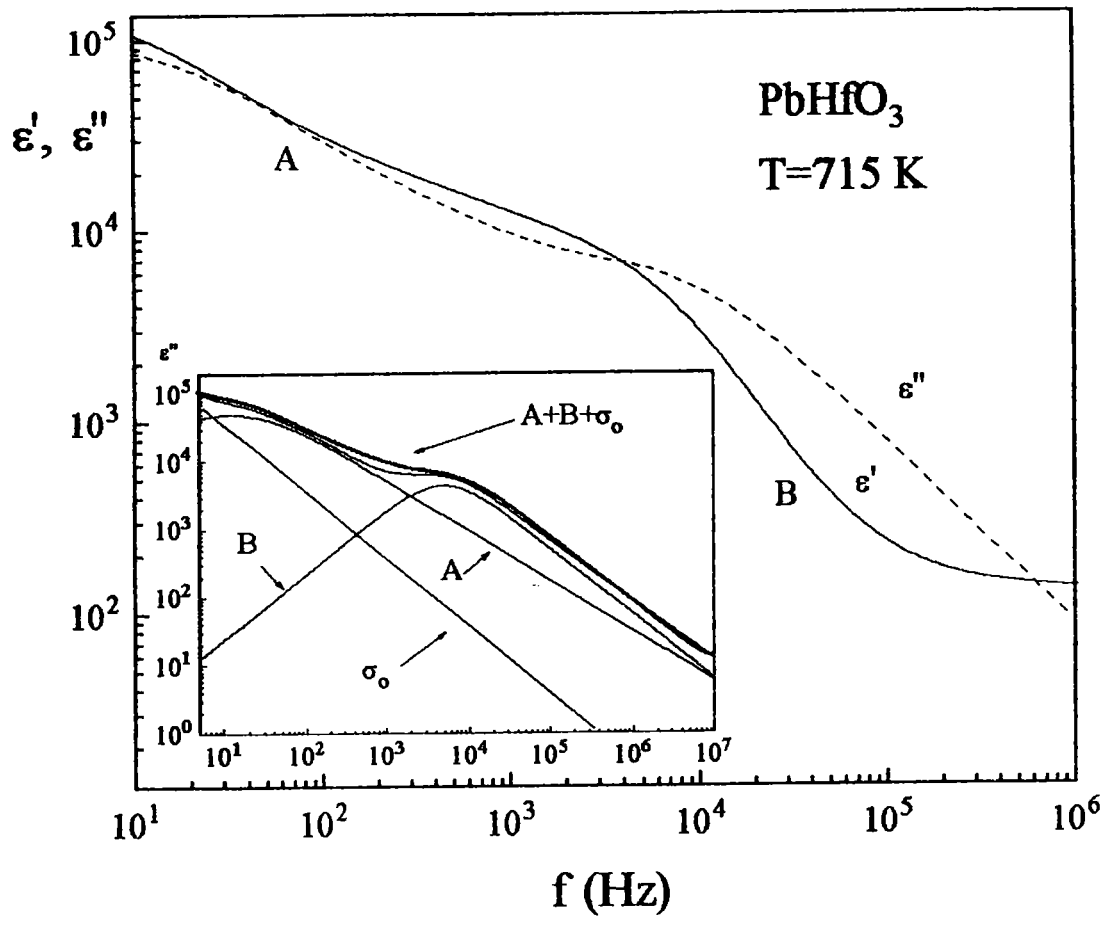


Figure 2.29. Frequency functions of real ε' and imaginary ε'' parts of dielectric permittivity for $PbHfO_3$ at the temperature T=715 K. The inset presents the way of fitting of the two relaxation processes **A** and **B** to the imaginary part of dielectric permittivity.

For the **A** relaxation the mean relaxation time τ_A is temperature dependent but does not follow the Arhenius law (Fig 2.30a). τ_A has an anomaly near the temperature T=670 K and next anomaly can be observed near 610 K. Near T_c, τ_A reaches the value 0.02 s.

Contrary to the **A** process in the paraelectric phase the temperature variation of τ_B of the **B** relaxation may be described by Arhenius law. The relaxation times τ_B are reported in Figure 2.31 in the form $\ln\tau(1/T)$. Using the simple regression method the value of the activation energy in the paraelectric phase can be calculated and its value is 0.46 eV and $\tau_o = 1.52 \cdot 10^{-8}$ s. By fitting the lowest-frequency data of the ε'' the values of d.c. conductivity were calculated and presented in Figure 2.30b. Near the temperature 670 K an anomaly in the dependence $\ln\sigma(1/T)$ can also be observed.

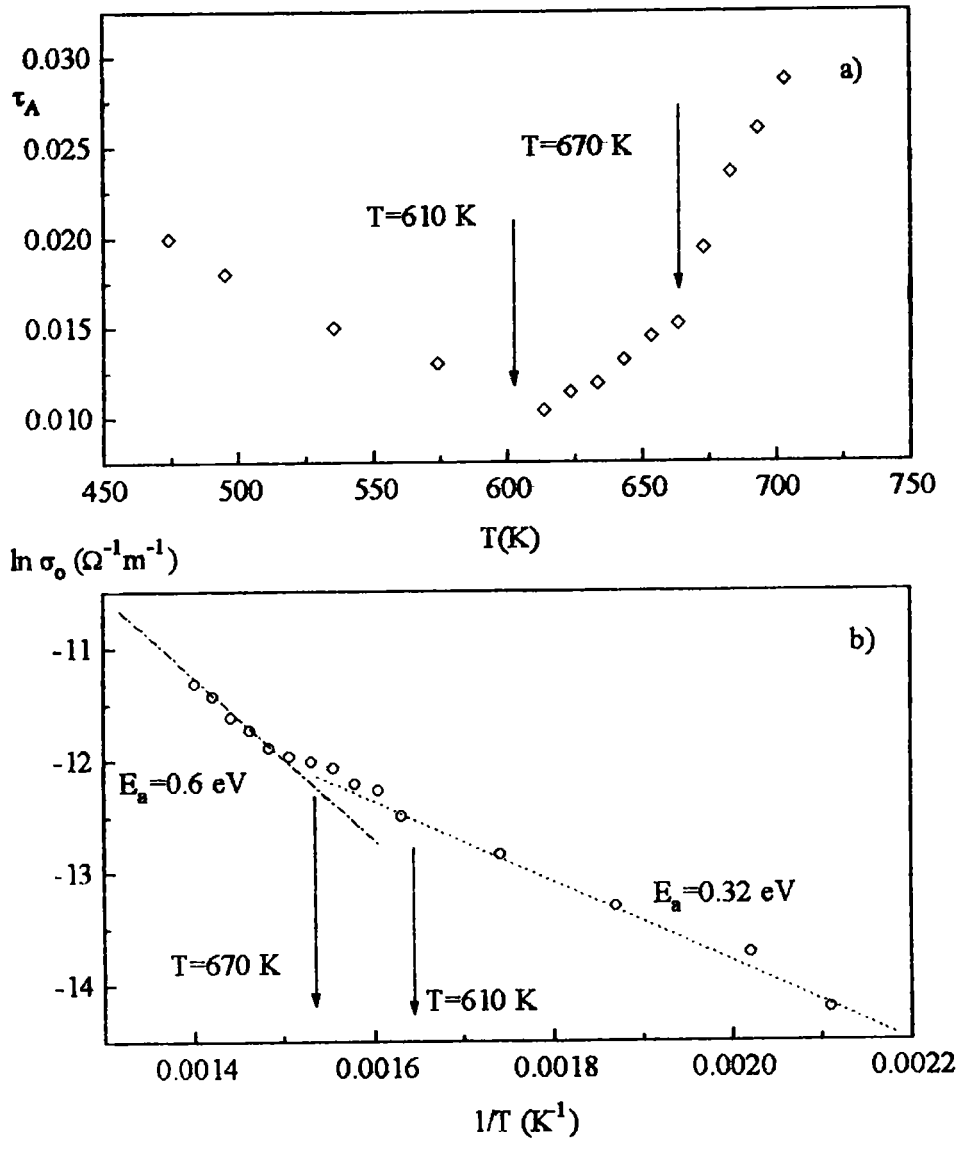


Figure 2.30. The calculated relaxation times τ of A relaxation (a) and values of d.c. conductivity (b).

Figure 2.31b presents the contribution of the B relaxation to the dielectric permittivity in all three phases (A_1, A_2 and P). Similarly to the $PbZrO_3$ single crystal $\Delta\varepsilon_B$ in the paraelectric phase seems to be temperature independent. In the transient phase A_2 the relaxation process B can be still observed but disappears when going to the A_1 phase. Just near the $A_2 \rightarrow A_1$ phase transition there a new very weak and strongly polydispersive relaxation process can be observed which exists on high frequencies (f~2000 kHz) (see Figure 2.32). It is easy to notice that the relaxation frequency of this weak process also shifts into lower frequencies. Down into A_2 phase all relaxations disappear.

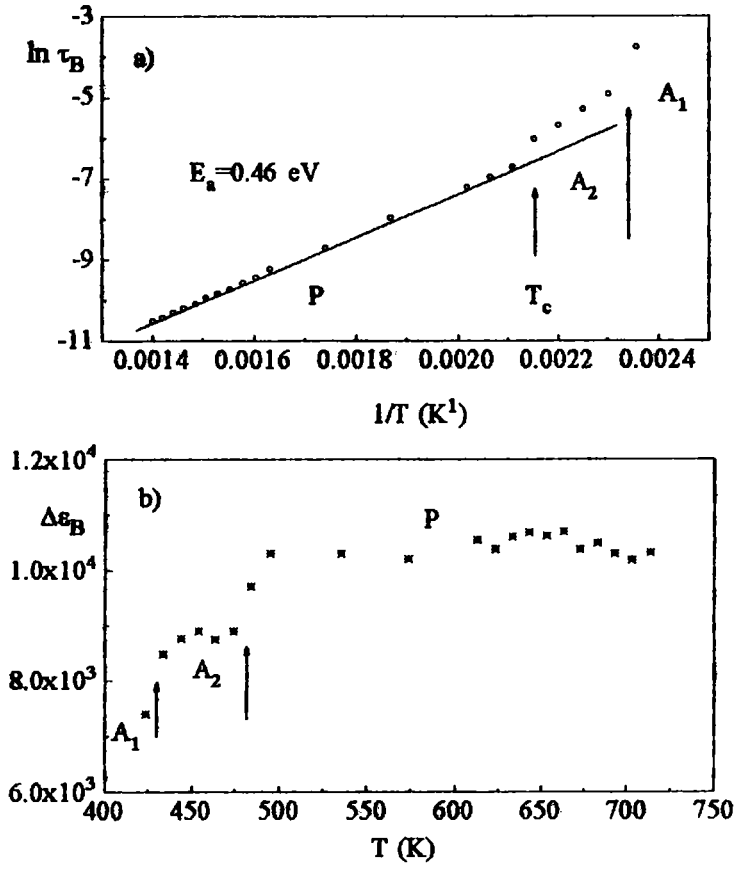


Figure 2.31. The calculated relaxation times τ_B and contribution of the **B** relaxation $\Delta\varepsilon$ to the dielectric permittivity in all three phases.

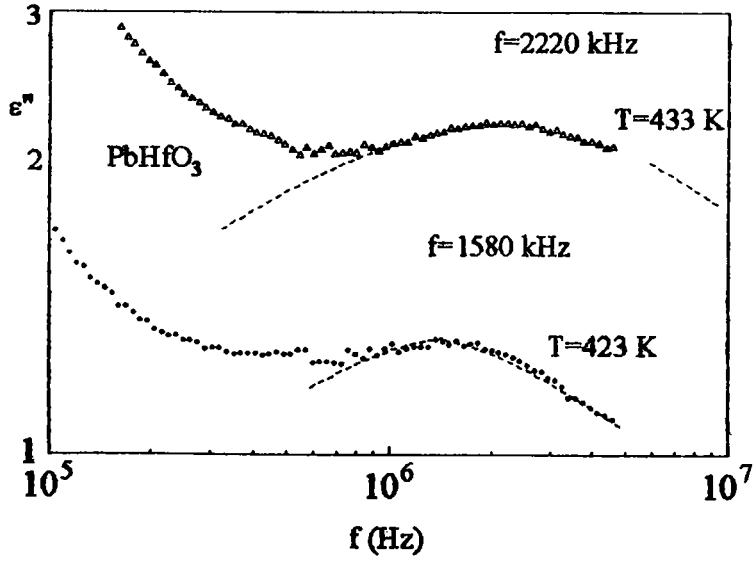


Figure 2.32. The imaginary parts of the $\varepsilon(f)$ of the higher frequency relaxation process detected in the vicinity of the A_1- A_2 phase transition

<u>$PbHfO_3$ doped with $PbTiO_3$: dispersion phenomena in $PbHf_{0.96}Ti_{0.04}O_3$ single crystal.</u>

Analogous measurements were made for the $PbHf_{0.96}Ti_{0.04}O_3$ sample and compared to the results obtained for pure $PbHfO_3$. An addition of Ti ions does not significantly impact the observed relaxations. In the Figure 2.33 two contributions **A** and **B** to ε and contribution of d.c. conductivity to ε'' are marked (see inset).

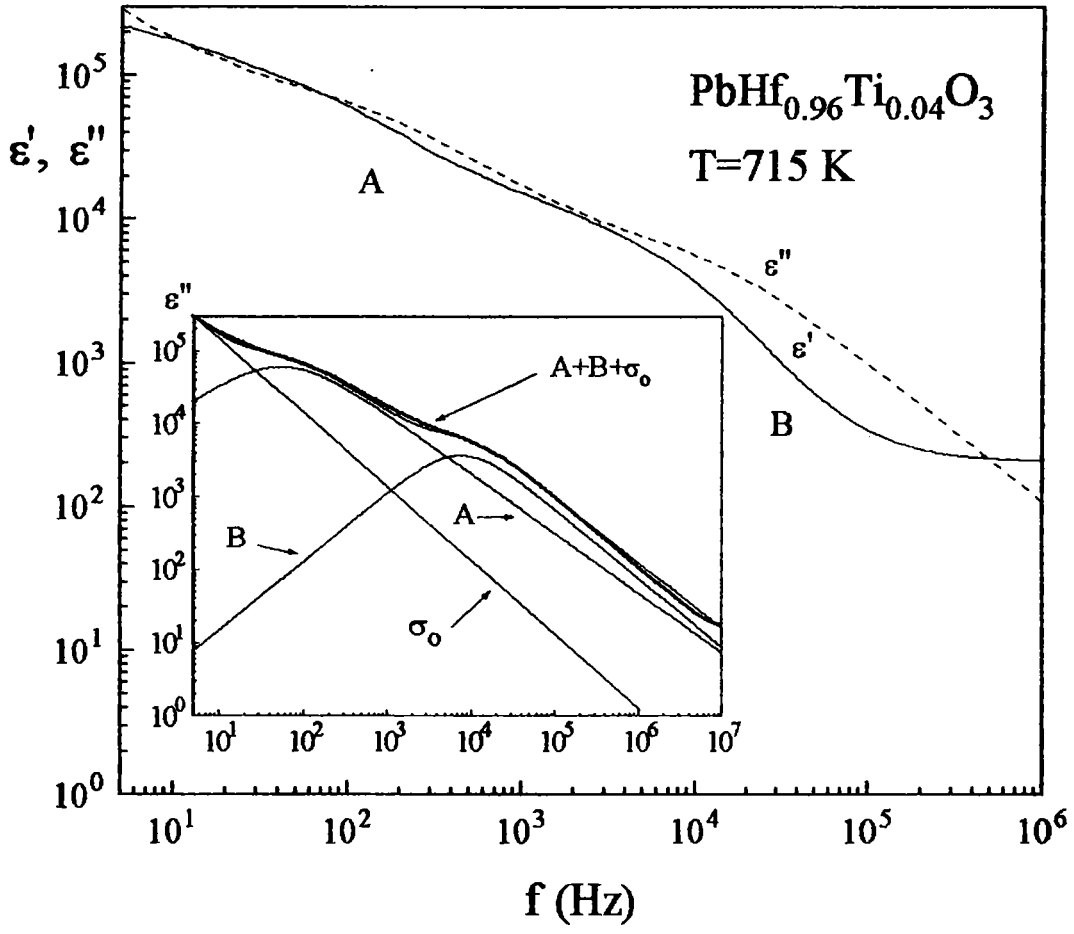


Figure 2.33. Frequency dependence of the ε' and ε'' at 715 K in paraelectric phase

The fitting process was made in the same way as for pure $PbHfO_3$. The results of fits for both **A** and **B** relaxation are presented in Figures 2.34 and 2.35 respectively. As to the **A** relaxation it behaves in similar way like in case of pure $PbHfO_3$. τ_A is also temperature dependent but does not follow the Arhenius law. The large $\Delta\varepsilon_A$ is almost temperature independent down to 600 K and then goes down step by step (Figure 2.34b). The values of d.c. conductivity are presented in Figure 2.34c, showing a clear anomaly near 670 K.

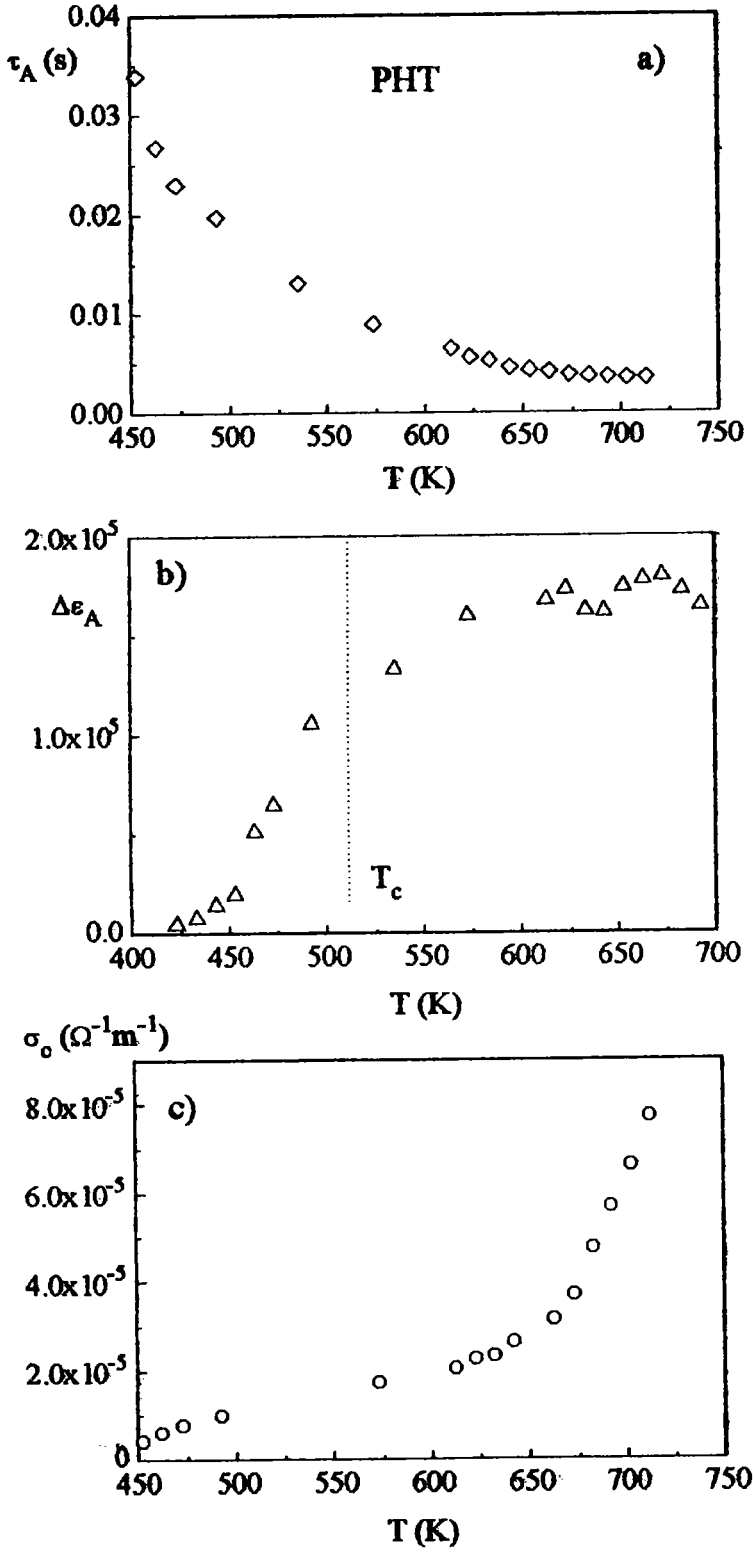


Figure 2.34. Calculated parameters of the A relaxation τ(T) (a) and Δε(T) (b) and values of d.c. conductivity (c)

In the paraelectric phase the relaxation times of the **B** relaxation can be described by classical Arhenius law (Fig. 2.35a) with the activation energy E_a=0.51 eV and $\tau_0=1.75\cdot10^{-9}$ s. Comparing these values to the ones obtained for $PbHfO_3$ one can say that the introduction of light Ti ions instead of heavy Hf ions moves the relaxation into higher frequencies. Contrary to $PbHfO_3$ the $\Delta\varepsilon_B$ step becomes temperature dependent in the paraelectric phase and at T_c takes slightly higher values than for PH. Besides both phase transitions are clearly visible on the $\Delta\varepsilon(T)$ dependencies for both of samples.

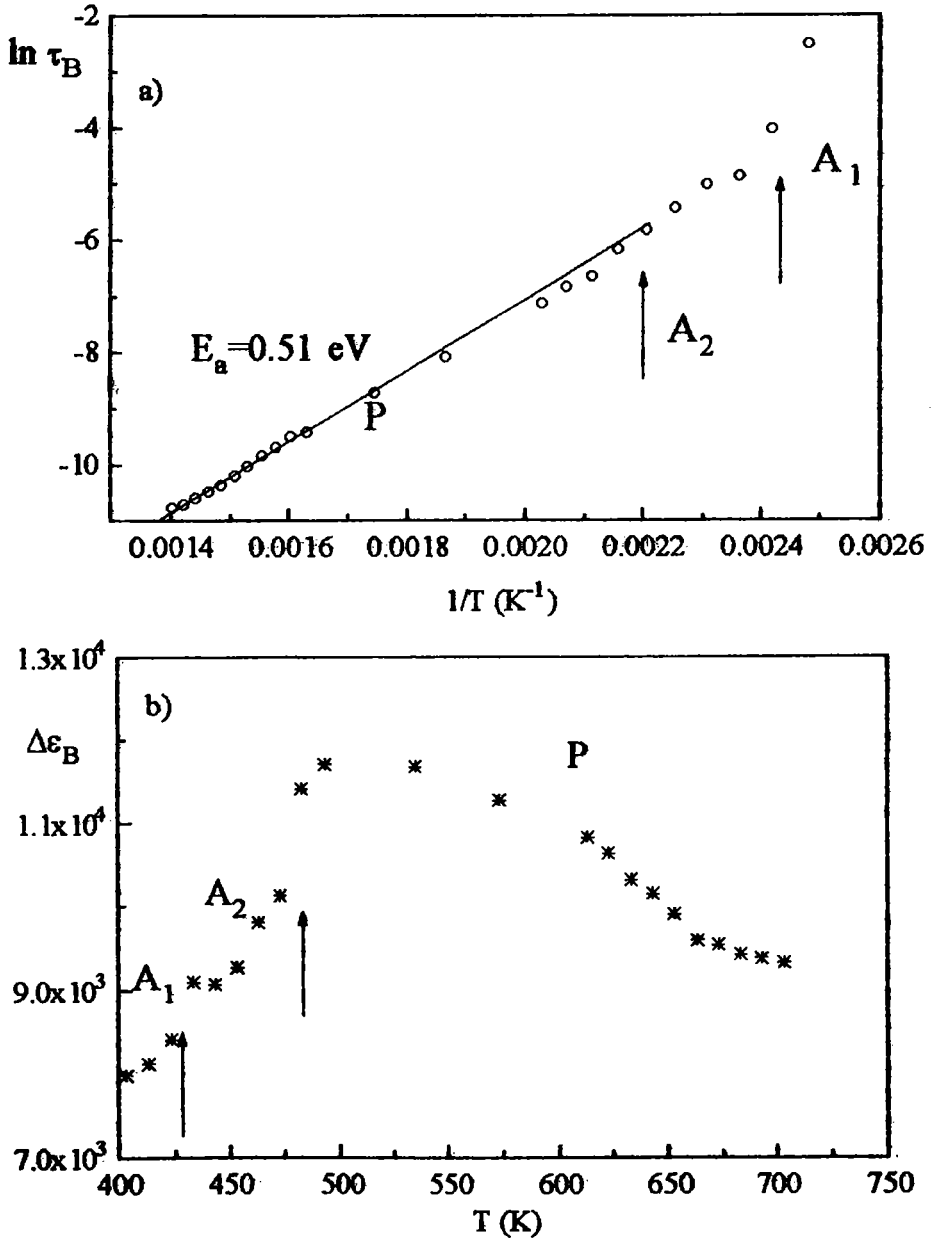


Figure 2.35. Calculated parameters of the **B** relaxation $\tau(T)$ (a) and $\Delta\varepsilon(T)$ (b).

Near the $A_2 \rightarrow A_1$ phase transition a very weak relaxation process can also be observed on higher frequencies (f~10^6 - $2 \cdot 10^6$ Hz) (Figure 2.36). In the A_1 phase all the relaxations disappear in the frequency range used.

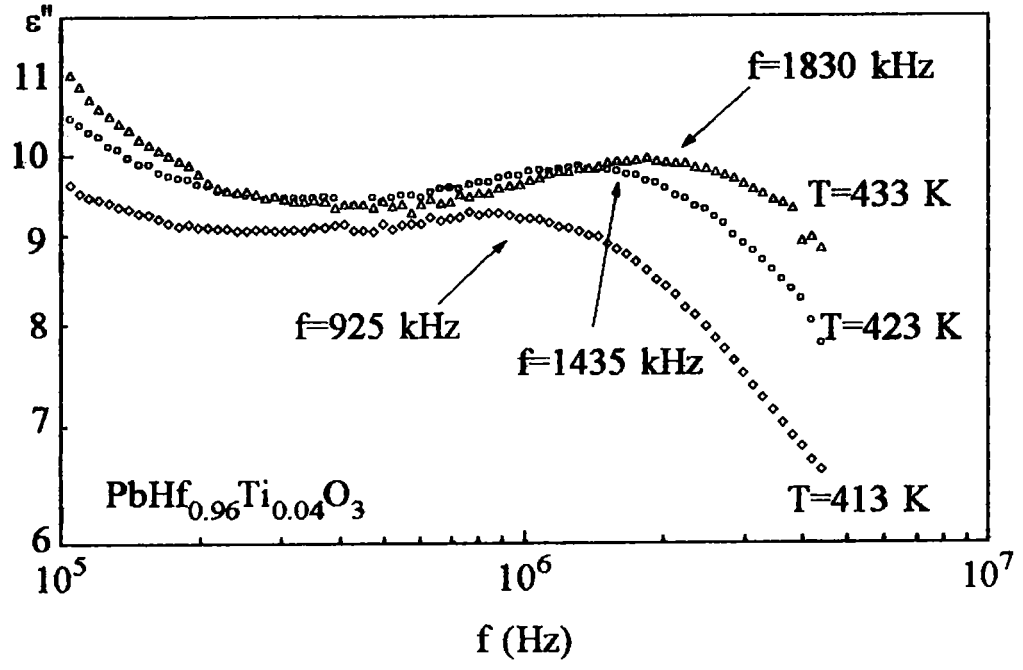


Figure 2.36. The imaginary part of the higher-frequency relaxation process for PHT in the vicinity of the A_1- A_2 phase transition.

2.4. DISCUSSION - POSSIBLE SOURCES OF RELAXATIONS BELOW 10 MHz.

In this work experimental results were presented in terms of dielectric permittivity calculated as C/C_0 with C_0 being the vacuum capacity related to crystal size. However we are aware that in many cases the LFD (low frequency dispersion) response of materials is carried out in terms of the capacitive equivalent of the complex susceptibility:

$$C(\omega) = C'(\omega) - jC''(\omega) = A(\varepsilon'(\omega) - j\varepsilon''(\omega)) \qquad 2.16$$

where $C(\omega)$ is the frequency-dependent complex capacitance and A is the geometrical factor of the sample. The reason is that in many problems of LFD the relevant geometry - when dealing e.g. with surface of interfacial transport - is not known. However the frequency spectrum is not influenced by the geometrical factors. Hence

unexpected huge values of ε for the lowest frequencies indicate unusual specific processes rather than abnormal high polarizability of the investigated material.

Case of $PbZrO_3$

The most important conclusion from the experiments is that a nearly monodispersive low-frequency relaxation exists in the lead zirconate without transient phase which slows down at T_c. This relaxation has a marked influence on the low-frequency ε(T) function due to very high dispersion step (ε_s-ε_∞). This is well demonstrated in Figure 2.37 where temperature dependence of real part ε' measured well above dispersion region (f=300 kHz) is compared with ε_s obtained from the calculations.

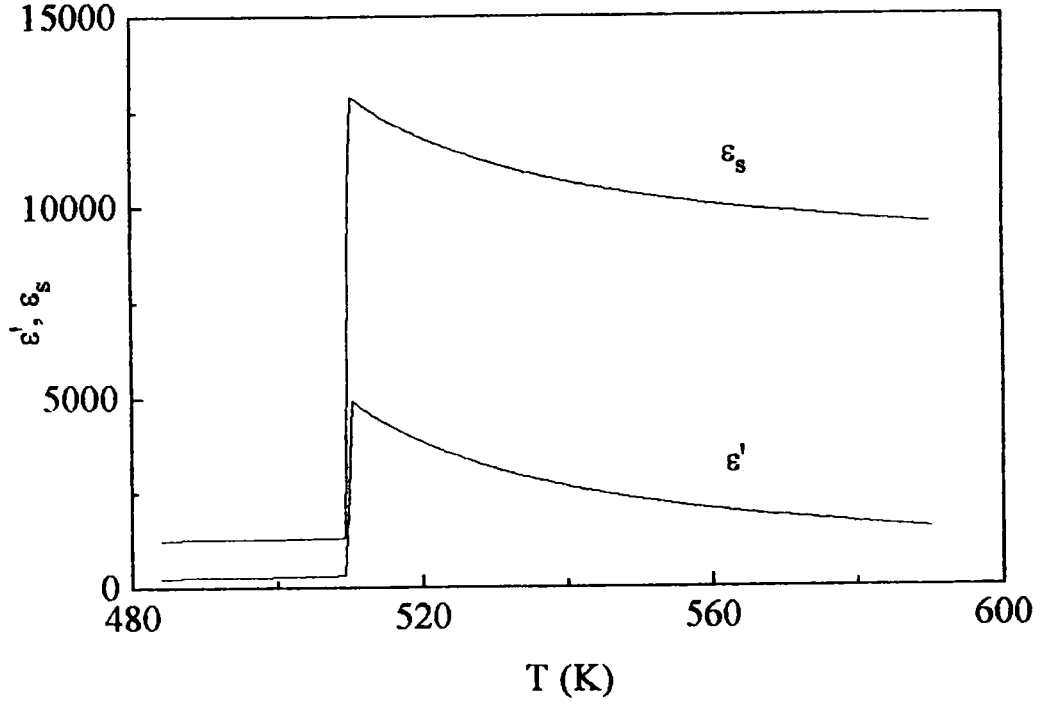


Figure 2.37. Comparison of the temperature dependence of the calculated dielectric permittivity ε_s with the real part ε' measured above dispersion region e.g. 300 kHz.

This comparison shows that the permittivity maximum seen at the phase transition for low frequencies is not completely dominated by one process although the share of the relaxation found is more than twice as large as the other. It should be mentioned that it is also difficult to decide on the nature of the smaller ε' maximum which can originate both

from the additional relaxation process taking place at much higher frequency or from the crystal lattice dispersion.

The intriguing question arises as to what physical mechanism is responsible for the appearance of the intense low frequency relaxation. In addition to the complex and strongly distorted crystal lattice determined by X-ray and neutron diffraction, Whatmore (1976) found another deviation of atom positions from their symmetric sites at room temperature. This concerned an oxygen atom sublattice in which disorder was found leading to the co-existence of two different distortions of the octahedra in the same crystal (see par.1.2.1). The same results were obtained from X-ray measurements performed on a single domain $PbZrO_3$ crystal (Glazer et al., 1993). While this disorder is frozen at room temperature, it could lead at high temperatures to a build-up of mobile dipoles consisting of regions of ZrO_6 octahedra relaxing with respect to the Pb sublattice. Their size and mass would confirm the low frequency dielectric dispersion coming from the polar relaxation mode.

Different models of dielectric relaxation in the low-frequency region which could be adopted here for antiferroelectrics was proposed by Bidault et al. (1994) who has observed thermally activated Debye relaxation at frequencies 10 Hz to 10 MHz in several ferroelectric perovskites. From the data reported in this paper, the relaxing dipoles have to be related to the density of oxygen vacancies and the relaxation rate has to follow the conductivity. From this the assumption was made that the free ionic carriers which were stored at the two dielectric-electrode interfaces caused a *space charge*. In fact this effect is well known in number of dielectric materials (Jonscher, 1983). The application of an electric field breaks the symmetry of this space charge and a macroscopic dipole is thus created. This could explain the presence of the electric dipole that is observed.

Dielectric relaxation found in lead zirconate also throws a new light on the problem of the transient phase appearing just below T_c and often recognised as ferroelectric. Only in $PbZrO_3$ crystal with one phase transition does this relaxation clearly appear. Shift of this relaxation to much lower frequencies in samples exhibiting transient phase may be linked with the concentration of point defects in the Pb and/or O sublattices so easily produced in the technological process. The defects diffusion model proposed by Glarum (1960) may be used to explain this problem. According to this model when a defect (hole) reaches the dipole it allows reorientation to occur more quickly than it otherwise would. If defects concentration becomes appreciably large, then virtually all the dipoles will relax at once

via the defects mechanism and disappearance of the dispersion can be observed. The large concentration of point defects in crystals with transient phase would be confirmed by the existence of dielectric losses (tan δ) several times higher at low frequencies (9.94 for 20 Hz at 625 K) than those found in crystals with one phase transition (2.02 for 20 Hz at 625 K). The other phenomenon which can be connected with the existence of point defects in this kind of crystal is the appearance of new very weak relaxation in range of 10^4 - 10^5 Hz in paraelectric phase. As mentioned in par. 1.2.2 if a sufficiently high concentration of point defects occurs, they can provoke a ferroelectric state below T_c. The same can also create polar regions above T_c which relax contributing to ε'(T) as presented in Figure 2.17.

$PbZr_{1-x}Ti_xO_3$.

Taking into account the part of discussion above concerning $PbZrO_3$, the overall dielectric response investigated for $PbZr_{1-x}Ti_xO_3$ single crystals at frequencies up to 10 MHz can be divided into three parts:

1) a strong very low-frequency response below 100 Hz at 623 K (Fig. 2.19) in the paraelectric phase visible in the imaginary and real part of the dielectric permittivity and related, to electrochemical processes contributing to the dielectric polarization whether it be a volume or a surface.

2) a strong low-frequency dipolar relaxation up to 1 kHz in the paraelectric phase giving a marked contribution to the ε'(T) dependence, which is contrary to the behaviour of pure $PbZrO_3$. For pure $PbZrO_3$ strong low-frequency relaxation for which Δε was invariant with temperature is found, similar to that for polarization limited by non-thermal forces, for example by elastic constrains (Jonscher, 1983). The introduction of Ti ions does not significantly change the frequency range of occurrence of this relaxation in comparison with pure $PbZrO_3$ but clearly changes the relaxation strength Δε which at the same time becomes temperature dependent. It is suggested that in $PbZrO_3$ single crystal with Ti ions replacing of Zr there is a specific coupling between local polarization induced by Ti, polarization limited by non-thermal forces and the electronic conductivity.

3) much weaker relaxation in the range of few kHz clearly visible in the transient phase and above T_c. This relaxation appears due to Ti introduction and generally may come from the interface dynamics both in the paraelectric and the intermediate phases. In the paraelectric phase the local polar regions are formed and their size increase with respect to

the paraelectric matrix on approaching T_c from the high temperature side. In a.c. electric field the behaviour of phase boundaries between the polar region and paraelectric matrix would thus be responsible for the relaxation observed. The deviation from the Curie-Weiss law is just because of this effects. In the intermediate phase of ferroelectric properties, dielectric relaxation may be related to motion of walls in the complex domain structure observed under a polarizing microscope. Polydispersive behaviour found in this phase would also favour the explanation proposed. The ε time variation observed by Roleder et al (1991) in the intermediate phase provides additional evidence for the existence of domain-wall relaxation in this phase. On the other hand the action of sufficiently strong d.c. electric field which eliminates or pins the domain structure, removes the relaxation process. This fact can also be seen as a further proof that this relaxation is due to interface dynamics.

$PbHfO_3$ and $PbHf_{0.96}Ti_{0.04}O_3$

In comparison with $PbZrO_3$ and PZT there are two kinds of relaxation below 10 MHz in $PbHfO_3$ and $PbHf_{0.96}Ti_{0.04}O_3$:

1. A strong low-frequency response (e.g. maximum of ε'' for about 100 Hz at T=715 K) visible in the real and imaginary parts of the dielectric permittivity and giving large contribution to ε'(T) measured in this frequency region ($\Delta\varepsilon_A$ - Figure 2.34b). This effect is related to the free ionic and electronic carriers in the bulk and stored at the dielectric - electrode interfaces (electrochemical processes, space charge) and is well known in a number of dielectric materials (Jonscher, 1983; Miga et al., 1996; Bidault et al., 1994). Since both σ_o and dielectric step $\Delta\varepsilon=\varepsilon_s-\varepsilon_\infty$ decrease with decreasing temperature on approaching T_c the above explanation seems to be justified (Fig.2.30 and 2.34b&c).
2. Another dipolar relaxation in the range up to several kHz in the paraelectric phase giving a marked contribution to the ε'(T) (Figure 2.31b and 2.35b)

Behaviour of this relaxation (**B**) is similar to that found in $PbZrO_3$ and $Pb(ZrTi)O_3$ which could be related to the presence of defects or disorder in the oxygen atom sublattice (Glazer et al., 1993; Jankowska-Sumara et al., 1995a) or following to Bidault (1994) space charge model related to the density of oxygen vacancies. The existence of some kind of disorder in the paraelectric phase was also proposed for pure $PbHfO_3$ and $Pb(HfTi)O_3$ on the basis of Raman scattering investigations (Jankowska-Sumara et al., 1995b). The

existence of the disorder but in Pb atom sublattice in the paraelectric phase of $PbHfO_3$ found in x-ray investigations by Kwapulinski et al. (1994) at about 670 K tends to support this supposition.

3. A very weak high frequency (f~2000 kHz) relaxation visible near the $A_2 \rightarrow A_1$ phase transition and probably related to the motion of domain walls when the domain structure is being reorganised in $A_2 \rightarrow A_1$ phase transition. It is worth to recall here that in this region, double antiferroelectric hysthercsis loops were easily observed (Fig. 2.32 and 2.36).

Discussing low frequency response (especially very high ε values) of materials under consideration one cannot forget about perhaps the dominating role of surface layers. For ABO_3 compounds such as $KNbO_3$, $BaTiO_3$, $PbTiO_3$ and $SrTiO_3$ it was found that chemical composition, together with structural properties of the surface, differs distinctly from the bulk. The surface is not a homogeneous region and existence of extended defects in it serves as fast diffusion path for oxygen and A type atoms. This leads to a segregation of A or AO-complexes, which is extremely easy at elevated temperatures, and a continuous transition between ABO_3 and $AO(ABO_3)_n$ in the surface region takes place (Szot et al., 1996). In such surface region, reduction and electroreduction processes may be forced and restricted to the neighbourhood of the extended defects. This kind of surface region effectively enlarges the area of electrical contact and gives rise to the observed anomalous increase of dielectric permittivity at low frequencies.

On the other hand, many experimental facts (Jonscher, 1996) suggests that LFD action is distributed throughout the inter-electrode space instead of being confined to same barrier regions near the electrodes. A model of electrochemical interactions involves the unique feature of „battery-like" action without which it is difficult to understand the very high values of effective $C'(\omega)$ and $C''(\omega)$ being reached at low frequencies. The electrochemical mechanism is proposed to explain this behaviour and it relies on the formation of neutral component molecules M_1M_2 out of slowly mobile ions M_1^+ and M_2^- following the symbolic equation:

$$M_1^+ + M_2^- \Leftrightarrow M_1M_2$$

where the corresponding densities ν_{M_1}, ν_{M_2} and $\nu_{M_1M_2}$ are determined by the external conditions such as - in broad meaning - the impurity content in bulk materials.

The presentation of LFD data seems to convince that they represent a special class of dielectric behaviour interpretation which is not easy. The LFD mechanism is clearly due to hopping charge carriers which are in our case ionic. Since similar relaxations were seen in all investigated materials one can state that LFD is independent from the detailed physical or chemical nature of materials, subjected mainly to the presence of localised carriers. One can distinguish three separate locations of LFD: in the volume, on the surface and across interfaces. Three relaxations clearly seen in the case of $PbZr_{1-x}Ti_xO_3$ single crystals nicely prove this hypothesis. Charge carriers responsible for LFD may be present in the materials „intrinsically" due to impurities (Ti), lattice defects (Pb, O vacancies) or other causes (electrochemical processes). It is worth to notice that nowadays theoretical interpretation of LFD is not as yet well established.

3. ELECTROSTRICTION

3.1. THEORETICAL BACKGROUND

The investigations of nonlinear effects near the phase transitions can give additional information on mechanisms of the phase transitions and structure of the investigated phases, since they exhibit much stronger anomalies than the linear effects and therefore they are much more sensitive for measurement. Electrostriction is such a nonlinear effect in dielectric crystals.

Electrostrictive effect follows from the second power dependence of $\varkappa$ on electric field E and it must be distinguished on the reverse piezoelectric effect which follows directly from the linear dependence of $\varkappa$ on E. A consequence of acting of electric field E on a crystal in electromechanical aspect is the appearance of deformation in the crystal. This deformation can be described by the following equation:

$$x_{jk} = d_{ijk}E_i + M_{ijjk}E_iE_l \qquad 3.1$$

where x_{jk} is the deformation tensor and E_i, E_l - the components of electric field vector. The first term of the right side describes the linear piezoelectric effect. d_{ijk} is the first derivative $\frac{\partial x_{jk}}{\partial E_i}$ for infinitely weak fields. The second term M_{ijjk} is equal to $\frac{\partial^2 x_{jk}}{\partial E_i \partial E_l}$ and describes the *electrostrictive effect*. Thus in the electrostriction the changes of dielectric permittivity in function of stress are connected by the second derivative with strain on electric field. When electric field changes its direction all of E_i components change their sign. Consequently in linear effects the deformation must also change the sign (i.e. stretches become abridgements). At the same time because of the quadratic dependence of second term on electric field the electrostrictive deformation is always positive (the crystal is always stretched). Coefficients M_{ijjk} create fourth order tensor which is symmetrical in relation to i and l such as j and k.

From the above it follows that the electrostrictive effect exists in all crystals, contrary to the piezoelectric effect which exists only in those crystals that do not posses center of symmetry.

The electrostrictive deformation can be then written as:

$$\text{or} \qquad \begin{aligned} x_{ij} &= M_{ijkl}E_kE_l \\ x_{ij} &= Q_{ijkl}P_kP_l \end{aligned} \qquad 3.2$$

For the cubic symmetry of Pm3m point group when no external stresses are present, the tensor Q_{ijkl} has the independent components Q_{1111}, $Q_{2211} = Q_{1122}$ and Q_{1212}. Substituting $Q_{1111}=Q_{11}$, $Q_{1122}=Q_{2211}=Q_{12}$ and $Q_{1212}=Q_{44}$ we can write the equation 3.2 in the form:

$$\begin{pmatrix} x_{11} \\ x_{22} \\ x_{33} \\ x_{23} \\ x_{31} \\ x_{21} \end{pmatrix} = \begin{pmatrix} Q_{11} & Q_{12} & Q_{12} & & & \\ Q_{12} & Q_{11} & Q_{12} & & & \\ Q_{12} & Q_{12} & Q_{11} & & & \\ & & & Q_{44} & & \\ & & & & Q_{44} & \\ & & & & & Q_{44} \end{pmatrix} \bullet \begin{pmatrix} P_1^2 \\ P_2^2 \\ P_3^2 \\ P_2P_3 \\ P_3P_1 \\ P_2P_1 \end{pmatrix} \qquad 3.3$$

The most commonly measured strains are longitudinal $x_{11}(x_1)$ and transverse $x_{22}(x_2)$ strains.

$$\begin{aligned} x_1 &= Q_{11}P_1^2 \\ x_2 &= Q_{12}P_1^2 \end{aligned} \qquad \text{or} \qquad \begin{aligned} x_1 &= M_{11}E_1^2 \\ x_2 &= M_{12}E_1^2 \end{aligned} \qquad 3.4$$

where P_1 denotes electric polarisation and E_1 is the strength of external electric field. The method of measurement of these two strains is presented in Figure 3.1

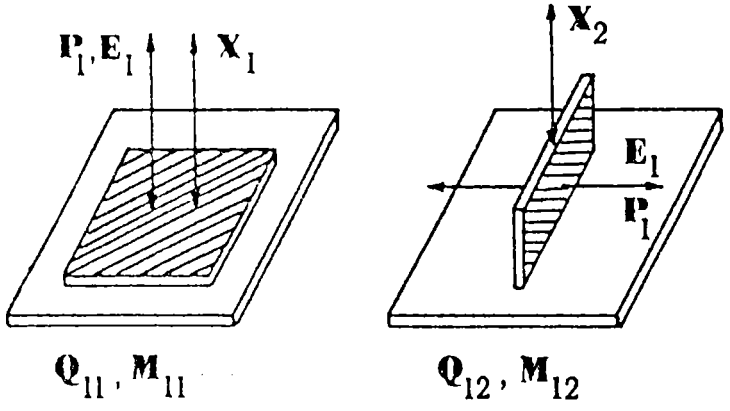


Figure 3.1. The manner of measuring of longitudinal and transverse strains.

Numerical values of electrostriction coefficients pertaining to the paraelectric phase are commonly calculated from experimental data of induced polarisation assuming that the strain is electrostrictively induced by the induced polarisation.

There are various available methods of measuring electrostrictive deformation x_i and determination of Q_{ij} coefficients (Jona & Shirane, 1962). The method most frequently

applied is the one in which a comparison is made of polarisation and corresponding mechanical deformation. In this case the magnitude of deformation is determined directly using capacitance dilatometers or special polyamide foils (Uchino & Cross, 1980; Nomura et al., 1979a; Nomura et al., 1979b).

3.2. EXPERIMENTAL SETUP

The method used here (Roleder, 1983) differs from the one used in dilatometers and polyamide foils. Here electrostrictive deformation is caused by constant (or slowly changing) electric field. Using of constant electric field in high temperature paraelectric phase can cause the electric break down of the sample. The electrostrictive deformation is caused by variable electric field of frequency f and strength E which increased up to $10^6 V/m$ applied perpendicularly to the sample surface. The mechanical vibrations are transmitted by a quartz rod which is attached to the electroded sample surface. The other end of the rod is glued to one plate of the measurement air condenser (Figure 3.2).

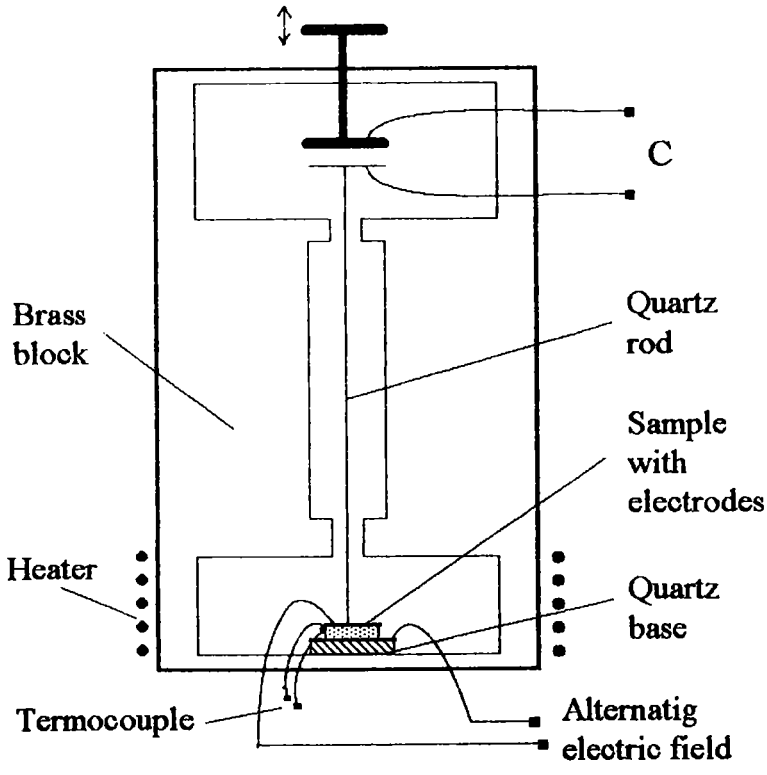


Figure 3.2. Layout for measurements of electrostrictive deformations by the capacity method

The sample and the condenser are placed in an air-tight brass block within which the temperature was stabilised with an accuracy of ±0.1 K. An electric field of amplitude E_o and frequency $\omega(=2\pi f)$ was applied to the sample by means of thin silver wires. In a sufficiently strong electric field of strength $E=E_o \sin\omega t$, electrostrictive vibrations of the sample proportional to $E_o^2 \sin^2 \omega t$ cause a change in distance between the plates of the measurement condenser, and hence in its capacity. To measure the amplitude of electrostrictive vibrations of the sample, the measurement condenser was connected up to a resistance R and a constant voltage source U (Figure 3.3).

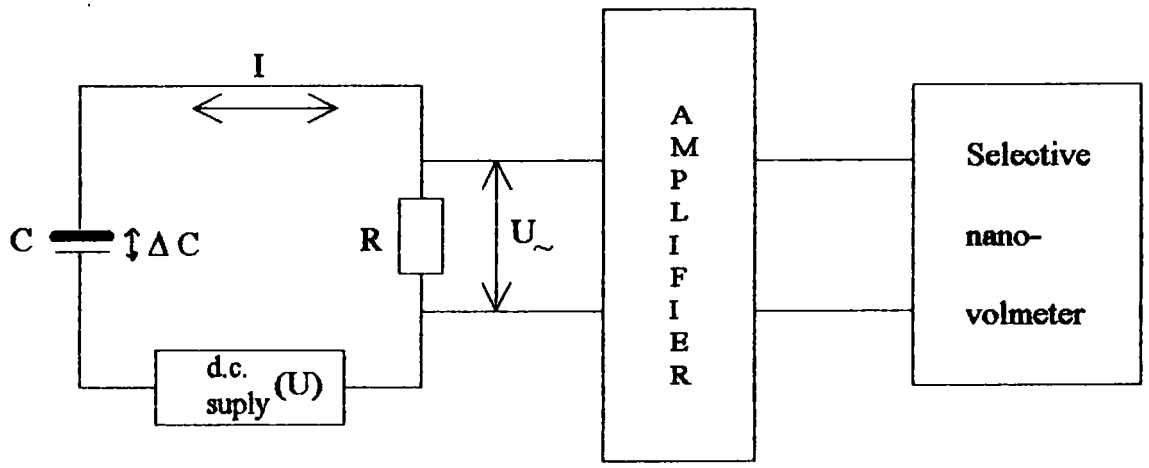


Figure 3.3. Measurement system for determining magnitude of electrostrictive deformation

Electrostrictive vibrations of the sample cause variations in charge of the condenser C and an alternating current I=dq/dt then flows in the circuit RC with the connected constant voltage U. The magnitude of strain x_1 was calculated on the basis of potential $U_\sim$ drop at resistance R measured with a selective nanovoltmeter.

$$x_1 = \frac{l_o}{d_o} \frac{U_\sim}{\omega RUC_o} \qquad 3.5$$

where l_o is the distance between measurement condenser plates when the sample is not vibrating, d_o is the thickness of the sample and C_o - the capacity of the measurement condenser when there are no electrostrictive vibrations.

The values of coefficients Q_{11} or Q_{12} can be calculated knowing the value of polarisation P_1 corresponding to application of electric field of strength E_1 (eq. 3.4) which is measured using the well known Sawyer-Tower system.

The details of measuring method is described in paper by Roleder (1983).

3.3. EXPERIMENTAL RESULTS

3.3.1. Electrostriction in $PbZrO_3$

The flux grown crystals in the form of thin plates of dimensions 3 x 3 x 0.05 mm^3 were used in experiments. As in the case of dielectric dispersion measurements, two kinds of specimens were used. The first one showed only one phase transition directly from the cubic (paraelectric) to the orthorhombic (antiferroelectric) phase at 514 K. In the second one, a transient phase (~3 K at cooling) was observed directly below the phase transition point T_c.

Because of the thickens of the samples only the longitudinal x_1 strain was measured and only Q_{11} coefficient could be calculated.

Strong low frequency electrostrictive strain in $PbZrO_3$ without transient phase

Figure 3.4 represents the frequency dependence of the polarization P_1 and electrostrictive strain x_1 at different temperatures in the paraelectric phase. The strong increase of P_1 and x_1 towards low frequencies (below 200 Hz) corresponds to the frequency range in which the dielectric dispersion was found.

According to the relation $x_1 = M_{11} \cdot E_1^2$ the magnitude of electrostrictive strain should be a quadratic function of electric field. For this reason the strain x_1 was measured as a function of electric field for different frequencies. In the measurements, the strength of electric field was limited to 10^6 V/m to protect the sample from the electric break-down. Departure from this relation for chosen frequencies in the logarithmic scale as a different slope of presented functions is shown in figure 3.5.

It should be noted that for defined temperature the strain electric-field relation is in fact quadratic only for frequencies lying over the relaxation frequency. The calculated values of slopes at different temperatures above T_c are added to the figure 3.5.

Analysing the shape $P_1(f)$ and $x_1(f)$ and the dependence of x_1 on electric field E_1, the frequency 300 Hz was chosen to measure the behaviour of electrostrictive coefficient Q_{11} versus temperature. In the temperature region used in our measurements (T_c, T_c + 25 K)

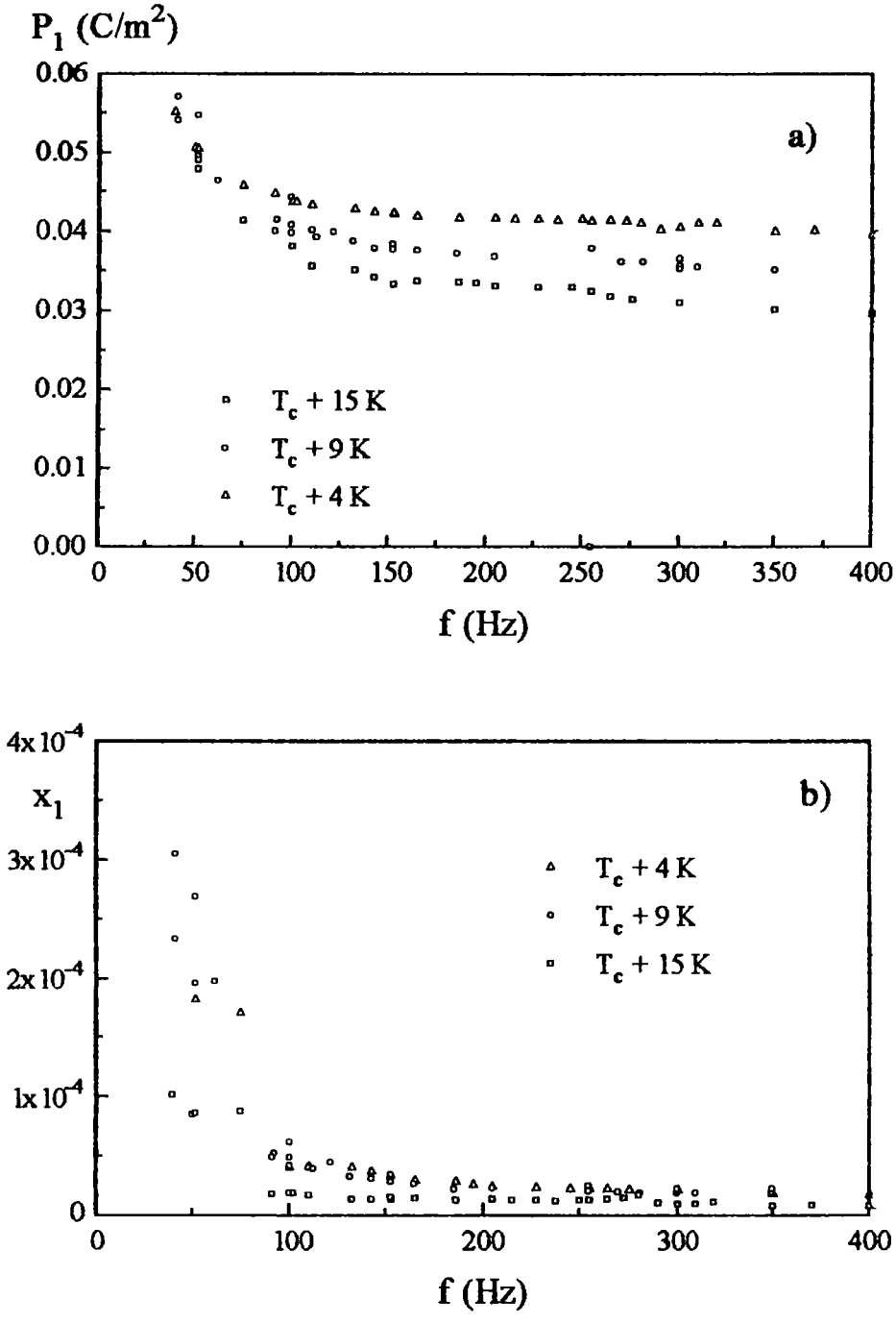


Figure 3.4. Frequency dependence of the polarization P (a) and strain x_1(b) at different temperatures in the paraelectric phase.

this frequency lies above the dispersion region. In agreement with the theoretical predictions the Q_{11} was temperature independent (Figure 3.6) (Jona & Shirane,1962; Barsch et al., 1981).

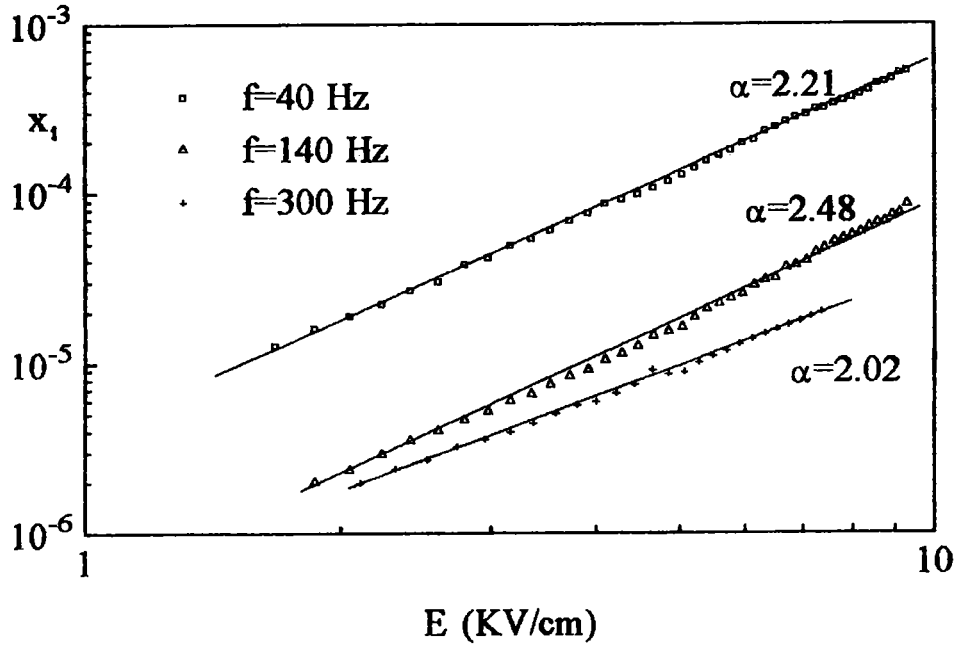


Figure 3.5. Field dependence of strain at different frequencies in the paraelectric phase in logarithmic scale for the sample without transient phase. $T=T_c+9$ K

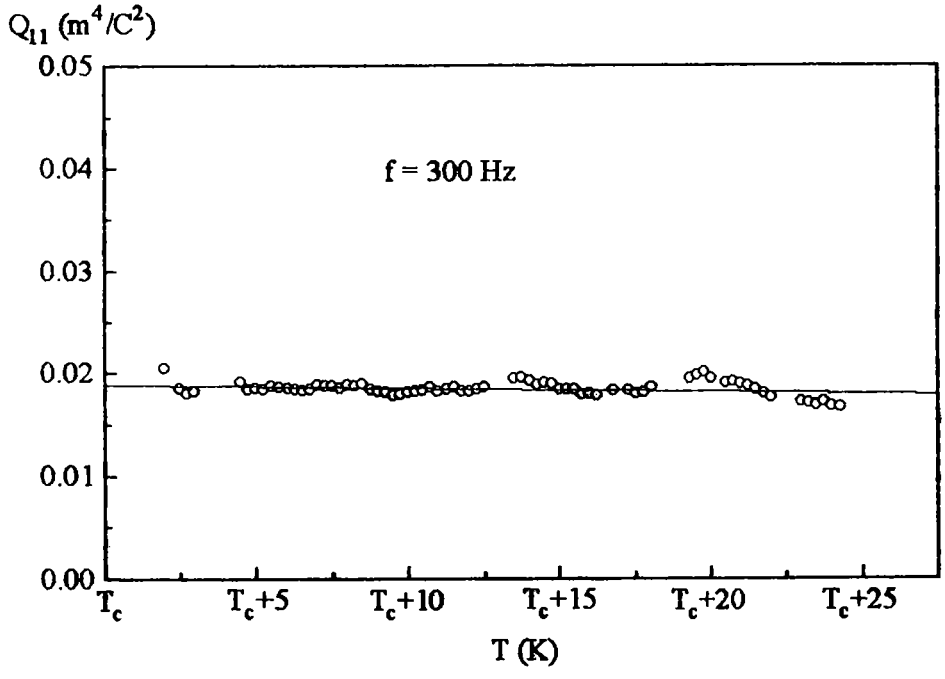


Figure 3.6. Temperature dependence of electrostrictive coefficient Q_{11} measured at 300 Hz for the sample without transient phase

Almost frequency independent electrostrictive properties in $PbZrO_3$ with an Intermediate Phase

The same measurements were repeated for the sample with transient phase (both on heating and on cooling). The obtained results are shown in Figures 3.7 - 3.9. It should be noted that for this kind of crystal the dielectric dispersion was not observed.

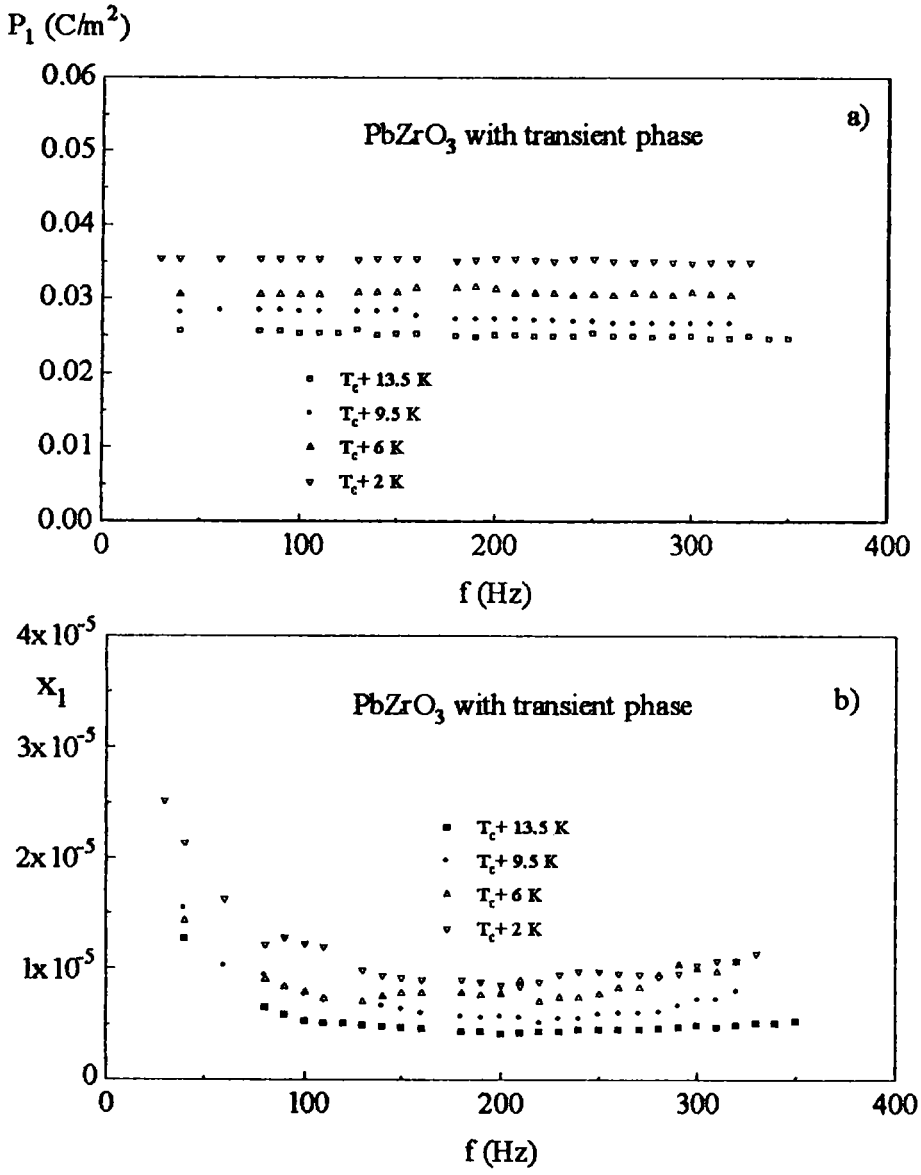


Figure 3.7. Frequency dependence of the polarization P_1 (a) and strain x_1 (b) at different temperatures in the paraelectric phase for the sample with transient phase.

Although the polarization is frequency independent (Figure 3.7a) the measurement sensitivity of strain x_1 allowed to detect a slight increase in very low frequencies

(Figure 3.7b). The relation $x_1 \sim E_1^2$ verified in the same way as for previous sample is well satisfied as shown in figure 3.8. The electrostrictive coefficient Q_{11} is not only temperature, but also frequency independent in the whole measured frequency region but its values are smaller than those obtained for the sample without transient phase (Figure 3.9)

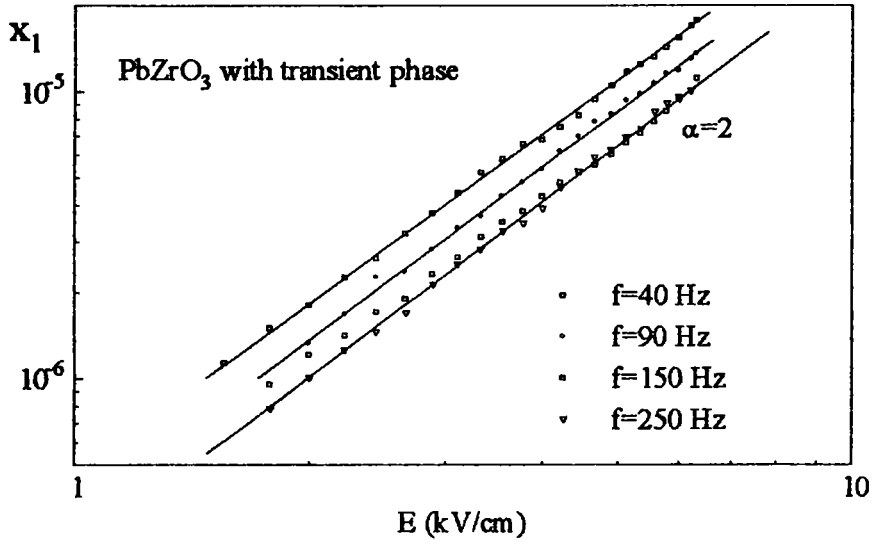


Figure 3.8. Field dependence of strain at different frequencies in the paraelectric phase in logarithmic scale for the sample with transient phase. The slope of all lines is equal 2.

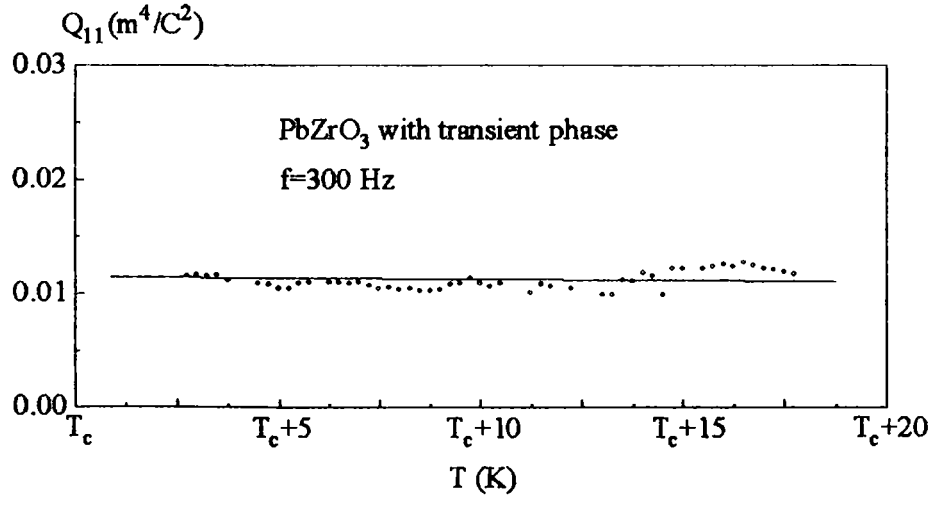


Figure 3.9. Temperature dependence of electrostrictive coefficient Q_{11} measured at 300 Hz for the sample with transient phase. The frequency was chosen for comparison with figure 3.6.

3.3.2. Strain dispersion in the $PbZr_{1-x}Ti_xO_3$ single crystal.

For the measurements two compositions of $PbZr_{1-x}Ti_xO_3$ were chosen in which the real concentrations were: 0.018, 0.03. Both specimens showed the existence of transient phase below the phase transition point T_c (see par. 1.2.2). The results represented here for PZT samples were obtained for $T>T_c$ using the same procedure as for pure $PbZrO_3$.

Because of the observed relation between the frequency dependence of electrostrictive deformation and the dielectric relaxation in $PbZrO_3$, the measurements of electrostriction in PZT compounds were performed, especially in order to verify the observed relation. For this reason for two samples of PZT the quadratic behaviour of the electrostrictive deformation on electric field i.e. relation $x_1 = M_{11}E_1^2$ was tested. To simplify the measurements the dependence of $x_1(E_1)$ was measured at different temperatures for one chosen frequency.

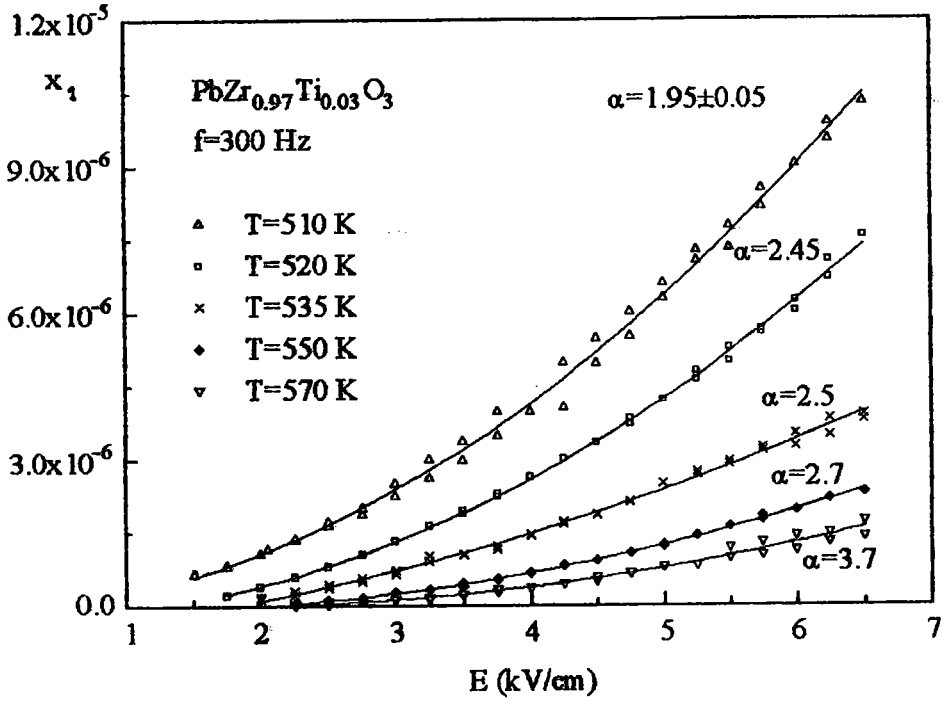


Figure 3.10. Strain electric field dependence for $PbZr_{0.97}Ti_{0.03}O_3$ at the frequency 300 Hz .

For the $PbZr_{0.97}Ti_{0.03}O_3$ single crystal the dependencies of $x_1(E_1)$ for the frequency 300 Hz are presented in Figure 3.10. For each temperature the departure from quadratic strain-electric field relation was calculated as the value of exponent of the equation $x_1 = M_{11}E_1^{\alpha}$. For pure electrostriction α should be equal to 2. For example for the frequency 300 Hz,

some degrees above T_c (T_c=508K) the deviation from the quadratic behaviour of the electrostrictive curve is seen. The higher temperature in the figure, the stronger is the observed deviation. In Figure 3.11 the dependence of polarization P_1 on the frequency of electric field at different temperatures is presented.

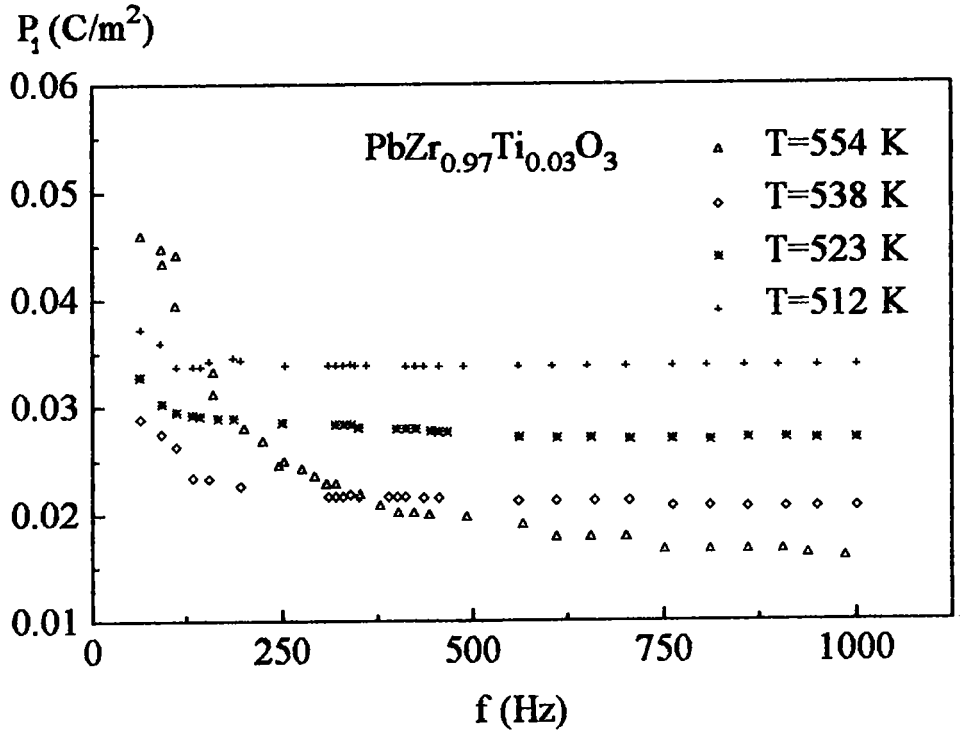


Figure 3.11. Frequency dependence of polarization P_1 at different temperatures in paraelectric phase, measured in Sawyer-Tower setup.

The strong non-linear increase of P_1 towards low frequencies corresponds to the frequency range in which the dielectric dispersion was detected (see Fig. 2.19). Comparing the two figures 3.10 and 3.11 one can observe that for the temperature 510 K the frequency 300 Hz lies over the frequency region and the strain- electric field relation becomes pure electrostrictive. The calculated values of exponents for each temperature are marked in the Figure 3.10.

Similar procedure was repeated for the sample $PbZr_{0.982}Ti_{0.018}O_3$. For this sample the dielectric dispersion measurements evidenced the shift of the dipolar relaxation to the lower frequencies in comparison with $PbZr_{0.97}Ti_{0.03}O_3$ and $PbZrO_3$. This is reflected in the measurement of polarisation P_1 versus frequency f and electromechanical measurements which are presented in Figures 3.12 and 3.13.

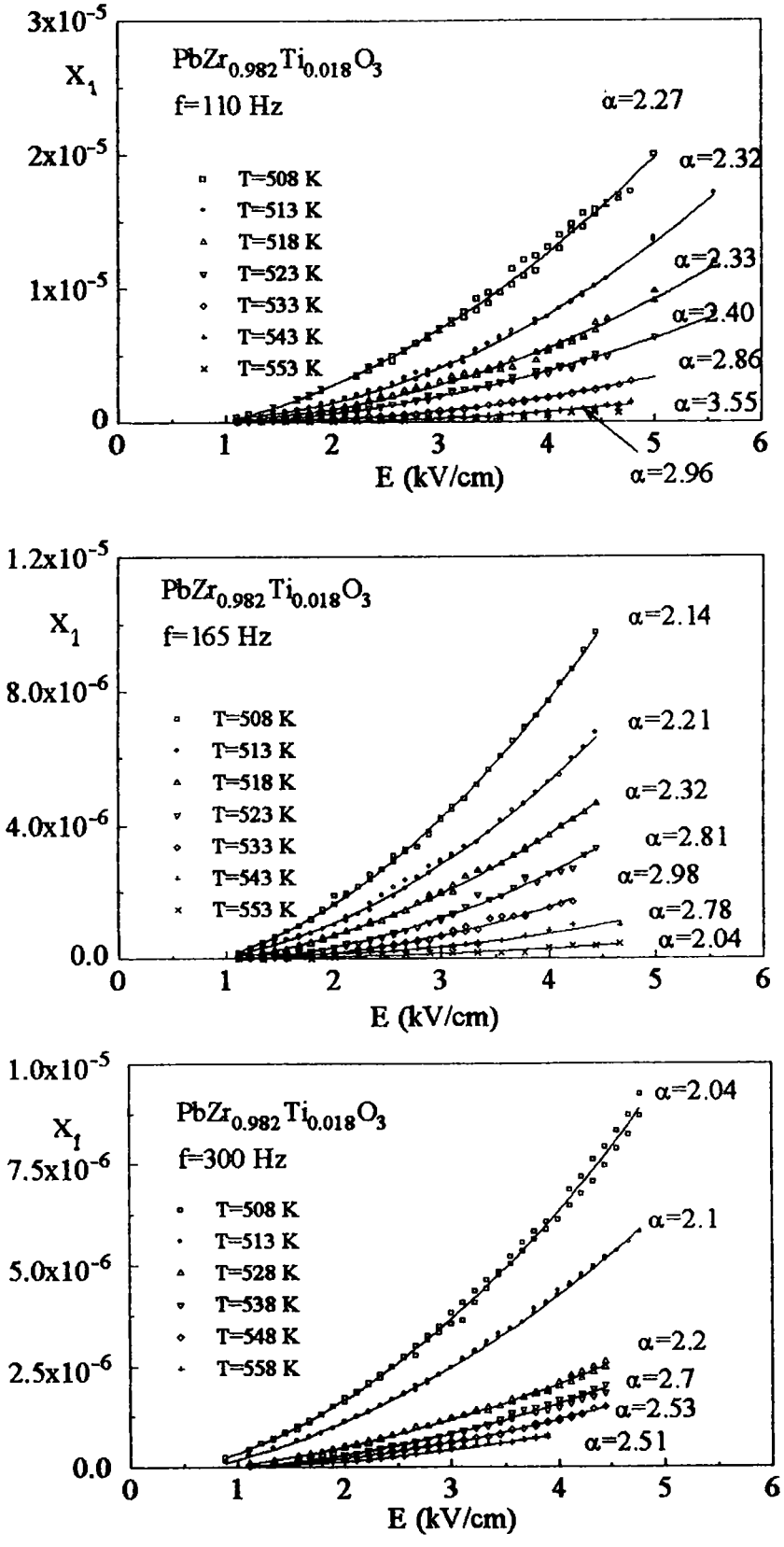


Figure 3.12. Strain electric field dependencies for $PbZr_{0.982}Ti_{0.018}O_3$ at three measuring frequencies and different temperatures in the paraelectric phase.

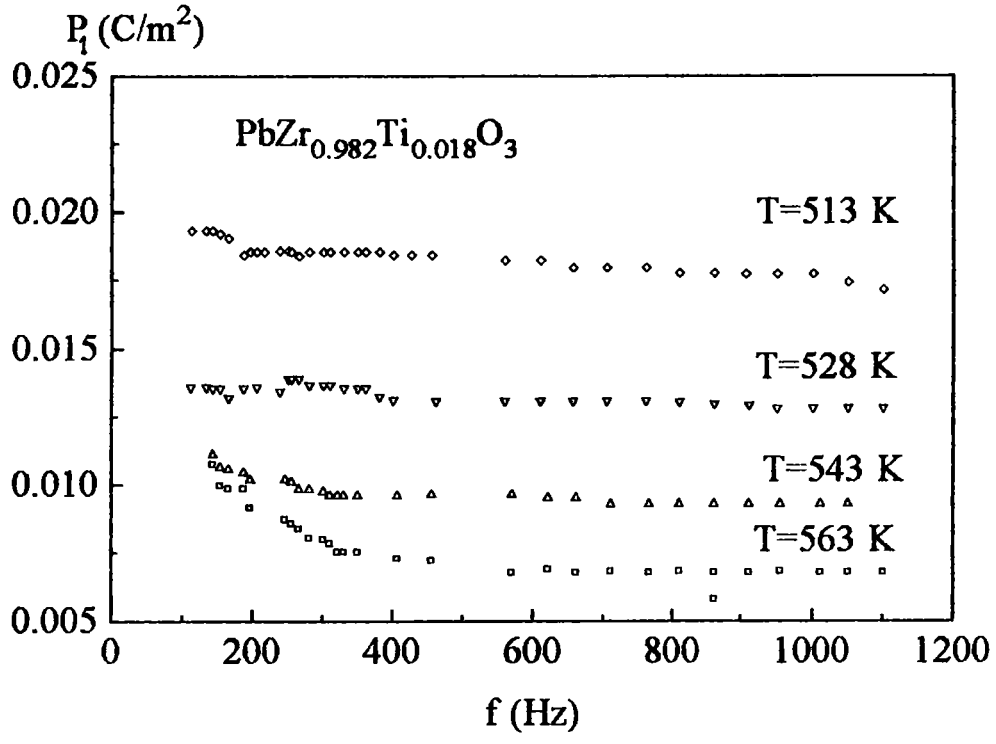


Figure 3.13. Temperature-frequency dependence of polarization P_1 for $PbZr_{0.982}Ti_{0.018}O_3$.

3.3.3. Electrostriction in $PbHfO_3$ and PHT

A completely different behaviour than the one described for $PbZrO_3$ and PZT was observed for lead hafnate and lead hafnate doped by $PbTiO_3$ - $PbHf_{0.98}Ti_{0.02}O_3$. Although on the basis of dielectric measurements some relaxations in the region of low frequencies were detected (see par 2.3.3.) the electromechanical measurement showed that the electrostriction is not correlated to any of the observed relaxations. For both of samples the $x_1(E_1)$ relation is always quadratic (in the limits of errors) and polarisation P does not depend on frequency as was shown in Figures 3.14 - 3.17.

The electrostrictive coefficients Q_{11} which are presented in Figure 3.18 for both samples $PbHfO_3$ and PHT are according to the theoretical predictions, temperature independent and take values typical for ferro/antiferroelectrics material of perovskite type (Yamanda, 1972).

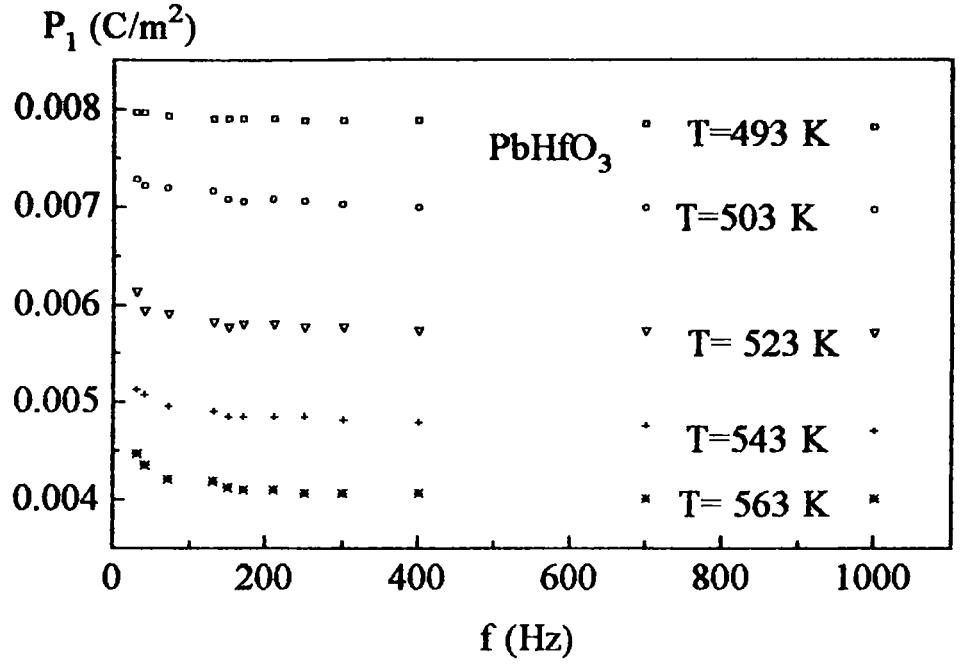


Figure 3.14. Temperature-frequency dependence of polarization P for $PbHfO_3$.

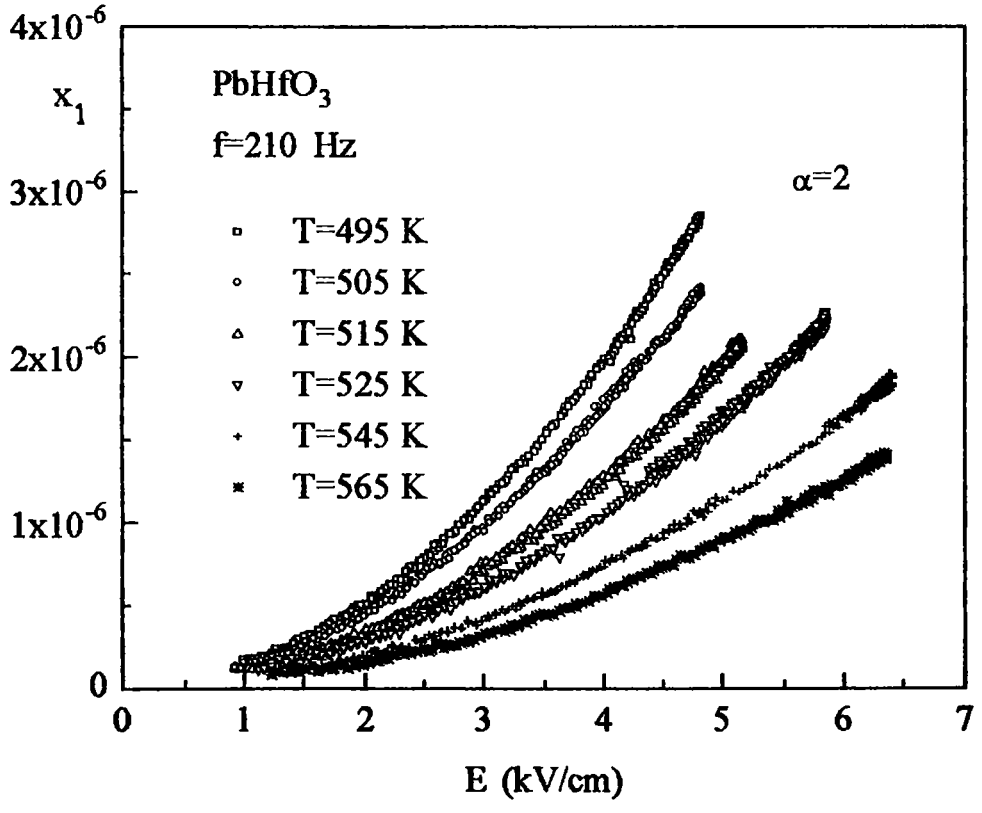


Figure 3.15. Strain electric field dependence for $PbHfO_3$ at one chosen frequency and different temperatures from the paraelectric phase.

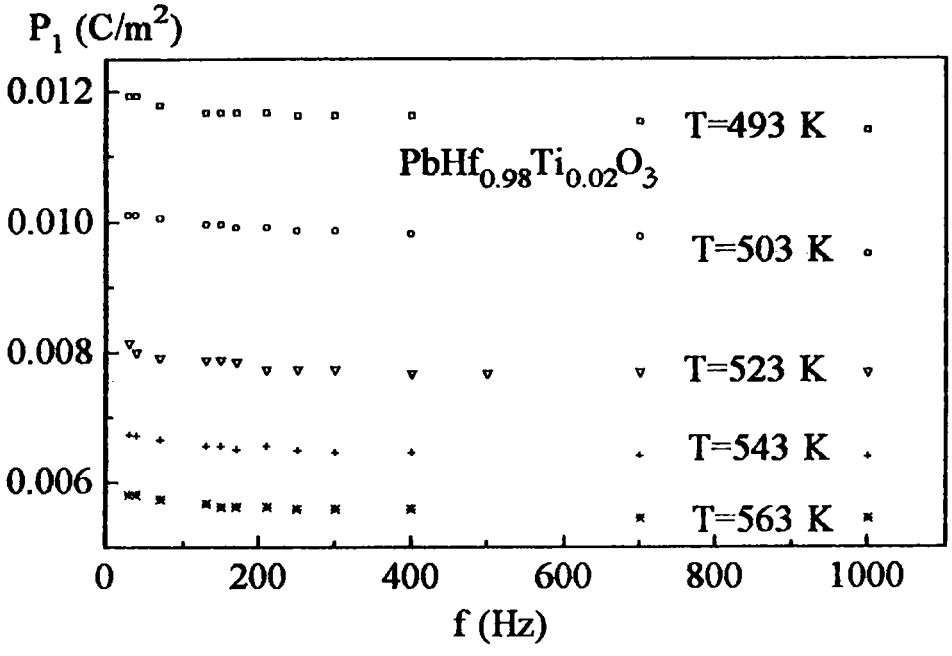


Figure 3.16. Temperature-frequency dependence of the polarization P for $PbHf_{0.98}Ti_{0.02}O_3$.

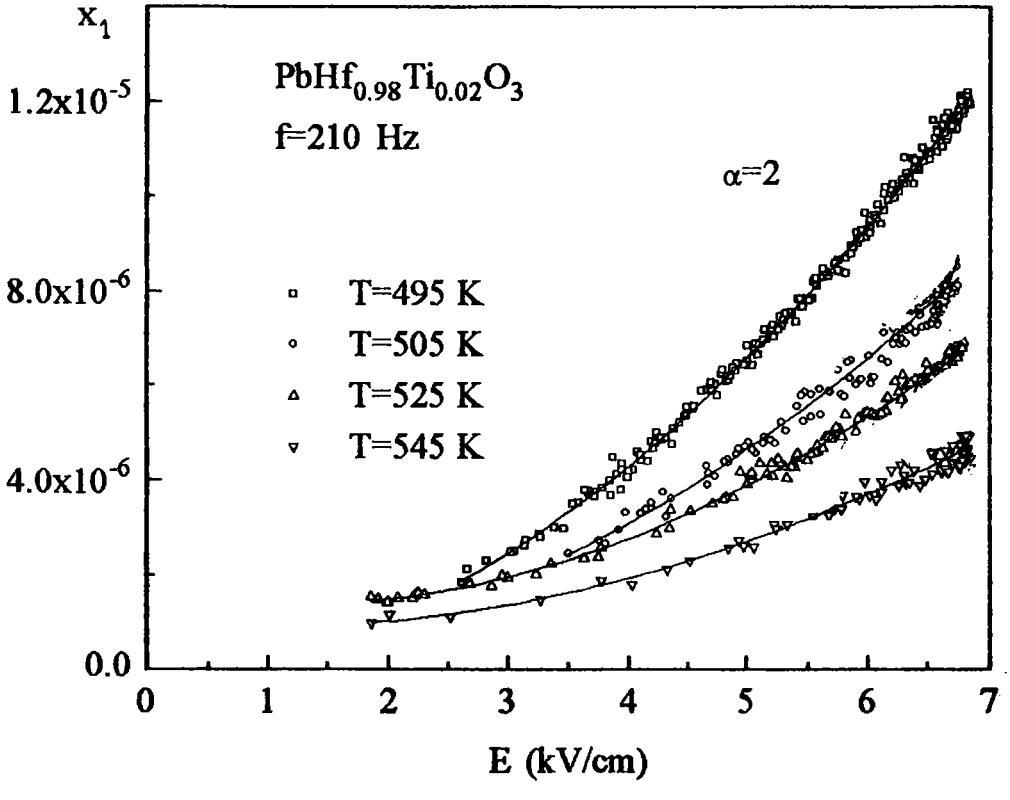


Figure 3.17. Strain electric field dependencies and $PbHf_{0.98}Ti_{0.02}O_3$ at the frequency 210 Hz and at different temperatures from the paraelectric phase.

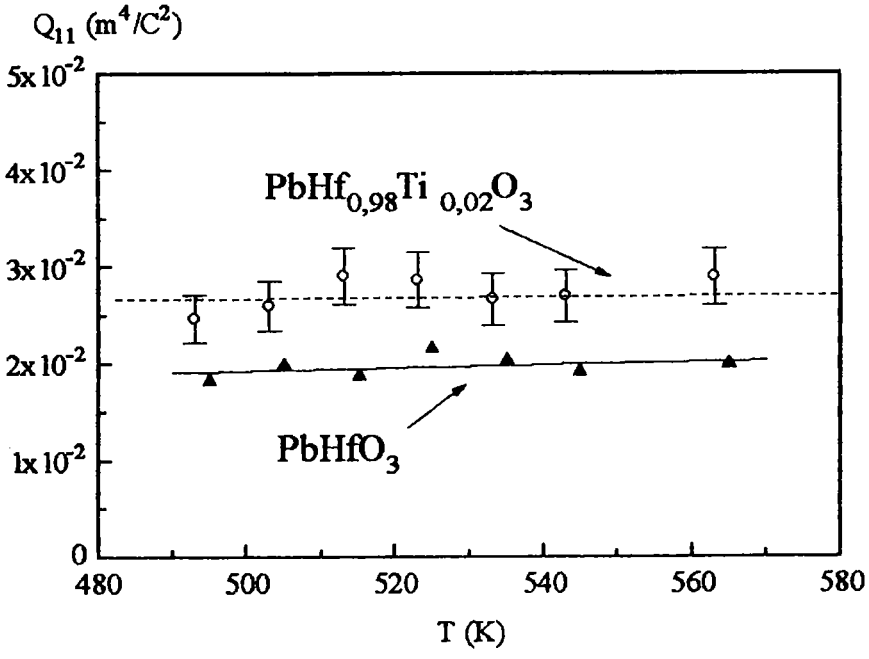


Figure 3.18. Temperature dependence of the electrostrictive coefficients Q_{11} measured at frequency 210 Hz for $PbHfO_3$ and $PbHf_{0.98}Ti_{0.02}O_3$ single crystals in the paraelectric phase.

3.4. DISCUSSION - ELECTROSTRICTION AND LOW-FREQUENCY DIELECTRIC RELAXATIONS

Case of pure lead zirconate and PZT compositions

The experiment showed, that in the frequency range where the dipolar relaxation was evidenced by dielectric experiments the electrostrictive strain in $PbZrO_3$ increases at low frequencies. On the basis of the data from Figure 3.5 the calculation of the difference between strain measured below (40 Hz) and above (200 Hz) dipolar relaxation showed that the main share (~90 %) in the x_1 at low frequencies came from the change of dipole orientation in the external electric field. It means that in the alternating electric field of frequency ω ($\omega=2\pi f$) the dipoles orientation varies with frequency 2ω, i.e. in the same way as electrostrictive vibrations of induced polarization. For this reason the strain-electric field relation should be modified to the form $x_1 = M_{11}(E_1)\cdot E_1^2$ for example. However, not only electric dipole can give a 2ω response while being excited at ω. One can introduce a non-linear behaviour of the susceptibility versus electric field, or to consider the defect elastic quadrupoles which would interact with elastic waves and change the electrostrictive

interaction. In this case the electric dipoles and elastic quadrupoles, which are both related to the defects, should have the same frequency spectrum. (Sommer et al., 1991; Kleeman et al, 1991)

In a frequency region above the dispersion the share of dipoles in the strain is switched off and the vibrations of the sample are purely electrostrictive ($x_1(E_1) = M_{11} \cdot E_1^2$, M_{11}=const), i.e., the strain-electric field relation is quadratic (Figure 3.5).

For the sample $PbZrO_3$ for which the transient phase occurs, in which no dispersion was found, the variation in the electrostrictive strain with frequency is inconspicuous.

As possible explanation of the magnitude of electrostrictive coefficients above the dispersion region a crystallographic rigid-ion model which explains the relationship between Q_{11} and the degree of the ordering of the structure, proposed by Uchino et al. (1980b), can be transformed into our situation.

The main idea is that the densely packed structure in the ordered perovskites gives much larger strain than disordered "rattling" structure. For $PbZrO_3$ the concentration of defects in any sublattice made the structure more loose and that is why the electrostrictive coefficient decreases from $Q_{11} \cong 2.0 \cdot 10^{-2}$ m^4/C^2 in condensed $PbZrO_3$ without transient phase to $Q_{11} \cong 1.2 \cdot 10^{-2}$ m^4/C^2 in $PbZrO_3$ exhibiting the above phase and possessing higher defect concentration.

Similar situation can be observed in PZT compounds. In both investigated samples $PbZr_{0.97}Ti_{0.03}O_3$ and $PbZr_{0.982}Ti_{0.018}O_3$ the measurements of polarisation P_1 and strain x_1 in function of frequency have proved the clear correlation between the electromechanical properties and dielectric relaxation observed in this compounds which is evidenced in Figures 3.10 - 3.13. The measurements made on PZT compounds can be thus treated as the evidence that the relaxation observed in $PbZrO_3$ single crystal with one phase transition below 10 kHz and PZT compounds doped by small amount of Ti, is of the same physical nature.

<u>Lead hafnate and lead hafnate doped by Ti.</u>

The measurements showed that the behaviour of strain-electric field relation in both investigated samples is quadratic i.e. the vibrations of the sample in the external electric field are purely electrostrictive. Polarization P_1 is not frequency dependent except small increase at the range of few Hz's. It should be pointed out that the electrostrictive

measurements were performed at high electric field strength comparing to that used in the dielectric dispersion tests (0.2 and 10 kV/cm respectively). Moreover, the ε value - and also the polarization P_1 - was calculated from the $P_1(E_1)$ relation taken in the Sawyer-Tower setup. Using conductivity compensation this relation was found to be linear in the whole range of temperature and electric field strength used and ε' values could be thus easily determined. These values of ε' were not however so huge as those obtained from dielectric dispersion measurement but comparable to those detected from ε'(T) at 1 kHz. It would mean that in the frequency range used (<400 Hz) the electristrictive strain is not influenced by the lowest relaxation found in $PbHfO_3$. It would also mean that this LFD (Low Frequency Dispersion) is connected with „induced" - rather than „intrinsic" - conductivity connected with the presence of surface layers. From the other hand it means that in the case of $PbZrO_3$, in which dielectric ($P_1(f)$ and ε'(f)) and electrostrictive dispersion occur in the same frequency range, the relaxation is of bulk character.

The second LFD found in $PbHfO_3$ and attributed to the bulk appears at considerably higher frequency (above 1 kHz). That is why the electrostrictive response measured only up to 400 Hz was unable to show any dispersion. These results for both $PbZrO_3$ and $PbHfO_3$ seem to prove the hypothesis that these relaxations are of bulk character. They are connected with the presence of defects which act as localised dipoles (hopping ions) and in this way can influence - as it is clearly seen in $PbZrO_3$ - the mechanical properties of the lattice.

In $PbHfO_3$ as well as PHT no variation of the electrostrictive coefficient with temperature have been observed and Q_{11} values are respectively $2 \cdot 10^{-2}$ m^4/C^2 and $2.6 \cdot 10^{-2}$ m^4/C^2 and are almost equal to coefficient values for other ferro- or antyferroelectric ABO_3 perovskites.

Appendix

In ordinary dielectrics the application of an electric field causes a stress due to the electric attraction between the oppositely charged plates on a condenser. For a sample with an area s and spacing d with the permittivity ε, the capacitance is $C = \frac{\varepsilon \cdot s}{d}$, charge - $Q = C \cdot V = \frac{\varepsilon \cdot s \cdot V}{d}$ and the force F between the plates is following (Jonscher, 1996):

$$F = \frac{Q^2}{2 \cdot \varepsilon \cdot s} = \frac{Q^2}{2 \cdot C \cdot d} = \frac{CV^2}{2d} \qquad 3.6$$

The stress $\sigma = \frac{F}{s}$ (force per unit area) can be written as:

$$\sigma = \frac{F}{s} = \frac{CV^2}{s \cdot 2d} = \frac{Q \cdot V}{s \cdot 2d} = \frac{\varepsilon V^2}{2d^2} = \frac{\varepsilon E^2}{2} \qquad 3.7$$

$$q = \frac{Q}{s} = \frac{\varepsilon \cdot V}{d}$$

It means that the stress is independent from the geometry and depends on the E^2 and ε. Taking typical value E=7 kV/cm, ε=3000 and $C \approx 10^{-11}$ [m^2/N] the strain is of the order of $7 \cdot 10^{-8}$ which is far lower than the observed electrostrictive deformation. Thus this effect can be neglected in the considerations.

4. RAMAN SPECTROSCOPY

4.1. THEORETICAL ASPECTS OF RAMAN LIGHT SCATTERING

Raman light scattering is often used for the investigation of dynamical aspects connected to structural phase transitions especially in crystalline materials developing of ferro- or antiferroelectric behaviour. Raman spectroscopy, by determination of the lattice vibrational frequencies provides valuable information on both static and dynamic microscopic phenomena accompanying the structural phase transitions. These vibrations are strongly influenced by the variations of the electronic polarization in a lattice of given crystal.

4.1.1. Scattering of light by material media

When a light beam of angular frequency ω_j propagates in material media, the oscillating electric field of the radiation causes forced vibrations of the electronic clouds associated to the atoms, ions or molecules. Oscillating electric dipoles are induced and each one will emit electromagnetic waves in all directions.

Three physical phenomena are associated with the scattering light:

- Rayleigh scattering or quasi-elastic scattering in which the frequency of the scattered light is the same (or nearly the same) as the incident one,
- inelastic scattering by acoustic phonons which is also called Brillouin scattering,
- inelastic scattering by optical phonons, so called Raman scattering.

In the case of inelastic scattering, the frequencies of the scattered light are shifted with regard to incident light of about $\Delta\omega = 0.05 - 1$ cm^{-1} for Brillouin scattering and $\Delta\omega = 10 - 3000$ cm^{-1} for Raman effect, corresponding to the vibrational frequencies of the acoustic and optic phonons respectively.

4.1.2. Inelastic Raman light scattering.

Consider a monochromatic light beam of angular frequency ω_j incidenting on a crystal sample with a wave vector $\vec{k}_j$:

$$\vec{E}_j(\vec{r},t) = \vec{e}_j E_j \cos(\vec{k}_j \bullet \vec{r}_j - \omega_j t) \qquad 4.1$$

where $\vec{e}_j$ is the vector of polarization and E_j the amplitude of the electric field.

This radiation propagating in the crystal induces the dipole moment $\vec{p}$ which is related in a first-order approximation to the electric field $\vec{E}$ of the radiation by:

$$\vec{p} = \begin{bmatrix} \alpha_{xx} & \alpha_{xy} & \alpha_{xz} \\ \alpha_{yx} & \alpha_{yy} & \alpha_{yz} \\ \alpha_{zx} & \alpha_{zy} & \alpha_{zz} \end{bmatrix} \cdot \vec{E} \qquad 4.2$$

where α_{si} is the second order dielectric polarizability tensor which describes the anisotropic response of electronic clouds submitted to an oscillating electric field.

The scattering of the light is related to the existence of fluctuations in material media. The thermal agitation of the nuclei induces fluctuations in the components of α_{si}. The electronic polarizability can therefore be expanded in a power series of the normal phonon mode coordinates $Q_k(\vec{q},t)$:

$$Q_k(\vec{q},t) = Q_k^{(o)} \cos(\vec{q}_k \bullet \vec{r} - \omega_k t) \qquad 4.3$$

where $\vec{q}_k$ and ω_k is the wave vector and frequency of k^{th} phonon and $Q_k^{(o)}$ contain information of the polarisation of the vibrational mode k.

such as

$$\alpha_{si} = \alpha_{si}^{o} + \sum_k \alpha_{si}^{k} Q_k + \sum_k \sum_{k'} \alpha_{si}^{kk'} Q_k Q_{k'} \qquad 4.4$$

where:

$$\alpha_{si}^{k} = \left(\frac{\partial \alpha_{si}}{\partial Q_k}\right)_0 \text{ and } \qquad \alpha_{si}^{kk'} = \left(\frac{\partial^2 \alpha_{si}}{\partial Q_k \partial Q_{k'}}\right)_0 \qquad 4.5$$

α_{si}^{k} and $\alpha_{si}^{kk'}$ are the first and second derivatives of the components of the polarizability with respect to normal mode coordinates evaluated at the equilibrium position. They give rise to the first-order and second-order Raman scattering, respectively. We will restrict our analysis to the first-order scattering.

If a particular mode $Q_k(\vec{q},t) = Q_k^{(o)} \cos(\vec{q}_k \bullet \vec{r} - \omega_k t)$ induces fluctuations in the component α_{si} of the electronic polarizability in such a manner that it increases the polarizability in a half-cycle and decreases in the other half cycle then the polarizability is not null. This mode modulates the component α_{si} of the polarizability in the direction of its wave vector $\vec{q}$. A plane monochromatic light wave $\vec{E} = E_j \cos(\vec{k}_j \bullet \vec{r} - \omega_j t)$

transversing crystal gives rise to oscillating dipoles whose component in this direction is given by:

$$p_s = \alpha_{sj} E_j = \alpha^{\circ}_{sj} E_j \cos(\vec{k}_j \bullet \vec{r} - \omega_j t) + \alpha^{k}_{sj} E_j \cos(\vec{k}_j \bullet \vec{r} - \omega_j t) Q^{\circ}_k \cos(\vec{q} \bullet \vec{r} - \omega_k t) \quad 4.6$$

The first term of the above equation corresponds to the elastic Rayleigh scattering and the second one to the Raman scattering. This second term can be written as:

$$\frac{1}{2}\alpha^{k}_{sj} E_j Q^{\circ}_k \left\{ \cos\left[\left(\vec{k}_j - \vec{q}\right) \bullet \vec{r} - \left(\omega_j - \omega_k\right)t\right] + \cos\left[\left(\vec{k}_j + \vec{q}\right) \bullet \vec{r} - \left(\omega_j + \omega_k\right)t\right] \right\} \quad 4.7$$

or

$$\frac{1}{2}\alpha^{k}_{sj} E_j Q^{\circ}_k \left\{ \cos\left(\vec{k}_s \bullet \vec{r} - \omega_s t\right) + \cos\left(\vec{k}_{as} \bullet \vec{r} - \omega_{as} t\right) \right\} \quad 4.8$$

where

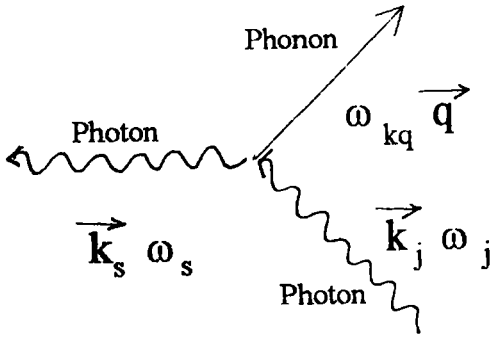
$$\begin{aligned} \omega_s &= \omega_j - \omega_k \\ \vec{k}_s &= \vec{k}_j - \vec{q} \end{aligned} \quad 4.9$$

and

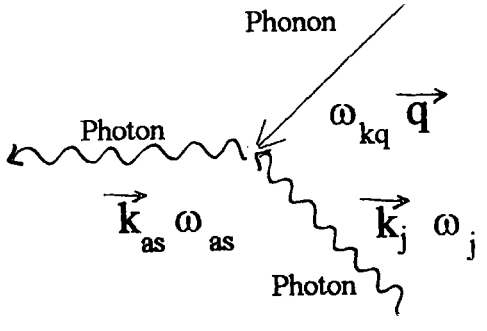
$$\begin{aligned} \omega_{as} &= \omega_j + \omega_k \\ \vec{k}_{as} &= \vec{k}_j + \vec{q} \end{aligned} \quad 4.10$$

The equations for frequencies and wave vectors express the energy and momentum conservation associated to the Stokes (s) and anti-Stokes (as) scattering of photons by phonons.

In both cases, an incident photon of angular frequency ω_j and wave vector $\vec{k}_j$ is absorbed, a phonon of frequency ω_k and wave vector $\vec{q}$ is created or destroyed and a scattered photon of frequency ω_s and vector $\vec{k}_s$ is emitted.



Stokes process



Antistokes process

In the case of polar crystals the macroscopic electric field which accompanies the polar vibrations also induces fluctuations in the polarizability. We have to add a new kind of derivative in the expression of polarizability such as:

$$\alpha_{sj} = \alpha^{o}_{sj} + \sum_{k} \alpha^{k}_{sj} Q_k + b_{sjn} E_n \qquad 4.11$$

where:

$$b_{sjn} = \left(\frac{\partial \alpha_{sj}}{\partial E_n} \right) \qquad 4.12$$

The last component is the electronic contribution to the electrooptic constants which describes the modulation of the polarizability by the macroscopic electric field E_n.

In scattering experiments using a visible light ($\lambda \approx 5000$ Å), the frequency of incident light is very close to the scattered light frequency ω_s. Therefore the modulus of the wave vector of the scattered light is very close to that of the incident $|k_s| \approx |k_j| \approx 2 \cdot 10^5 cm^{-1}$. From the conservation of momentum it is easy to show that:

$$|q| = 2|k_j| \sin \frac{\theta}{2} \qquad 4.13$$

Then the maximum wave vector of a phonon which can be investigated is $|q| = 2|k_j| \cong 4 \cdot 10^5 cm^{-1}$. Since the wave vector of the first Brillouin zone cannot be greater than the dimension of the first Brillouin zone $|\vec{q}| \approx 10^8 cm^{-1}$, this means that only phonons localised very closely to the first Brilloun zone centre ($\vec{q} \rightarrow 0$) can be observed in a first-order Raman scattering.

4.1.3. Symmetry analysis

As shown previously, only vibrations with a wavelength greater than λ_k=5000 Å can be observed in a first-order Raman scattering. Therefore in order to determine by Raman scattering the symmetry of the investigated modes, we have to consider only those modes for which the wave vector $\vec{q}$ =0. Each vibration mode Q_j is associated with one irreducible representation Γ_j of the point group of crystal. To find the symmetry of vibrational mode, we need to decompose the reducible representation Γ_{vib} of the Cartesian co-ordinates of the nuclear displacements as a sum of Γ_j.

$$\Gamma_{vib} = \sum_j a_j \Gamma_j \qquad 4.14$$

where a_j is the number of times the representation Γ_j appears in the decomposition Γ_{vib}. The coefficient a_j can be calculated using the characters $\chi^{\Gamma}(R)$ of the representation Γ_{vib}.

$$a_j = h^{-1} \sum_R \chi^j(R)\chi^{\Gamma}(R) \qquad 4.15$$

where: h - is the number of symmetry elements of the point group,

R - represents the elements of symmetry of the group,

$\chi^j(R)$ - are the characters of the representation Γ_j,

$\chi^{\Gamma}(R)$ - is the character of the representation Γ_{vib} which can be calculated by the expression:

$$\chi^{\Gamma}(R) = \sum_i \pm b_k(1+2\cos\theta_R) \qquad 4.16$$

The above sum is done over all nuclei i of the unit cell. The sign + or - indicates if the symmetry element R is a pure rotation of an angle θ_R or if R is a rotation followed by an inversion symmetry operation. The coefficient b_k takes value 1 if nuclei after the symmetry operation are carried to the same equivalent positions in the net and 0 otherwise.

Let us consider the above analysis in practice taking as an example the orthorhombic symmetry of two antiferroelectric crystals $PbZrO_3$ and $PbHfO_3$ at room temperature in A_1 phase.

Table 4.1. Table of characters for D_{2h}^9 space group.

D_{2h}^9	E	$C_2(z)$	$C_2(y)$	$C_2(x)$	i	$\sigma(x,y)$	$\sigma(x,z)$	$\sigma(y,z)$	Selection rules
A_g	1	1	1	1	1	1	1	1	$\alpha_{xx}\alpha_{yy}\alpha_{zz}$
B_{1g}	1	1	-1	-1	1	1	-1	-1	R_z α_{xy}
B_{2g}	1	-1	1	-1	1	-1	1	-1	R_y α_{xz}
B_{3g}	-1	-1	-1	1	1	-1	-1	1	R_x α_{yz}
A_u	1	1	1	1	-1	-1	-1	-1	
B_{1u}	1	1	-1	-1	-1	-1	1	1	T_z
B_{2u}	1	-1	1	-1	-1	1	-1	1	T_y
B_{3u}	1	-1	-1	1	-1	1	1	-1	T_x
χ_R^{Γ}	3	-1	-1	-1	-3	1	1	1	

These crystals belong to the D_{2h}^9 space group. The table of characters of the corresponding D_{2h}^9 space group is presented in Table 4.1.

With this table, in which we added the calculated characters of the irreducible representation Γ_{vib} and according to the previously quoted consideration it is possible to calculate the number of the vibrational modes.

$$\Gamma_{vib} = 16A_g + 8B_{1g} + 12B_{2g} + 12B_{3g} + 4A_u + 20B_{1u} + 24B_{2u} + 24B_{3u} \qquad 4.17$$

4.1.4. Selection rules for Raman scattering

From the equation 4.6, it is clear that the induced dipoles responsible for Raman scattering associated with the frequency ω_k will be zero unless at least one of the components of the derived polarizability tensor α_{ai}^k is non-zero:

$$\alpha_{ai}^k = \left(\frac{\partial \alpha_{ai}}{\partial Q_k}\right)_0$$

Thus the condition for Raman activity is that, for at least one component of the polarizability tensor, a plot of that component against the normal coordinate must have non-zero gradient at the equilibrium position. The corresponding condition for infrared activity is that at least one of the dipole moment component derivatives with respect to the normal coordinate Q_k taken at the equilibrium position should be non-zero.

Based on this selection rule, we can extract from the above presented symmetry analysis those vibrational modes which will be active for the space group in consideration:

$$\Gamma_{vib\text{-}Raman} = 16A_g + 8B_{1g} + 12B_{2g} + 12B_{3g} \qquad 4.18$$

4.1.5. Selection rules from a quantum-mechanical point of view.

Raman scattering process involves the absorption of an incident phonon of frequency ω_j, the emission of a scattered phonon of frequency $|\omega_j - \omega_{kq}|$. In other words, the incident photon induces an electronic transition from an initial state $|o,i\rangle$ to a virtual state $|v\rangle$, and a scattered photon is emitted when the electrons undergo a transition from the virtual state $|v\rangle$ to the final state $|o,s\rangle$ (the first index in the ket corresponds to a set of electronic

quantum numbers, and the second one specifies a vibrational level). A Raman transition occurs if electric dipole matrix between the initial and virtual states, and between the virtual and final states that is $\langle o,i|er|v\rangle\langle v|er|o,s\rangle \neq 0$. Since Raman transition involves two electronic dipoles, the phonon Q_k created or destroyed must belong to an irreducible representation present in the direct product of representations that transform like the components of a vector. Therefore Raman scattering occurs if the phonon Q_k belongs to an irreducible representation which contains as basis functions bilinear terms x^2, y^2, z^2, xy, yz and zx.

If the crystal point group contains a centre of symmetry operation, its irreducible representations have odd or even parity representations. Therefore the same phonon cannot appear in both Raman and infrared spectra. This is called the mutual exclusion principle. Only in piezoelectric crystals a phonon can appear simultaneously in the Raman and infrared spectra.

4.1.6. The temperature dependence of Raman intensities

The intensity of the scattered light in Stokes and anti-Stokes processes which correspond to the creation and annihilation of the phonon of the ω_k frequency and radiation of the light beam of frequency ω_s, following Poulet & Matieu (1970) is presented in following way:

$$\begin{aligned} I_s &\propto (\omega_j - \omega_k)^4 (n+1) \\ I_{as} &\propto (\omega_j + \omega_k)^4 n \end{aligned} \qquad 4.19$$

where factor:

$$n(\omega) = \frac{1}{\exp\frac{\hbar\omega_k}{k_B T} - 1} \qquad 4.20$$

is so-called Bose-Eistein temperature factor.

Comparing the Stokes and anti-Stokes intensities of the scattered light we get:

$$\frac{I_{as}}{I_s} \propto \frac{(\omega_j - \omega_k)^4}{(\omega_j + \omega_k)^4} \exp\left(-\frac{\hbar\omega_k}{k_B T}\right) \qquad 4.21$$

Because $\omega_j \rangg \omega_k$, then the $\frac{(\omega_j - \omega_k)^4}{(\omega_j + \omega_k)^4} \approx 1$, and the relation 4.21 is equal:

$$\frac{I_{as}}{I_s} \propto \exp\left(-\frac{\hbar\omega_k}{k_B T}\right) \qquad 4.22$$

From the equation 4.22 it is evident that at very low temperatures the values of the anti-Stokes intensities will be considerably lower than the Stokes intensities.

4.2. THE LYDDANE-SACHS-TELLER RELATION

Lyddane-Sachs-Teller relation (LST) firstly derived by Lyddane et al (1941) (for a double ionic crystal) is the relationship between dielectric permittivity $\varepsilon(0)$ (static dielectric permittivity) and $\varepsilon(\infty)$ (dielectric permittivity at high frequencies) and the longitudinal ω_L and transverse ω_T optical long-wavelength lattice vibration frequencies in form:

$$\frac{\varepsilon(0)}{\varepsilon(\infty)} = \frac{\omega_L^2}{\omega_T^2} \qquad 4.23$$

This relation may be obtained by examining the Kramers-Kronig integral:

$$\varepsilon'(\omega) - \varepsilon(\infty) = \frac{2}{\pi}\int_0^\infty \frac{x\varepsilon''(\omega)dx}{x^2 - \omega^2} \qquad 4.24$$

where the variable of the integration x is taken along the real frequency axis, at two special frequencies.

The LST relation contains information that the dielectric constant at high and low frequencies contains the frequency ω_T (transverse-optic mode frequency) which is specified as a region where the absorption was peaked and a frequency ω_L (longitudinal-optic mode frequency) when the dielectric permittivity is zero. This is the LST relation for the classical oscillator. The extension of the LST relation to the case of a sum of classical oscillator modes can be done (Lines & Glass, 1977) and the result is:

$$\frac{\varepsilon(0)}{\varepsilon(\infty)} = \frac{|\omega_{L1}|^2 \cdot |\omega_{L2}|^2 \cdots}{\omega_{T1}^2 \cdot \omega_{T2}^2 \cdots} \qquad 4.25a$$

or

$$\frac{\varepsilon(0)}{\varepsilon(\infty)} = \frac{\prod_{i=1}^{n} |\omega_{Li}|^2}{\prod_{i=1}^{n} \omega_{Ti}^2} \qquad 4.25b$$

Using the above equation we find that in phase transition one or more transverse modes ω_T can approach zero (mode softening) giving contribution to the $\varepsilon(T)$ function which comes

directly from the lattice vibrations. The possibility of ω_L approaching infinity must be rejected following Cochran's discussion who considers a specific lattice-dynamic model (Cochran, 1960) in which mode frequencies cannot approach infinity since masses cannot approach zero nor force constants approach infinity. Thus the divergence in ε(T) near the phase transition may be caused by either higher-frequency peak approaching zero or by so-called central peak. The most likely situation would be for the high-frequency peak to decrease its frequency mode forming a central peak when ω_T approaches zero. The occurrence of central peak does not imply necessary Debye dispersion. Any dielectric spectrum with suitable low-frequency form can be intrinsic to the material, resulting from coupling of allowed and forbidden modes, or it may be due to impurities.

4.3. CLASSICAL OSCILLATOR MODEL OF SPECTRAL FUNCTION

Consider a material composed of identical linear oscillators of reduced mass m, charge e, elastic constant β and friction coefficient f (Blinc & Žeks, 1974). Let E be the local field acting on each oscillator (we assume that the wave-length of the electromagnetic field is large with respect to the system).

The equation of the motion of each oscillator in the field direction x is:

$$m\ddot{x} = eE - \beta x - f\dot{x} \qquad 4.26$$

This equation is of the form:

$$m\ddot{x} + m\gamma\dot{x} + m\omega_o^2 x = eE \qquad 4.27$$

The second term involving the damping constant γ is put to include frictional effects and leads to absorption of energy from the electromagnetic wave.

Putting $E = E_o e^{i\omega t}$ to the equation 4.27, it can be solved to give the elementary dipolar moment:

$$\mu = ex = \frac{e^2}{m}\frac{E}{\left(\omega_o^2 - \omega^2 + i\omega\gamma\right)} \qquad 4.28$$

If N is the concentration of oscillators, then the polarization of the system is:

$$P = N\mu = Nex \qquad 4.29$$

and equation 4.30 takes the following form:

$$P = \frac{Ne^2}{m}\frac{E}{\left(\omega_o^2 - \omega^2 + i\omega\gamma\right)} \qquad 4.30$$

Since $P=\chi E$, where χ is the dielectric susceptibility, it can be written:

$$\chi = \frac{Ne^2}{m} \frac{1}{\left(\omega_o^2 - \omega^2 + i\omega\gamma\right)} \qquad 4.31$$

The susceptibility is thus a complex quantity and can be derived into real and imaginary parts:

$$\begin{cases} \chi' = \dfrac{Ne^2}{m} \dfrac{\omega_o^2 - \omega^2}{\left(\omega_o^2 - \omega^2\right)^2 + \omega^2\gamma^2} \\ \chi'' = \dfrac{Ne^2}{m} \dfrac{\omega\gamma}{\left(\omega_o^2 - \omega^2\right)^2 + \omega^2\gamma^2} \end{cases} \qquad 4.32$$

If we define the force of the oscillator as S_o:

$$S_o = \frac{Ne^2}{m\omega_o^2} \qquad 4.33$$

then we obtain a classical oscillator mode of strength S_o and damping γ:

$$\chi''(\omega) = \frac{\omega S_o \omega_o^2 \gamma}{\left(\omega_o^2 - \omega^2\right)^2 + \omega^2\gamma^2} \qquad 4.34$$

At this stage we have a spectrum defined by four parameters. ω_o is the frequency where χ'' is peaked as long as γ is not too large.

To summarise, the $\chi''(\omega)$ spectrum contains information on long-wave-length fluctuations of the polarization. Hence the spectra completely determine the dielectric function; once determined, they can be manipulated to fit equation 4.34 and if they do, the parameters ω_L and ω_T may be put into equation 4.25 to determine the ratio of dielectric constants.

4.4. THE EXPERIMENTAL CONDITIONS

The Raman scattering experiments were carried out on a Spex double monochromator for dispersion with a photon-counting readout system using a cooled RCA C31034 phototube for detection. The system was linked out with Datamate microprocessed controller and acquisition processor, and the data were stored on a floppy disk. As the excitation source the argon laser line of 5145 Å wave-length and helium neon laser line (6328 Å) were alternatively used. The low-temperature spectra were recorded with the crystal placed in

and Air-Product Displex cryostat driven by an automatic temperature indicator controller. For the measurements between room and high temperatures, the sample have been mounted in a temperature controlled furnace and the temperature was detected by a nickel chrome-nickel alloy thermocouple located near the sample. The whole system was arranged in the conventional 90° scattering geometry. The measuring set is schematically presented in Figure 4.1.

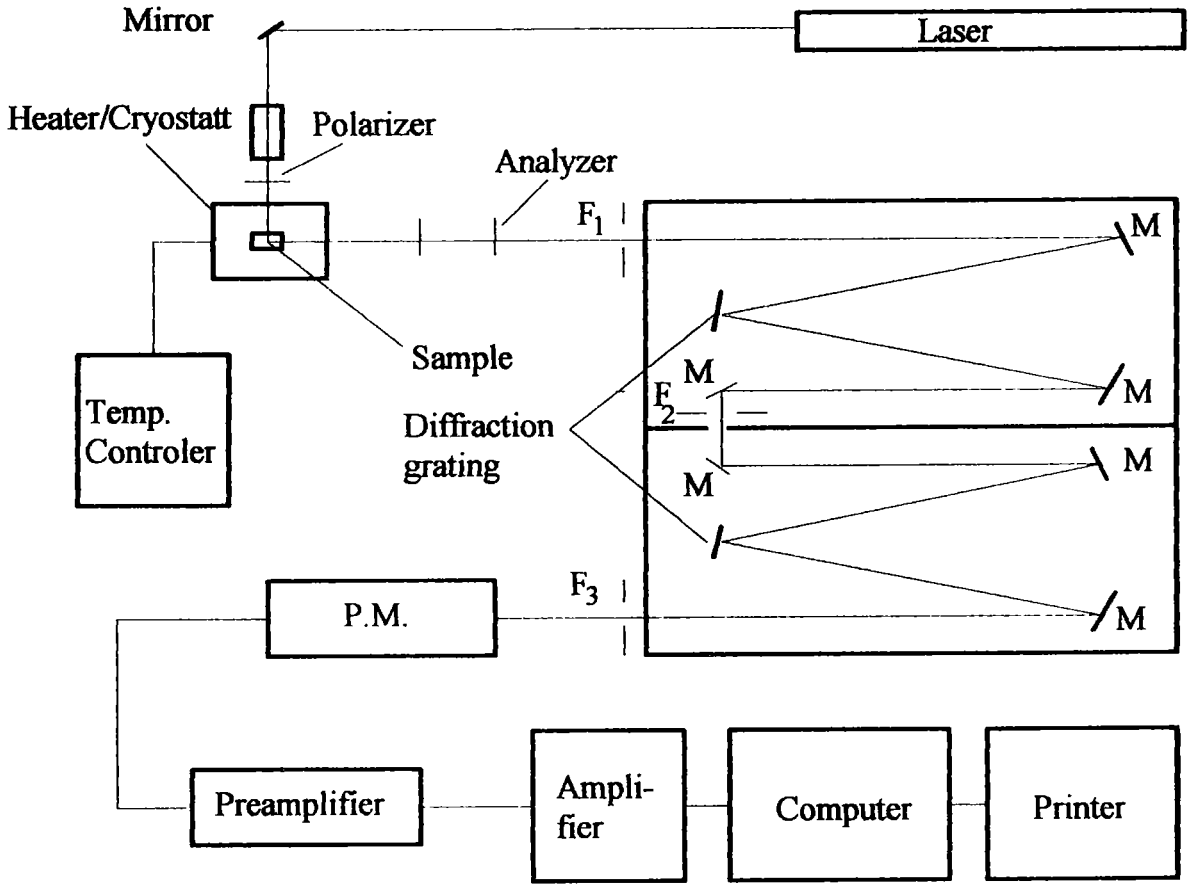


Figure 4.1. The layout for Raman scattering experiments.

The Raman scattering measurements were performed on the same crystals as those used in dielectric dispersion measurements. Details concerning the crystal growing are described in paragraph 2.2.1. Transparent crystals of $PbHfO_3$ and composition of $PbHf_{1-x}Ti_xO_3$ with x=0.04 were used for measurements. In the case of $PbZr_{1-x}Ti_xO_3$, concentration x was equal to 0.01. For the doped samples, the concentration x was established by X-ray microanalysis investigations.

Simultaneously to the Raman measurements and in order to have an accurate description of the phase transition temperatures, the variations of the dielectric susceptibility on cooling and heating were performed on a 1 MHz automatic capacitance bridge. The temperature dependencies ε'(T) of dielectric permittivity for pure $PbHfO_3$ and for $PbHf_{0.96}Ti_{0.04}O_3$ single crystals were already presented in the paragraph 2.3.3 in Figure 2.27 a and b. The ε'(T) dependence for $PbZr_{0.99}Ti_{0.01}O_3$ is presented in Figure 4.2 for comparison.

All the samples used in our experiments, revealed under a polarising microscope a polydomain structure in polar phases.

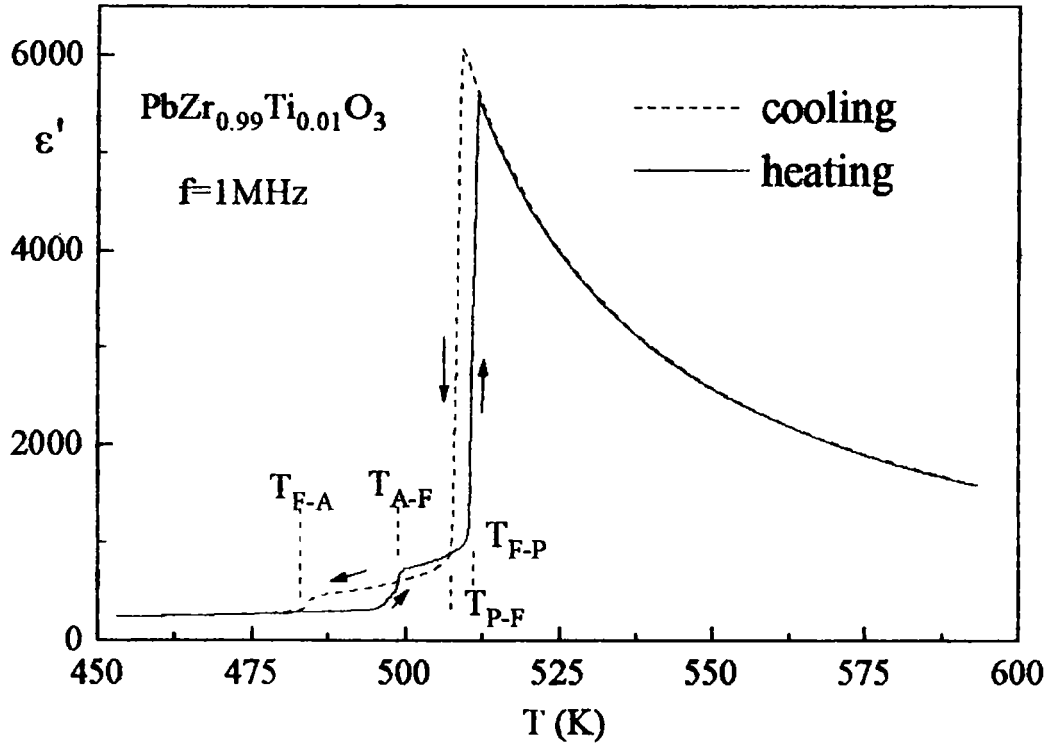


Figure 4.2. Temperature dependence of the dielectric permittivity for $PbZr_{0.99}Ti_{0.01}O_3$.

4.5. SYMMETRY ANALYSIS AND CALCULATIONS OF THE VIBRATIONAL MODES

4.5.1. Vibrational modes in $PbZrO_3$ pure and $PbZr_{1-x}Ti_xO_3$ (x<0.06)

It earlier studies at room temperature the $PbZrO_3$ crystal was supported to belong to orthorhombic antiferroelectric space groups Pba2 or Pbam (Sawaguchi et al., 1951).

Recently however Tanaka et al (1982), as well as Glazer et al (1993) studied the structure of $PbZrO_3$ in more details and described it as centrosymmetric Pbam (D^9_{2h})

The symmetry decomposition of the vibrational modes for this space group was already presented in the section 4.1.3. Thus the Pbam space group for perovskite $PbZrO_3$ is presented by a total number of 120 vibrational modes:

$$\Gamma_{vib} = 16A_g + 8B_{1g} + 12B_{2g} + 4A_u + 20B_{1u} + 24B_{2u} + 24B_{3u} + 12B_{3g} \quad 4.35$$

Three of these modes are acoustic modes and the others are optic modes. Using the selection rules for the Raman scattering only A_g, B_{1g}, B_{2g}, B_{3g} are Raman-active, while the modes described by index "u" are infrared-active. Then the number of Raman active vibrational modes reduces to 48.

The corresponding tensors of the polarizability corresponding to the particular modes are presented below:

$$A_g\begin{bmatrix} \alpha_{xx} & 0 & 0 \\ 0 & \alpha_{yy} & 0 \\ 0 & 0 & \alpha_{zz} \end{bmatrix} \qquad B_{2g}\begin{bmatrix} 0 & 0 & \alpha_{xz} \\ 0 & 0 & 0 \\ \alpha_{zx} & 0 & 0 \end{bmatrix}$$

$$B_{1g}\begin{bmatrix} 0 & \alpha_{xy} & 0 \\ \alpha_{yx} & 0 & 0 \\ 0 & 0 & 0 \end{bmatrix} \qquad B_{3g}\begin{bmatrix} 0 & 0 & 0 \\ 0 & 0 & \alpha_{yz} \\ 0 & \alpha_{zy} & 0 \end{bmatrix}$$

The cubic paraelectric phase, described by a Pm3m $\left(O^1_h\right)$ space group, is represented by 15 vibrational modes:

$$\Gamma_{vib} = 4F^{(3)}_{1u} + F^{(3)}_{2u} \quad 4.37$$

According to the selection rules, all these modes are not Raman-active and any first order structure, except the Rayleigh part, should not be observed in Raman scattering in the paraelectric phase.

For the PZT with small Ti concentration up to 0.06 the phase transition from cubic symmetry (P) (Pm3m - O^1_h) to an antiferroelectric (A) phase of orthorhombic symmetry (Pbam - D^9_{2h}) is realised via an intermediate F phase of R3m (C^5_{3v}) symmetry (usually called F^{ht}_R). This phase is represented by 10 vibrational modes. Decomposition of modes in particular phases appearing in $PbZr_{0.99}Ti_{0.01}O_3$ is shown in Table 4.2.

Table 4.2. Decomposition of the vibrational modes for $PbZr_{0.99}Ti_{0.01}O_3$

Phase	Paraelectric	Ferroelectric	Antiferroelectric
Symmetry	Cubic	Rhombohedral	Orthorhombic
Space group	Pm3m (O_h^1)	R3m (C_{3v}^5)	Pbam (D_{2h}^9)
Number of vibrational modes	15	10	120
Decomposition of vibrational modes	$4F_{1u}^{(3)} + F_{2u}^{(3)}$	$4A_1 + 5E + A_2$	$16A_g + 8B_{1g} + 12B_{2g} + 12B_{3g} + 4A_{1u} + 20B_{1u} + 24B_{2u} + 24B_{3u}$
Raman active modes	0	$3A_1 + 4E + A_2$	$16A_g + 8B_{1g} + 12B_{2g} + 12B_{3g}$

4.5.2. Vibrational modes in $PbHfO_3$ and $PbHf_{1-x}Ti_xO_3$ solid solutions.

Both $PbHfO_3$ and $PbHf_{1-x}Ti_xO_3$ system doped with small amount of $PbTiO_3$, both exhibit two temperature induced phase transitions (at 436 K and 484 K for $PbHfO_3$) . Doping of Ti shifts the lower phase transition several degrees towards lower temperatures (see Fig. 2.27). Both, the low temperature A_1 and the intermediate A_2 phases are antiferroelectric with orthorhombic structure. The P (paraelectric) phase exhibits cubic perovskite structure Pm3m (O_h^1).

The A_1 phase in $PbHfO_3$ was usually considered as isomorphous with that of $PbZrO_3$, so lets consider the symmetry of the A_1 phase in $PbHfO_3$ as centrosymmetric Pbam. In the symmetry analysis of the vibrational modes, the symmetry of the intermediate A_2 phase is not clearly defined. The possible space groups to which the system could belong are as follows: $P222_1$ (D_2^2), Pmm2 (C_{2v}^1), Pmmm (D_{2h}^{13}) or P222 (D_2^1) (see 1.2.3.). On the basis of the subgroups sequence analysis, the space group Pmmm (D_{2h}^{13}) can be excluded from the further considerations. The space groups $P222_1$ (D_2^2) and P222 (D_2^1) are described by the same kinds and number of the vibrational modes thus we can simplify the considerations into two most probable (C_{2v}^1 and D_2^2). In both cases all the vibrational modes are Raman active and their number should be equal to 120 unlike the low temperature phase A_1 in which only 48 modes are active. Hence the structural phase transition should be characterised by activation (on heating) of previously Raman silent phonon modes.

The theoretical group analysis of the vibrational modes in $PbHfO_3$ in the three phases A_1, A_2 and P using two assumptions of the A_2 phase is reported in Table 4.3.

Table 4.3. Decomposition of the vibrational modes for $PbHfO_3$

Phase	Paraelectric	Antiferroelectric		Antiferroelectric
symbol	P	A_2		A_1
space group	Pm3m (O_h^1)	Pmm2 (C_{2v}^1)	$P222_1$ (D_2^2)	Pbam (D_{2h}^9)
symmetry	cubic	orthorhombic		orthorhombic
number of $PbHfO_3$ in the unit cell	Z=1	Z=8		Z=8
number of vibrational modes	15	120	120	120
symmetry decomposition of vibrational modes	$4F_{1u}^{(3)} + F_{2u}^{(3)}$	$36A_1 + 12A_2 + 36B_1 + 36B_2$	$20A + 28B_1 + 36B_2 + 36B_3$	$16A_g + 8B_{1g} + 12B_{2g} + 12B_{3g} + 4A_{1u} + 20B_{1u} + 24B_{2u} + 24B_{3u}$
Raman active modes	0	all the modes		$16A_g + 8B_{1g} + 12B_{2g} + 12B_{3g}$

4.6. RAMAN SCATTERING LITERATURE DATA IN PURE $PbZrO_3$

In contrast with the number of dielectric structural and electromechanical investigations and certainly because of difficulties in obtaining crystals of sufficiently good quality for optical studies, the experimental Raman spectroscopy studies are rather scarce. Pasto and Condrate (1972) measured the Raman spectra on powders and multidomain single crystals of $PbZrO_3$ from room temperature to 250°C. They considered only the antiferroelectric-paraelectric transition and interpreted their results in comparison with the spectra for PbO and ZrO_2. Some Raman data on PZT solid solution are available but concern essentially results on ceramic samples with Ti greater than 0.10 (Bauerle & Pinczuk, 1976; Bauerle et al., 1974; Bauerle et al., 1977). In these PZT's in which the ferroelectric transient phase of the rhombohedral symmetry exists, the ferro-paraelectric phase transition was correlated to

an E(TO) mode which was found to soften with increasing temperature (and also the $PbTiO_3$ concentration).

Roleder et al.(1989) investigated the Raman spectra of pure $PbZrO_3$ and PZT with low Ti concentration using single crystals of sufficiently good quality, and related the Raman data to the structural phase transition sequence and especially to the existence of the intermediate phase in PZT.

Though the theory predict the existence of the soft mode in $PbZrO_3$ ($\vec{q} = 0$), this kind of behaviour was not found using the Raman spectroscopy method since no mode is Raman active in the paraelectric phase. Only a 130 cm^{-1} line detected at room temperature (in antiferroelectric phase) shifted slowly towards lower frequencies and might have been considered as a soft mode but was strongly overdamped when approaching transition to the intermediate and then to the cubic phase (Roleder et al., 1989). The purpose of this work was to perform the additional experiments on a $PbZr_{1-x}Ti_xO_3$ single crystals with x=0.01 of better quality in order to detect the changes of spectra in broad temperature range (from 10 K to 600 K) and especially near the phase transition points and mainly to analyse, using the systematic fitting procedure, the temperature dependence of subsequent vibrations and quasielastic diffusion. Special attention was paid to the paraelectric phase in which unexpected first order Raman scattering has been previously observed. The obtained results were analysed and compared to dielectric measurements and the phase transition mechanism was discussed.

4.6.1. Raman spectra for two kinds of $PbZrO_3$ single crystals.

In order to compare the complete Raman spectra for PZT samples, we present in first Raman spectra recorded for pure $PbZrO_3$ single crystal (Roleder et al., 1989). The non-polarised spectrum for $PbZrO_3$ recorded at room temperature is presented in Figure 4.3a. Figure 4.3b shows the Raman spectrum for the $PbZrO_3$ single crystal without transient phase which has been used before in this work in the dielectric dispersion measurements (below 10 MHz). It can be seen that the form of both spectra are similair but the differences can be seen in the positions of pariculair lines.

According to the analysis performed in Roleder et al. (1989) the spectra contain three main frequency regions: 0 - 200 cm^{-1} (I), 200 - 400 cm^{-1} (II) and 400 - 800 cm^{-1} (III) and which are common features of the oxide perovskite crystals families. The origin of these

regions can be analysed within the framework of the phonon dispersion behaviour known in the cubic phase of similar perovskite crystals.

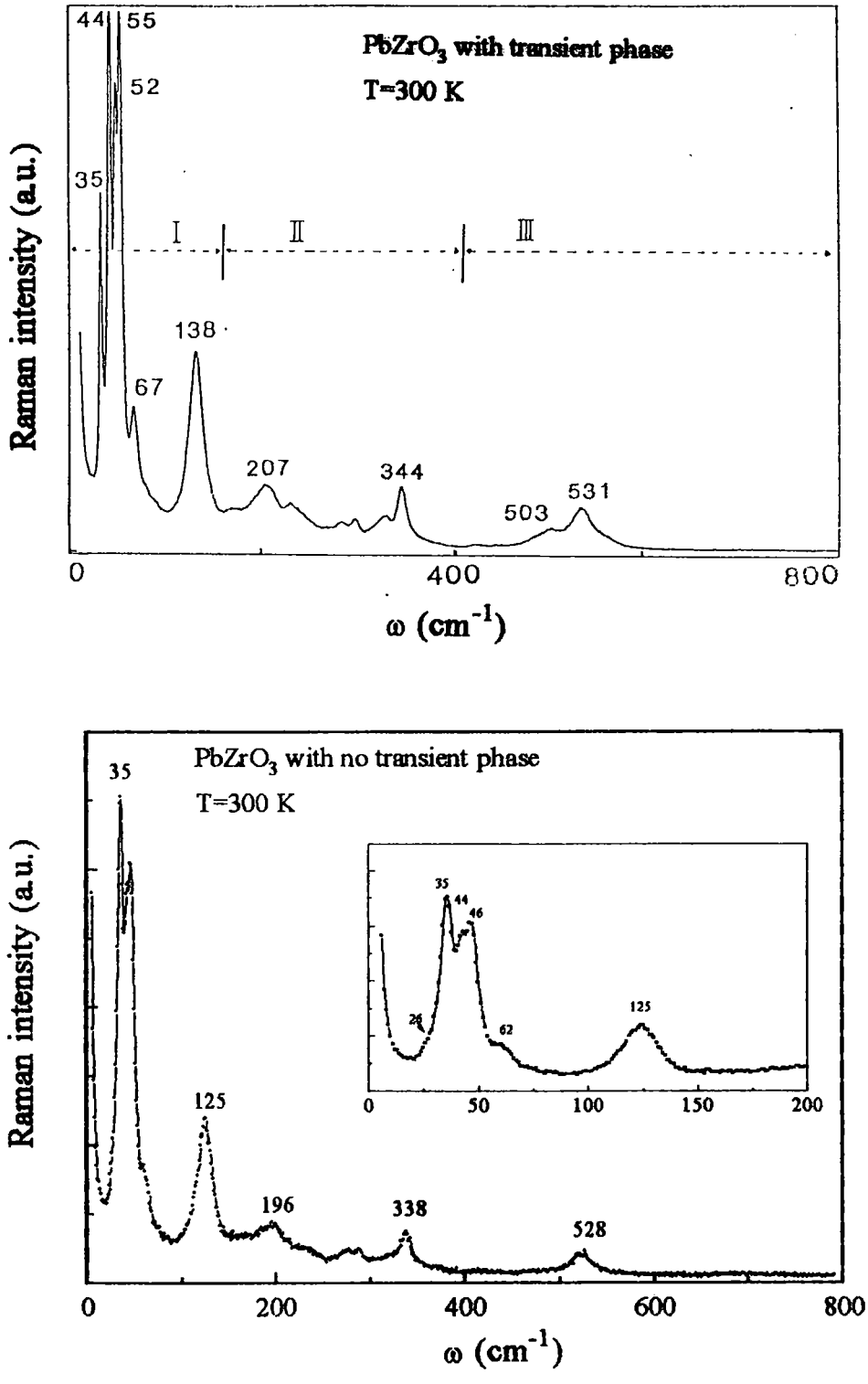


Figure 4.3. Raman spectrum for two kinds of $PbZrO_3$ single crystal at room temperature: (a) with the transient phase (Roleder et al., 1989), (b) without transient phase (this work).

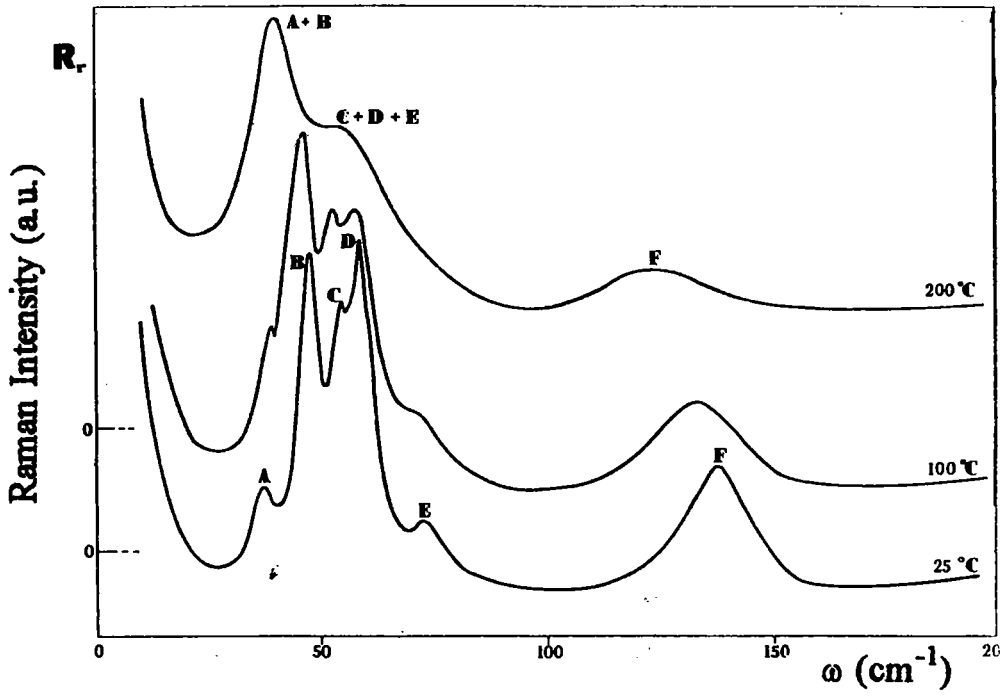


Figure 4.4. Evolution of the Raman lines in the antiferroelectric phase (Roleder, 1990)

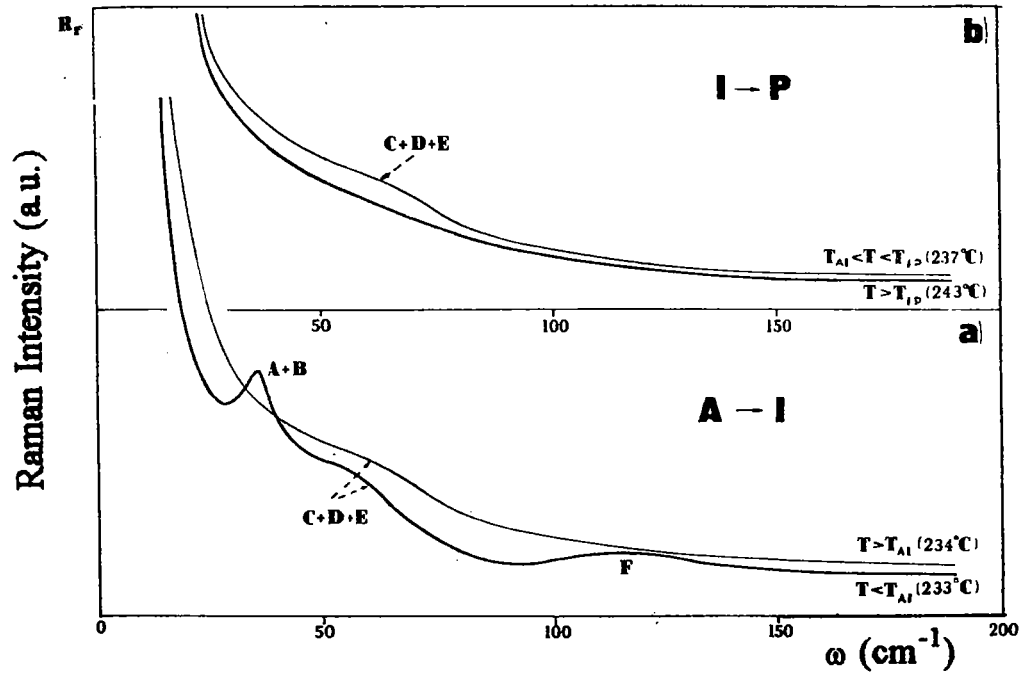


Figure 4.5. Changes of the Raman spectra near two phase transitions A-I (a) and I-P (b) in $PbZrO_3$ single crystal (Roleder, 1990).

The lowest-frequency range I (in Figure 4.3) contains lines of high intensity corresponding to the lowest-frequency optic and acoustic phonon branches activated by the

antiferrodistorsive transition leading to the antiferroelectric structure. The next two regions arise from the splitting and activation of the higher frequency phonons at this transition.

The evolution of the Raman spectra in the antiferroelectric phase is presented in Figure 4.4, and the behaviour of the Raman spectra near the phase transition points is represented in Figure 4.5. At the temperature T_{A-I} the lines marked as A, B and F disappear and the broad band C+D+E remains. At the temperature T_c this "broad band" (C+D+E) seems to disappear and slight changes of the quasielastic scattering above T_c can be only observed. (Fig. 4.5b).

4.7. EXPERIMENTAL RESULTS

4.7.1. Raman spectrum of $PbZr_{0.99}Ti_{0.01}O_3$ in the antiferroelectric phase

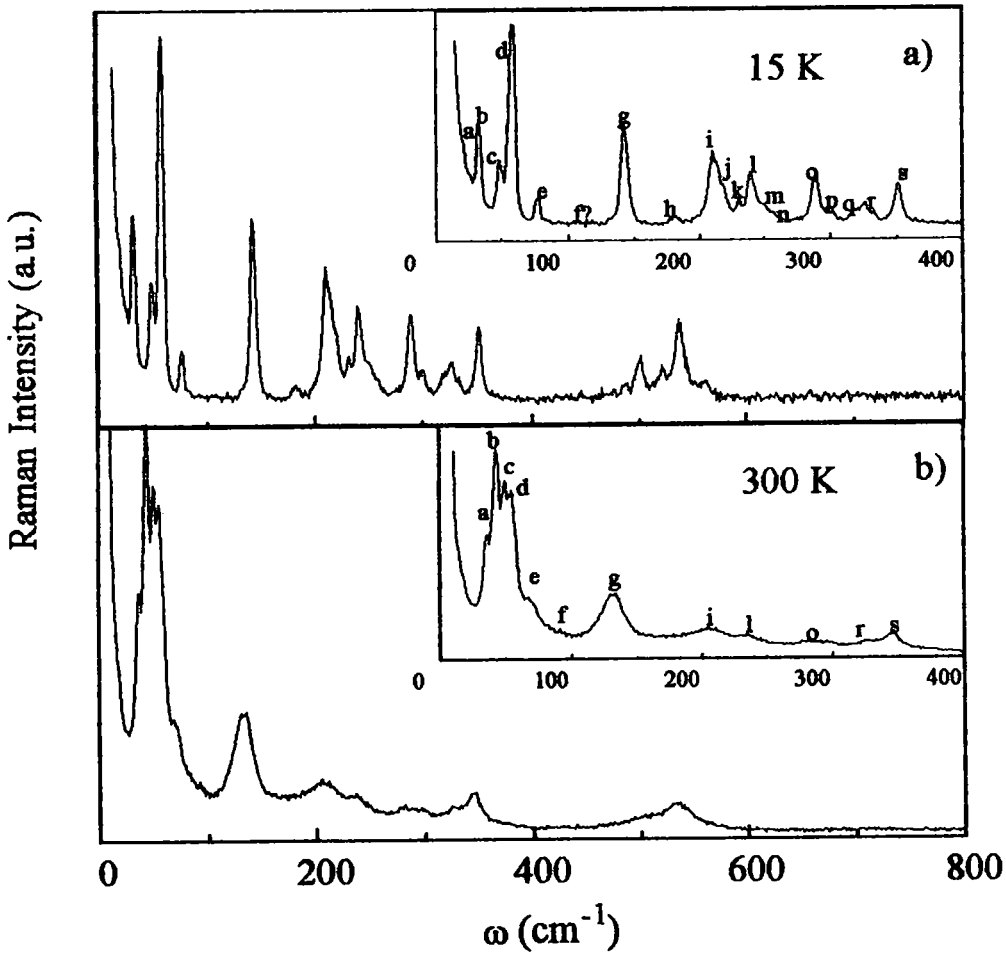


Figure 4.6. Raman spectra for $PbZr_{0.99}Ti_{0.01}O_3$ single crystal recorded at 15 K (a) and at room temperature (b).

Figure 4.6 compares the first-order Raman spectra recorded on a $PbZr_{0.99}Ti_{0.01}O_3$ single crystal at low (15 K) and at room temperature measured in frequency range 0 and 800 cm^{-1}. The analysis of the lines showed that the spectra in the antiferroelectric phase for the pure $PbZrO_3$ and $PbZr_{0.99}Ti_{0.01}O_3$ are almost the same.

By symmetry analysis, maximum 48 modes should be observed in the antiferroelectric phase in this crystal. The Raman spectra from 15 K to room temperature do not exhibit abnormal modification in the number of lines, their positions and width, and thus exclude existence of any additional phase transition below room temperature. In the A phase the lines show the normal increase of damping with increasing temperature and gradual shifting down in frequency of two lines marked in Figure 4.6 as *a* and *g*. This fact will be analysed in more detail in section 4.8.2. No other significant changes were observed in the spectra up to the A-F phase transition

4.7.2. The evolution of the Raman spectra near the A-F phase transition.

Figure 4.7 presents the evolution of the low-frequency Raman spectra (0 - 400 cm^{-1}) on heating towards the A-F phase transition (T_{A-F} ~ 490 K). Above T_{A-F} the Raman spectra contain a broad shoulder (see arrow in the Figure), which can consist of more than one line but strongly overdamped. Unfortunately because of this damping at higher temperature, it

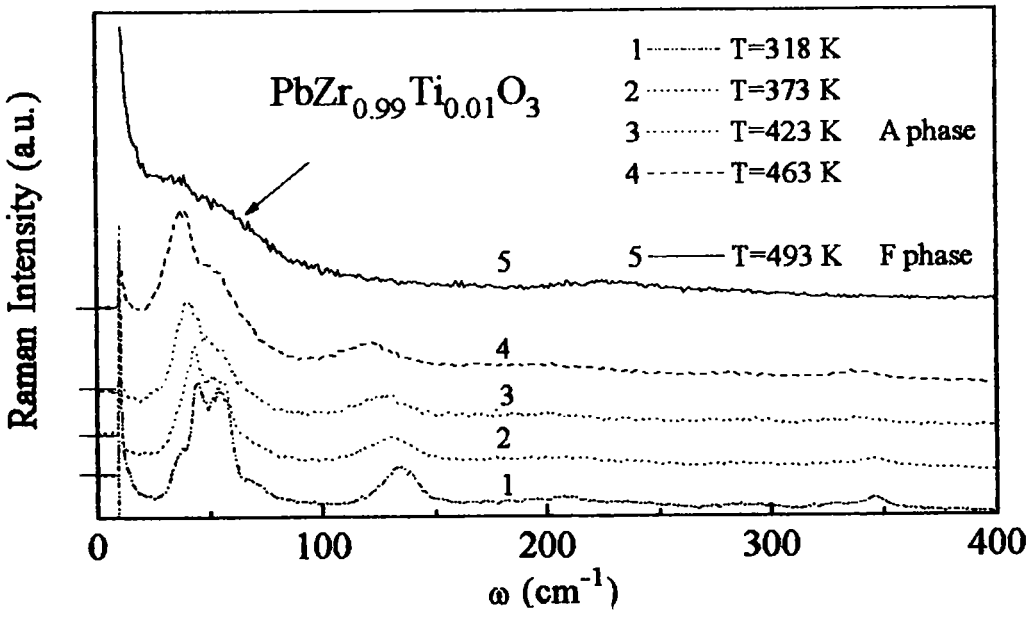


Figure 4.7. Raman spectra in A phase and near T_{A-F} phase transition

is difficult to distinguish directly from the spectra the number and exact positions of lines characteristic for the F phase. This work will be done on the basis of systematic fitting procedure described in the next paragraph.

4.7.3. Raman spectra at the F-P phase transition

The transition from the rhombohedral F phase to the cubic P phase is presented in Figure 4.8. As can be seen, at the F-P transition the Raman spectra do not show any deep modification. The characteristic broad shoulder observed in F phase remains present even up to temperatures far from the transition point (see inset.) (similar behaviour was also observed by Roleder et al. (1989)).

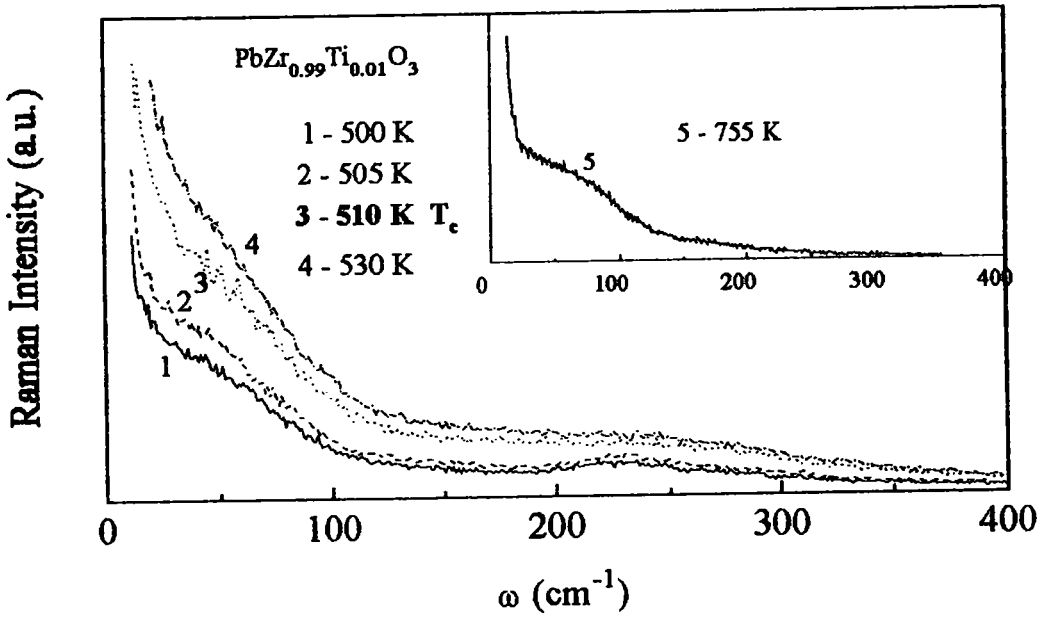


Figure 4.8. Changes of the Raman spectra near the F-P phase transition. An inset shows the broad shoulder which exists even deeply in paraelectric phase.

The most significant modification in these spectra is growing of the global scattering intensity in low frequency range, when approaching T_c from low temperature side.

Furthermore it should be stressed that clear decrease of this intensity takes place just several degrees above T_c, taken as a maximum of the dielectric permittivity measured simultaneously during spectra detection. This phenomenon can be due to the changes in the quasielastic scattering intensity around phase transition, although the share of the *broad shoulder* in the P phase cannot be completely omitted.

4.7.4. Raman spectra around antiferroelectric phase transition in $PbHfO_3$ and $PbHf_{1-x}Ti_xO_3$

The investigations were made on two kinds of crystals $PbHfO_3$ pure and $PbHf_{0.96}Ti_{0.04}O_3$ (PHT) single crystals. The variations with temperature of the ε' were previously shown in paragraph 2.3.3.

$PbHfO_3$ single crystal

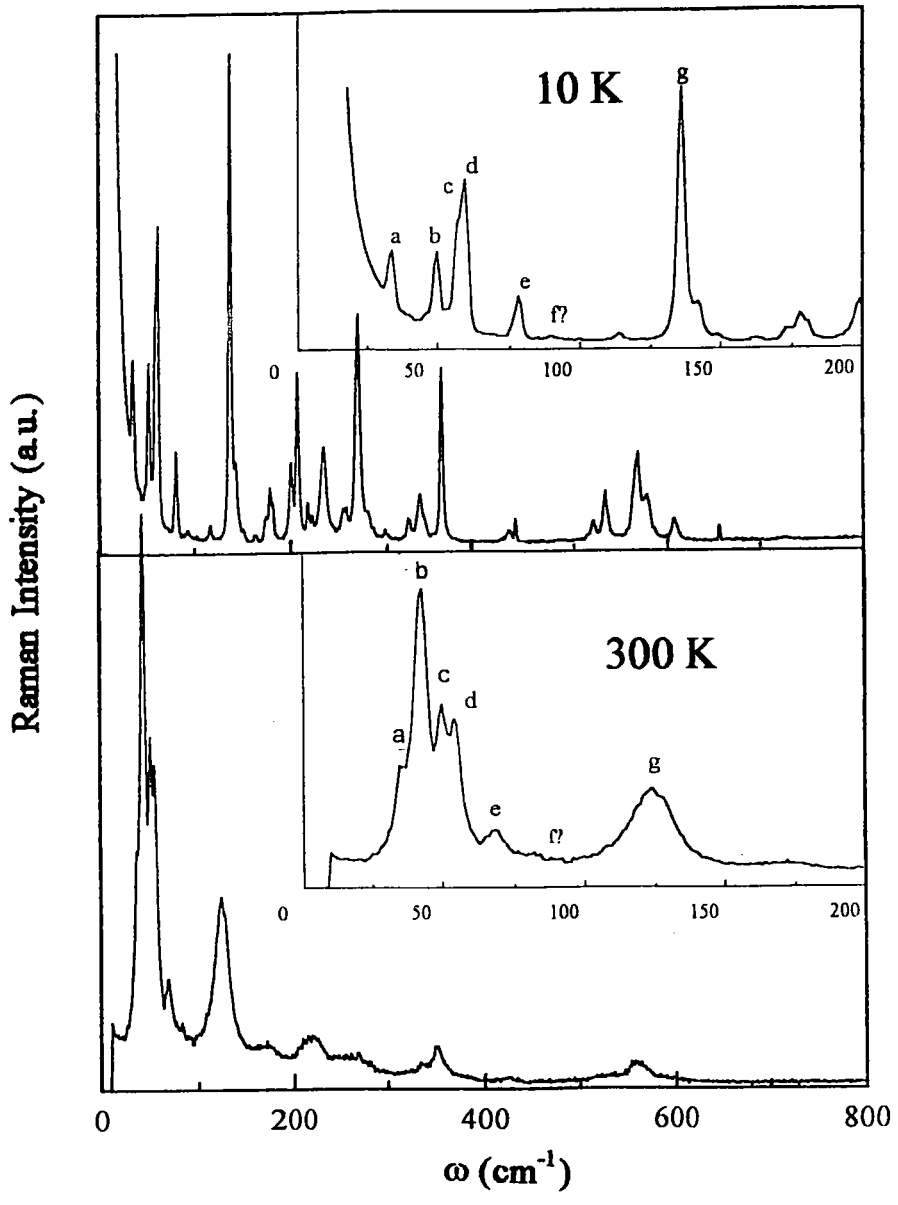


Figure 4.9. Raman spectra recorded for pure $PbHfO_3$ at 10 K and at room temperature.

A comparison of Raman spectra recorded in the usual frequency range from 0 to 800 cm^{-1} at 10 K and at room temperature is given in Figure 4.9. In both cases the low-frequency (0-200 cm^{-1}) range is presented in more detail (see inset). The spectra obtained at 10 K exhibit about 40 structures of various intensities what means that the majority of the Raman active modes are seen. Exact symmetry indexation was, however, impossible because of the polydomain character of the sample. Heating from 10 K to room temperature leads to Raman spectra in which the peaks exhibit a normal increase in damping, a shift in frequency but no drastic change in the spectrum, indicating the absence of any transition between 10 and 300 K. Since the clearest part of the spectrum appears in the frequency part lower than 200 cm^{-1}, description of the temperature-dependent Raman spectrum will be undertaken in this range only (where lines are more intense and changes of lines frequency are most significant from the point of view of LST relation) on the basis of Raman lines *a*, *b*, *c*, *e*, *f* and *g* as labelled in Figure 4.9.

Figure 4.10 presents Raman spectra recorded near the $A_1 \rightarrow A_2$ transition which are typical for the A_1 phase (434 K) and A_2 phase (441 K) as well as the transition range at 438 K.

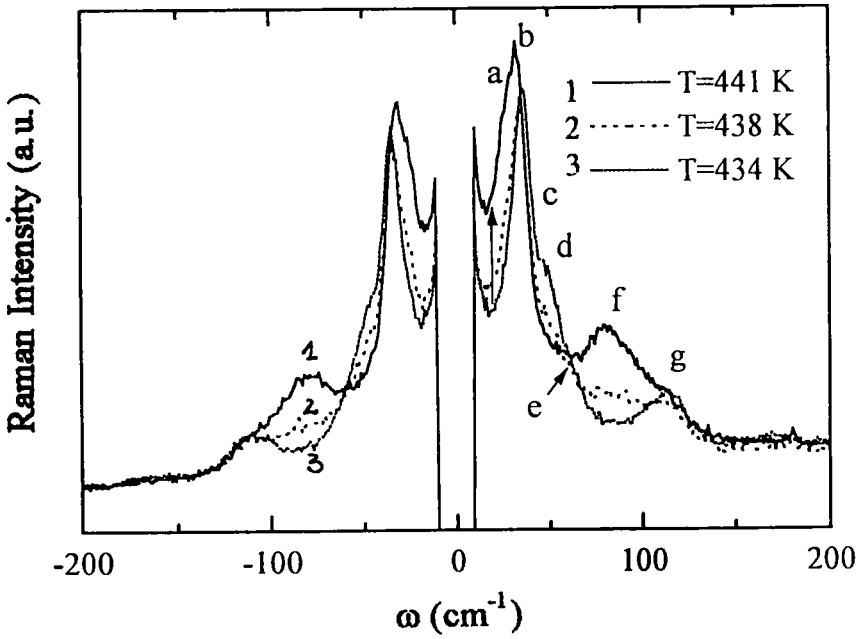


Figure 4.10. Raman spectra recorded on heating for pure $PbHfO_3$ below (434 K) near (438 K) and above (441 K) the phase transition $A_1 \rightarrow A_2$

The main modifications through the transition are as follows:

(i) a shift downward in the low-frequency *a* and *b* lines with simultaneous increase in low-frequency scattering (see arrow);

(ii) disappearance of the shoulders *d* and *e* and the formation of the one main band;

(iii) strong activation of a mode at about 85 cm^{-1} (called *f*);

(iv) clear softening of the *g* line.

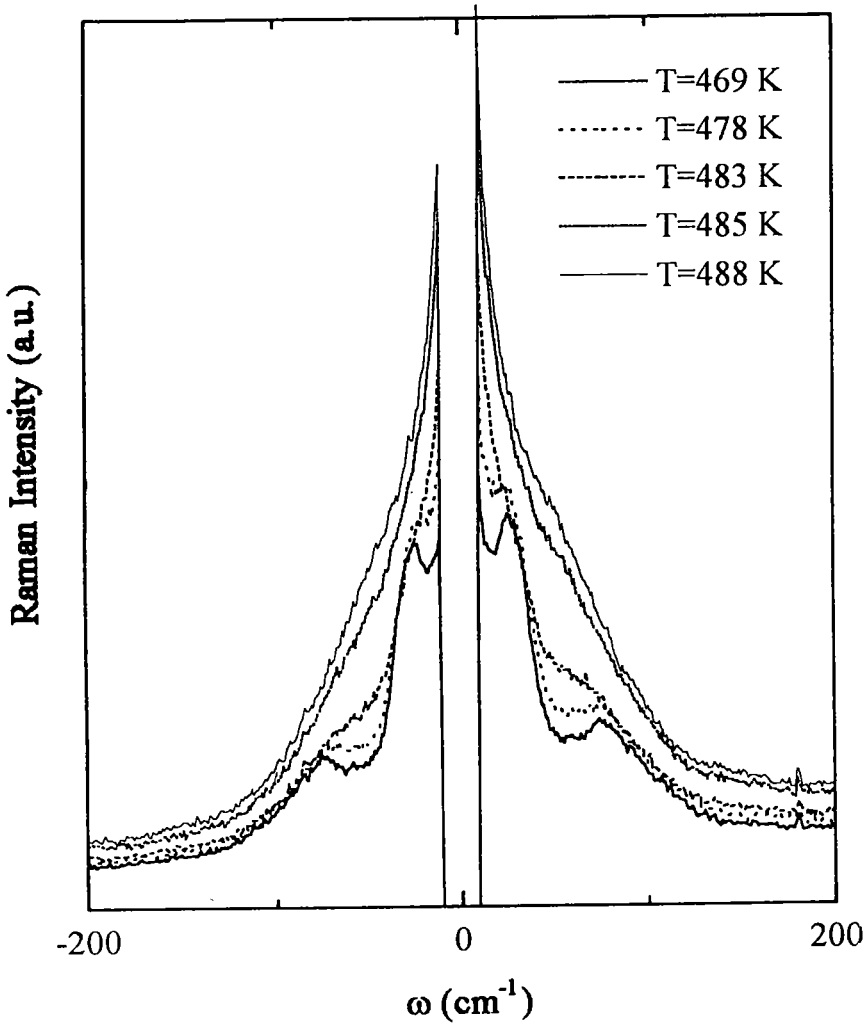


Figure 4.11. Raman spectra recorded in the heating process for pure PH through the $A_2 \rightarrow P$ transition (T_{A2-P}=484 K)

The phase transition from the intermediate A_2 phase to the cubic P phase given in Figure 4.11 shows an abrupt disappearance of the Raman structures. The P phase is characterised by the persistence of strong quasielastic scattering and temperature dependent low-frequency bump. The temperature dependence of this spectrum will be shown and analysed in section 4.8.6.

It is also noteworthy that the modifications in Raman spectra through the $A_1 \leftrightarrow A_2$ and $A_2 \leftrightarrow P$ transitions on heating and on cooling are in excellent agreement with the hystheresis phenomenon seen in the dielectric response (Figure 2.27).

$PbHf_{0.96}Ti_{0.04}O_3$ (PHT)

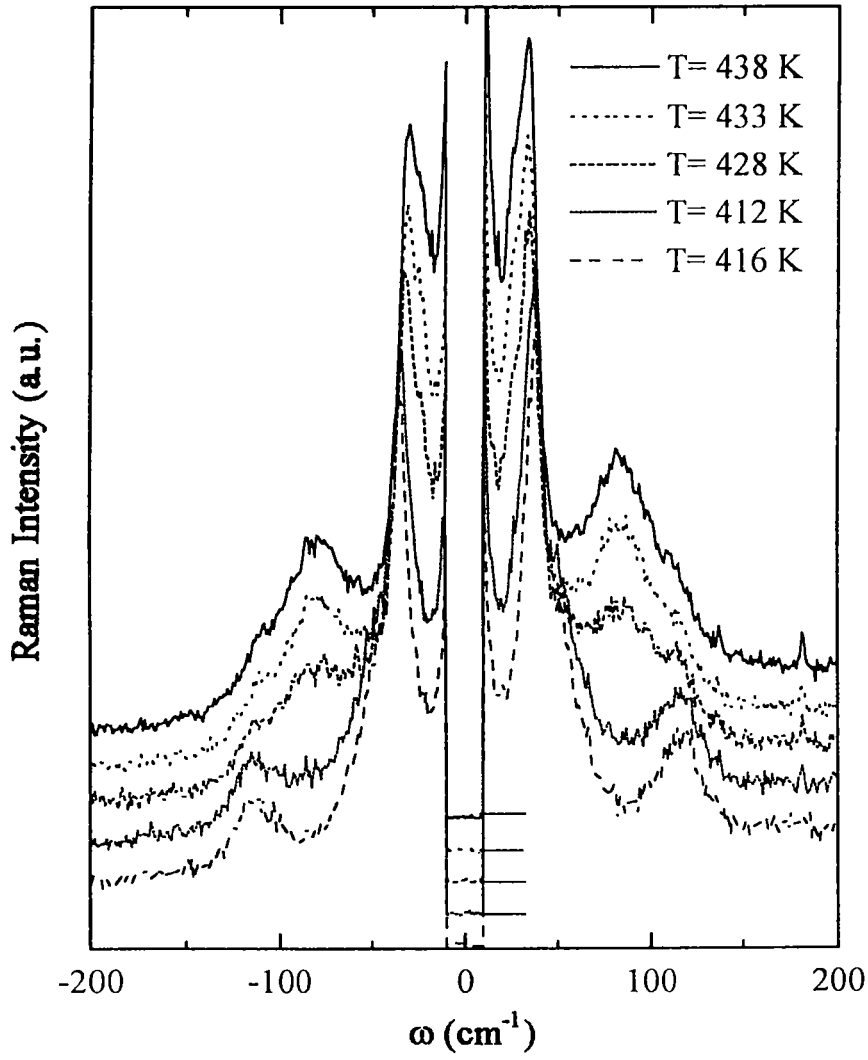


Figure 4.12. The evolution of low-frequency Raman spectra for PHT between the $A_1 \rightarrow A_2$ phases (on heating)

Comparison of the PHT spectra with those obtained for $PbHfO_3$ indicates that a small addition of Ti does not significantly modify the shape and number of Raman lines in the A_1, A_2 and P phases. The most significant change is connected with the broader temperature range of the $A_1 \leftrightarrow A_2$ transformation and the decrease in its temperature. For

illustration, the temperature evolution of the Raman spectra in the vicinity of the $A_1 \rightarrow A_2$ phase transition in PHT is presented in Figure 4.12. In agreement with the behaviour of the dielectric permittivity (figure 2.27), the transition $A_1 \leftrightarrow A_2$ occurs in a relatively wider temperature range than in the case of $PbHfO_3$.

4.8. ANALYSIS OF THE RAMAN RESULTS

4.8.1. Introduction

The phonon lines were analysed in the framework of the usual damped-harmonic oscillator model (see par. 4.3). The intensity due to the scattered phonon was therefore adjusted to the following function:

$$I_{oi}(\omega) = \begin{Bmatrix} n(\omega)+1 \\ n(\omega) \end{Bmatrix} \frac{S_i \omega_i^2 \gamma_i \omega}{(\omega_i^2 - \omega^2)^2 + \gamma_i^2 \omega^2} \qquad 4.38$$

where S_i, ω_i, γ_i are respectively: the oscillator strength, the frequency and the damping of i^{th} phonon and the factors $n(\omega)+1$ and $n(\omega)$ are so-called Bose-Einstein factors and correspond to Stokes and anti-Stokes scattering respectively. The frequency, damping and intensity of each mode were thus determined as a function of temperature.

For the quasielastic part of scattering, the Debye-like function originating from relaxational behaviour was used:

$$I_R(\omega) = \begin{Bmatrix} n(\omega)+1 \\ n(\omega) \end{Bmatrix} \frac{\omega S_r \gamma_r}{\omega^2 + \gamma_r^2} \qquad 4.39$$

where S_r and γ_r describe the strength and the relaxation rate of the relaxator respectively.

Thus the whole Raman spectra consist of the sum of one relaxator and several oscillators.

$$I_s(\omega) = k\left[I_R(\omega) + \sum_i I_{oi}(\omega) \right] \qquad 4.40$$

where the coefficient k in the equation (4.40) is the factor related to experimental conditions.

4.8.2. Calculations of the Raman spectra intensities and frequencies in the A and F phases for $PbZr_{0.99}Ti_{0.01}O_3$.

Figure 4.13a shows an example of fitting with function from eq. 4.40, the low frequency Raman spectrum at room temperature i.e. in the A_1 phase. The fit of spectrum to the most probable structures existing in the F phase is presented in Figure 4.13b (For all samples used we failed to detect all Raman lines predicted by theory). All the calculations and fits were made using the computer program Origin 3.5.

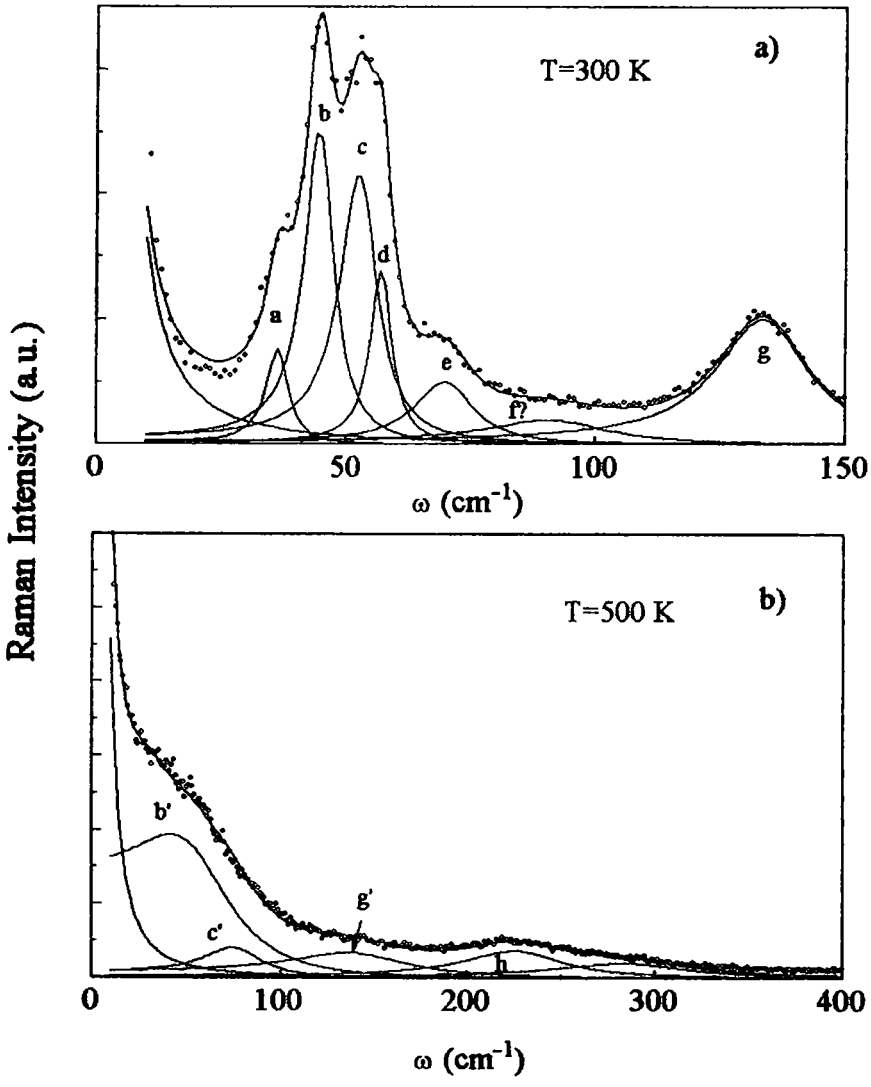


Figure 4.13. Example of fitting of the low–frequency Raman spectrum in (a) A phase , and (b) F phase (number of lines used in the fit is taken according to the symmetry consideration).

The calculated temperature dependence of the frequency positions of highest intensity lines in the low frequency region (0-150 cm^{-1}) are presented in Figure 4.14.

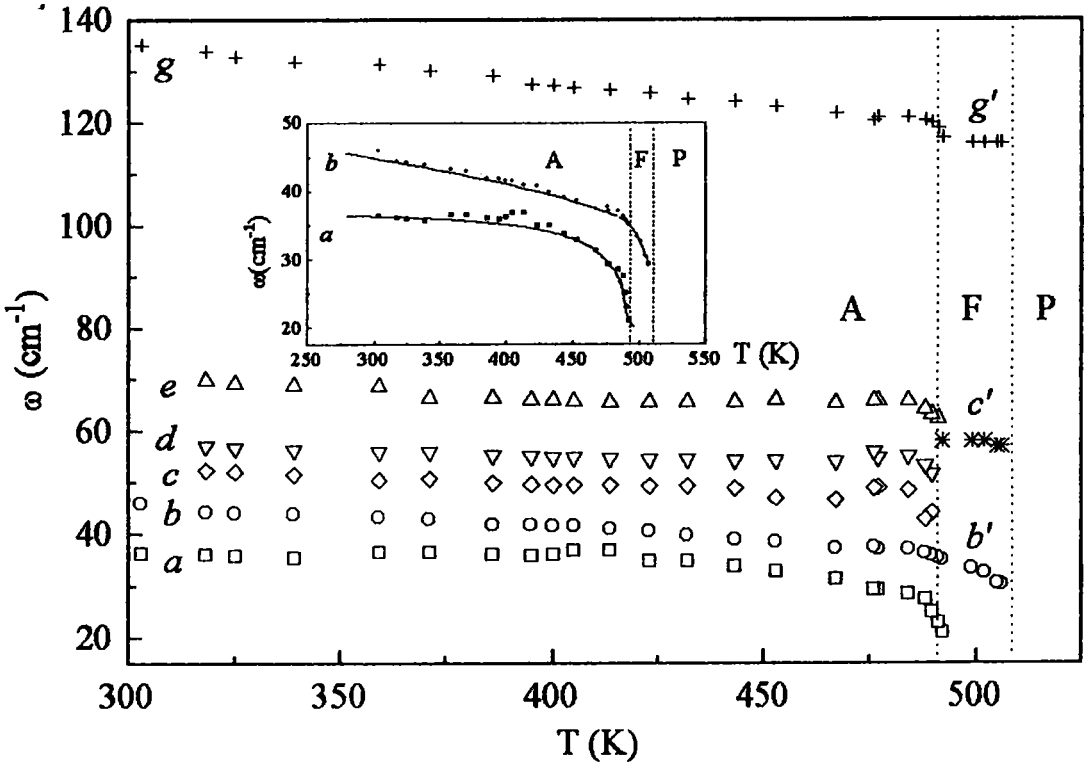


Figure 4.14. Temperature dependence of the Raman lines frequencies in the low-frequency region in the A and F phases. An inset shows more precisely the behaviour of the two most interesting lines *a* and *b(b')*.

Since they are perfectly reliable down to 15 K (Figure 4.6), the figure exhibits only the values above room temperature. The performed calculations confirmed that in the A phase positions of two lowest frequency lines *a*, *b* and line *g* gradually move towards the lower frequencies. Near the A-F phase transition line *a* softens rapidly and strong decrease in intensity is observed. The other modes seem to keep their positions with normal increasing of their damping.

Taking into account the symmetry analysis presented for ferroelectric phase (par. 4.5.1) it has to be said that it was impossible to find all lines. The shoulder remaining in the F phase can be constructed of a doublet *b'* and *c'* from which line *b'* seems to be a continuation of the line b from the A phase and a structure *c'* at the frequency 60 cm^{-1} can be continuation of lines *c*, *d* and *e*. The inset in the Figure 4.14 shows in details an interesting behaviour of *a* and *b* lines around the A-F transition. The observed strong

softening of the *a* line is accompanied by increase of the quasi-elastic scattering at the A-F transition as seen in (Figure 4.15).

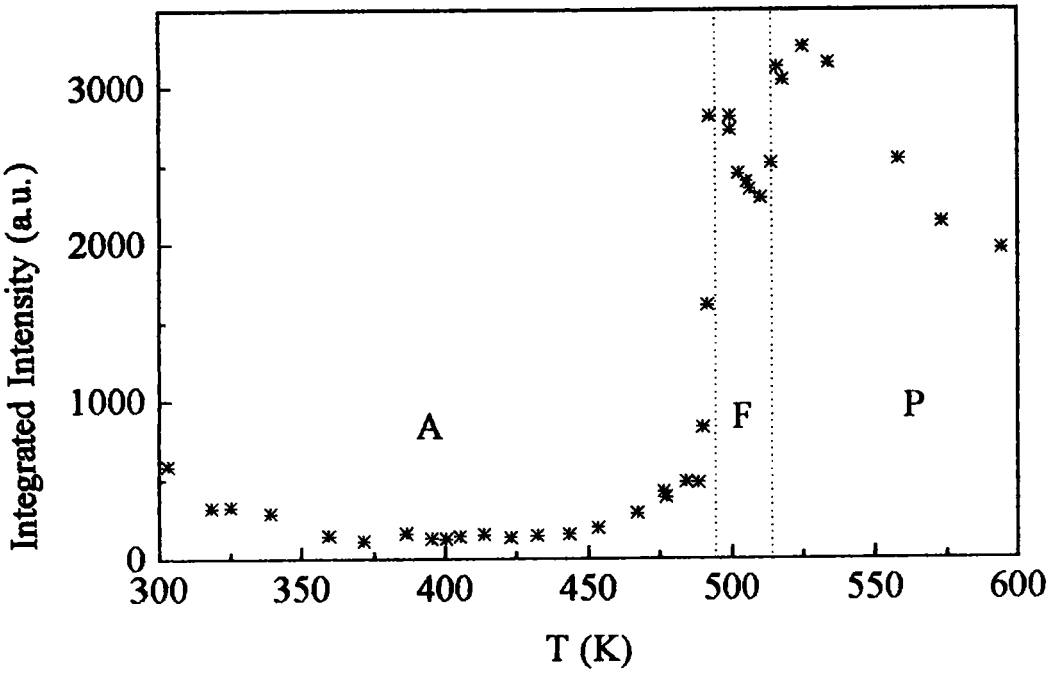


Figure 4.15. Temperature dependence of quasielastic scattering intensity on heating for the $PbZr_{0.99}Ti_{0.01}O_3$ single crystal.

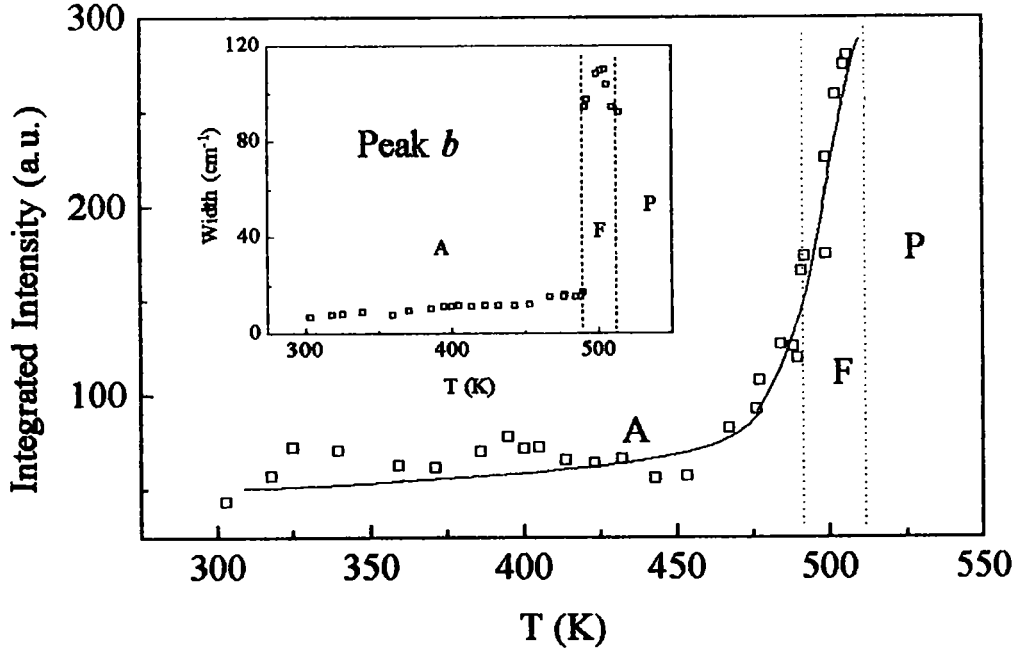


Figure 4.16. Changes with temperature of the Integrated intensity (and half-width in the inset) near the A-F transition for the *b(b')* - most interesting line.

Both, softening of the line and changes in quasielastic scattering may - since we could not exclude an influence on scattering the domain structure reorganisation - indicate that this phase transition exhibits both a displacive and order-disorder character. The *b* line is prolonged in the F phase by the *b'* structure which softens toward the F-P phase transition.

These features show that this transition exhibits both displacive and order-disorder as well as a strong first order character. As it is calculated in the analogous sample $PbHfO_3$ (Jankowska-Sumara et al. 1995b), a conclusion might be drawn that the small jump in the dielectric constant at A-F phase transition could find his origin in the softening of the *a* and *b(b')* lines.

4.8.3. Raman scattering in the P phase of $PbZr_{0.99}Ti_{0.01}O_3$ - modes share in dielectric response

As was mentioned, the spectra at the F-P phase transition do not show any visible modification in their shape and contain in the P phase together with strong quasielastic scattering a broad mode similar to that observed in the F phase. It is curious that this mode does not disappear even at very high temperatures deeply in the paraelectric phase. According to the symmetry analysis and selection rules developed for Raman scattering in the cubic paraelectric phase, no optic mode of the first order can be Raman active. The observed behaviour is thus in contrast to the usually known theoretical predictions. However similar features have already been observed for various perovskite compounds, voluntary or involuntary doped with impurities like $KTaO_3$:Nb, $KTaO_3$:Li (Yacoby, 1978; Uwe et al., 1986; DiAntonio et al., 1993; Toulouse et al., 1992) and more recently $SrTiO_3$:Ca (Bianchi et al., 1994). Several theories which describe these activation processes and which yield the temperature dependent line shape and intensities have been reported in above mentioned papers.

Before going into details and in order to have a basic idea on the temperature dependence of the low frequency bump, we performed systematic fitting with the function 4.40 of the structure in the paraelectric phase up to the temperature of about 800K.

The light scattering spectra observed in paraelectric phase in the low frequency range consist in most intense of strong quasi-elastic diffusion, which decreases on heating (see Figure 4.15), together with broad bump which was assigned to the lowest frequency phonon.

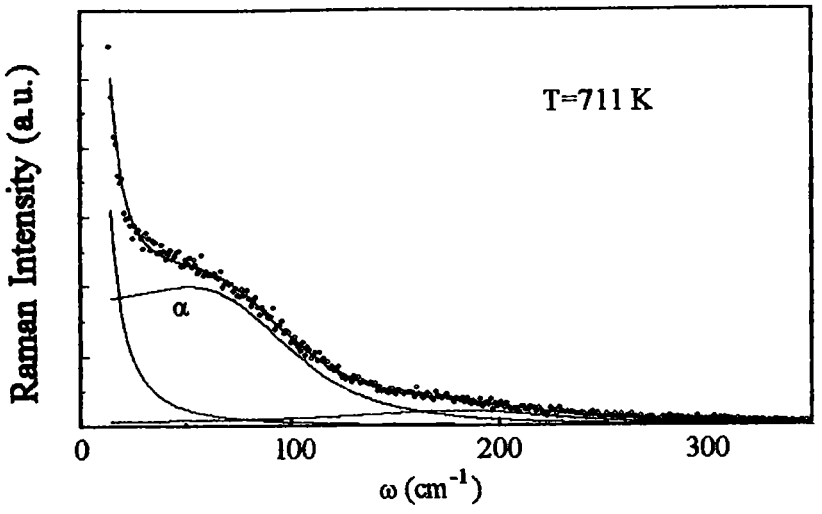


Figure 4.17. Example of fitting of the observed Raman spectra in P phase

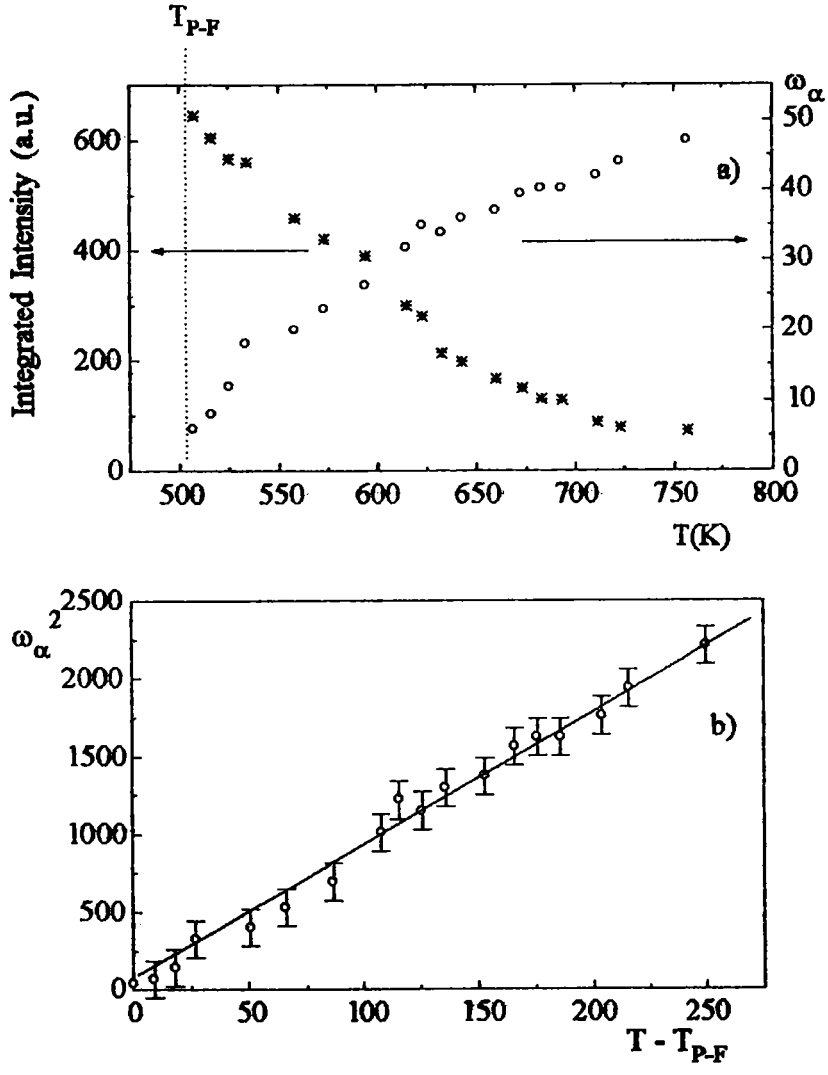


Figure 4.18. a) Temperature dependence of the frequency and integral intensity of the α line assigned in the P phase b) Dependence of the squared ω_α versus $(T-T_{P-F})$.

The example of fitting in P phase is presented in Figure 4.17 and the results of the calculations are reported in Figure 4.18. The line marked α clearly exhibits frequency soft character from 50 cm^{-1} at high temperature to about 10 cm^{-1} near the $T_{P\text{-}F}$, together with a divergence of scattered intensity when approaching $T_{P\text{-}F}$. In Figure 4.18b the frequency squared of this hypothetically assumed „soft" mode together with a linear fit is reported. It is seen that the soft mode behaves according to the Curie-Weiss law ($\omega^{-2} \sim a^*(T\text{-}T_o)$) with a value of T_o lying at about 500 K, which is about 10 K lower than $T_{P\text{-}F}$.

The appearance of the „soft mode" studied here, enables evaluation of its share in the $\varepsilon(T)$ dependence. In order to do this, we applied here lattice dynamic shell model in cubic phase of $PbZrO_3$ crystal on the basis of the model parameters of Lahlou et al.(1990). The dispersion curves of the transverse and longitudinal phonon modes in the high symmetry Δ direction are presented in Figure 4.19.

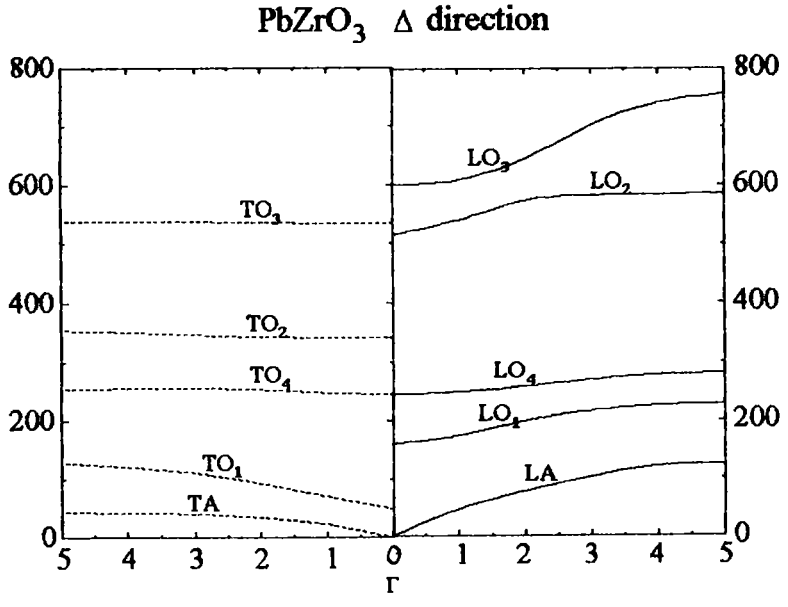


Figure 4.19. Dispersion curves of the phonon modes in the Δ[100] direction in the cubic phase of $PbZrO_3$

The zone centred optical modes are supposed to be constant versus temperature except to lowest transverse mode TO_1 assigned as the soft mode. Using the Lyddane-Sachs-Teller equation:

$$\frac{\varepsilon(0)}{\varepsilon(\infty)} = \frac{\prod_{i=1}^{n} \omega_{iLO}^2}{\prod_{i=1}^{n} \omega_{iTO}^2} \qquad 4.41$$

where ω_{LO}, ω_{TO} are the frequencies of the longitudinal and transverse modes respectively and $\varepsilon(\infty)$ is the high-frequency dielectric permittivity taken as the square of the optical refractive index (Roleder et al., 1989) the values of ε_{cal} involved by the net resonances were calculated and compared to the results of $\varepsilon'(T)$ dependence measured directly at the frequency 1 MHz (Figure 4.20). From figure 4.20 it is evident that the contribution of the soft mode α to $\varepsilon'(T)$ dependence is significant although an additional excitation (next relaxational process) should also take place in the observed dielectric response between the frequency of the presented dielectric data and the soft-phonon resonance as far as the temperature is above T_c.

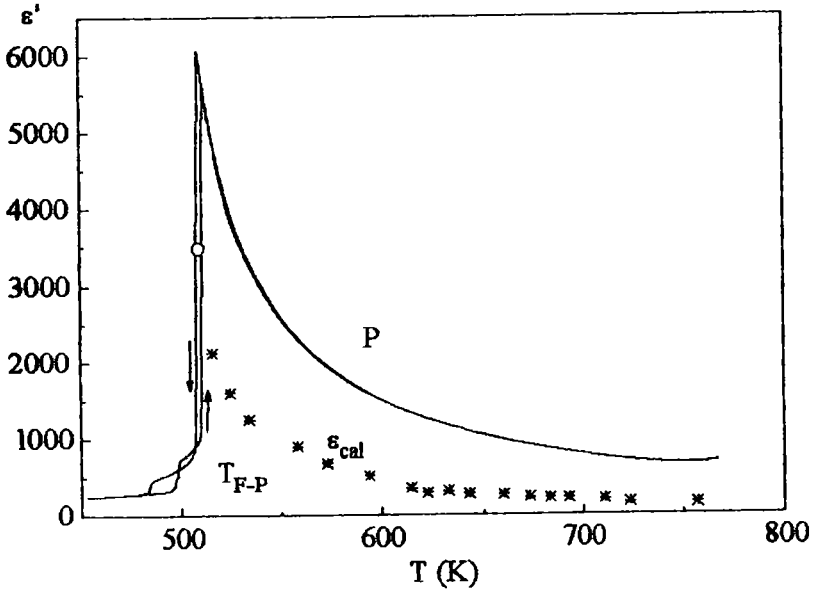


Figure 4.20. Temperature dependence of the lattice contribution obtained from LST relation for mode α. Continuous line in the Figure shows experimentally measured electric permittivity at frequency of 1 MHz. Value corresponding to open circle was obtained by extrapolation of the $\varepsilon_{cal}(0)$ to the T_{P-F} point.

4.8.4. $A_1 \rightarrow A_2$ and $A_2 \rightarrow P$ phase transitions in $PbHfO_3$ and $PbHf_{1-x}Ti_xO$

Figure 4.21 shows the temperature dependence of the frequencies of the Raman lines *a*-*g* from 10 K to $A_2 \rightarrow P$ transition in $PbHfO_3$. The inset shows more clearly the $A_1 \rightarrow A_2$ phase transition. Our calculations indicate delicate softening of the two lowest lines *a* and *b* on approaching $T_{A1 \rightarrow A2}$. Above this temperature these modes stabilise. The line g, showing

continuous decrease with increasing temperature without any singularity at $T_{A1\rightarrow A2}$, unlike the lines *a* and *b*, is not connected with this transition. As mentioned in the symmetry considerations, the appearance of the line *f* can be attributed to the activation of previously silent Raman modes. No activation of other modes could be detected. This happens mainly because at these temperatures the main part of the vibrational modes are difficult to observe because of their small scattering strength and marked damping.

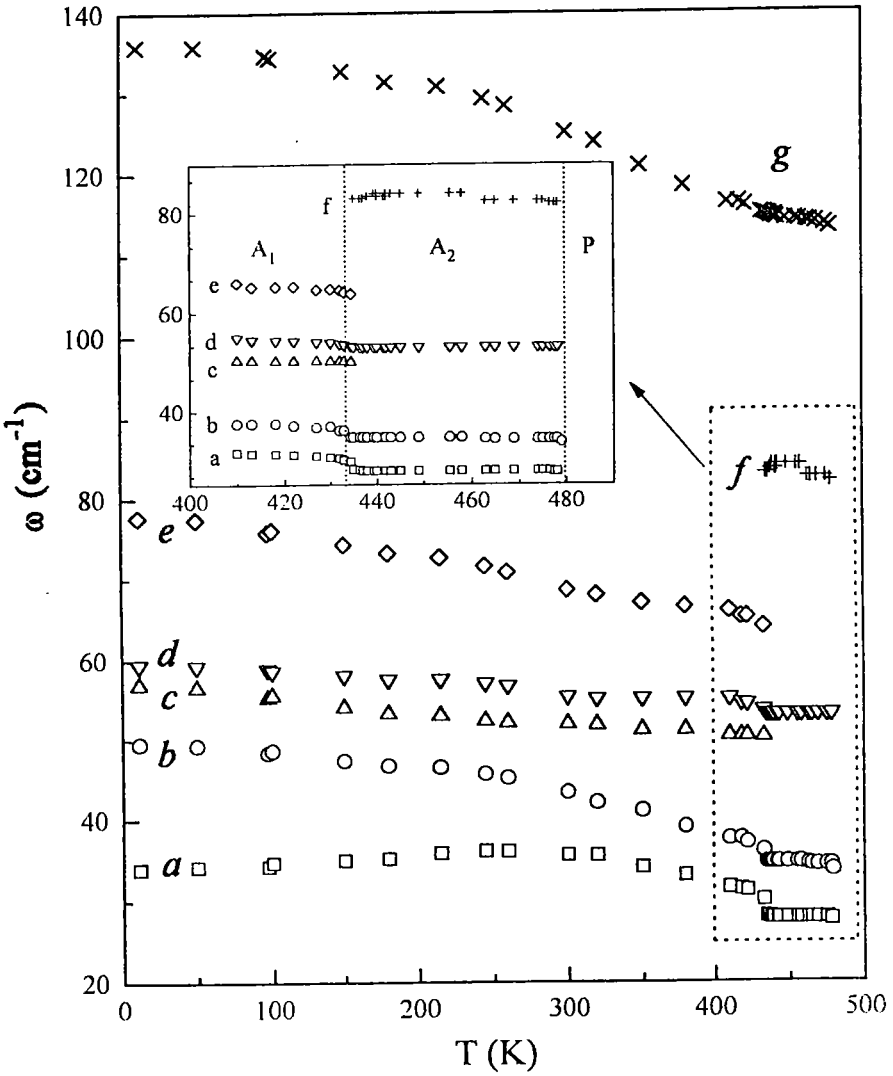


Figure 4.21. Temperature dependence of Raman lines frequencies throughout the whole experimental temperature range for $PbHfO_3$. The vicinity of both phase transitions is magnified in the inset.

The scattering strength intensity S_r for the relaxational mode obtained in our calculations is presented in Figure 4.22. This strength increases as the temperature approaches $T_{A2\rightarrow P}$, without any singularity at the $A_1\rightarrow A_2$ transition. This indicates that the

$A_1 \rightarrow A_2$ transition seems to be of a displacive nature and is not influenced by a relaxational process. This point of view for the $A_2 \rightarrow P$ transition will be considered separately.

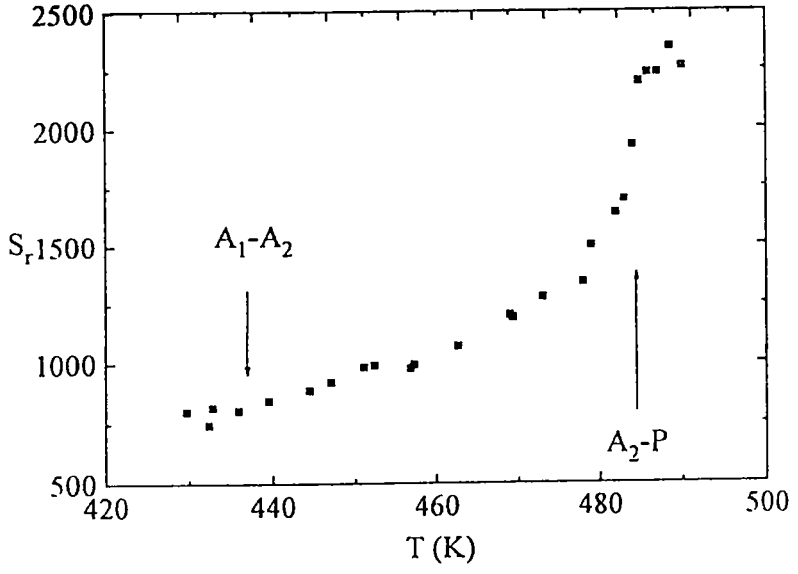


Figure 4.22. Temperature dependence of quasielastic scattering intensity for $PbHfO_3$ on heating.

Figure 4.23 shows the changes in the integrated intensity and damping parameter γ_i for the Raman lines detected i.e. *a* and *b* which play the most important role at the $A_1 \rightarrow A_2$ transition. The line *a* (Figure 4.23a) is of particular importance is exhibiting marked changes in the parameter γ_i which causes experimentally observed quasielastic scattering. It should be pointed here that the value of the integrated intensity of the scattering is proportional to the value of the real part of the dielectric permittivity (ε') i.e. the temperature changes of the integrated intensity of the particular Raman line illustrate its contribution to the ε'(T) dependence.

Similar calculations were systematically performed for the $PbHf_{0.96}Ti_{0.04}O_3$ sample. Results of the line frequencies in the vicinity of the $A_1 \rightarrow A_2$ and $A_2 \rightarrow P$ phase transitions are shown in Figure 4.24. The dashed lines corresponding to the equivalent frequencies in the pure PH samples are added for comparison and they enable distinguishing the modes which indicate motion involving Ti(Hf) ions. This appears to be the case for the lines *a*, *b*, *f* and *g* which exhibit as could be expected, increase in mode frequency after Ti introduction.

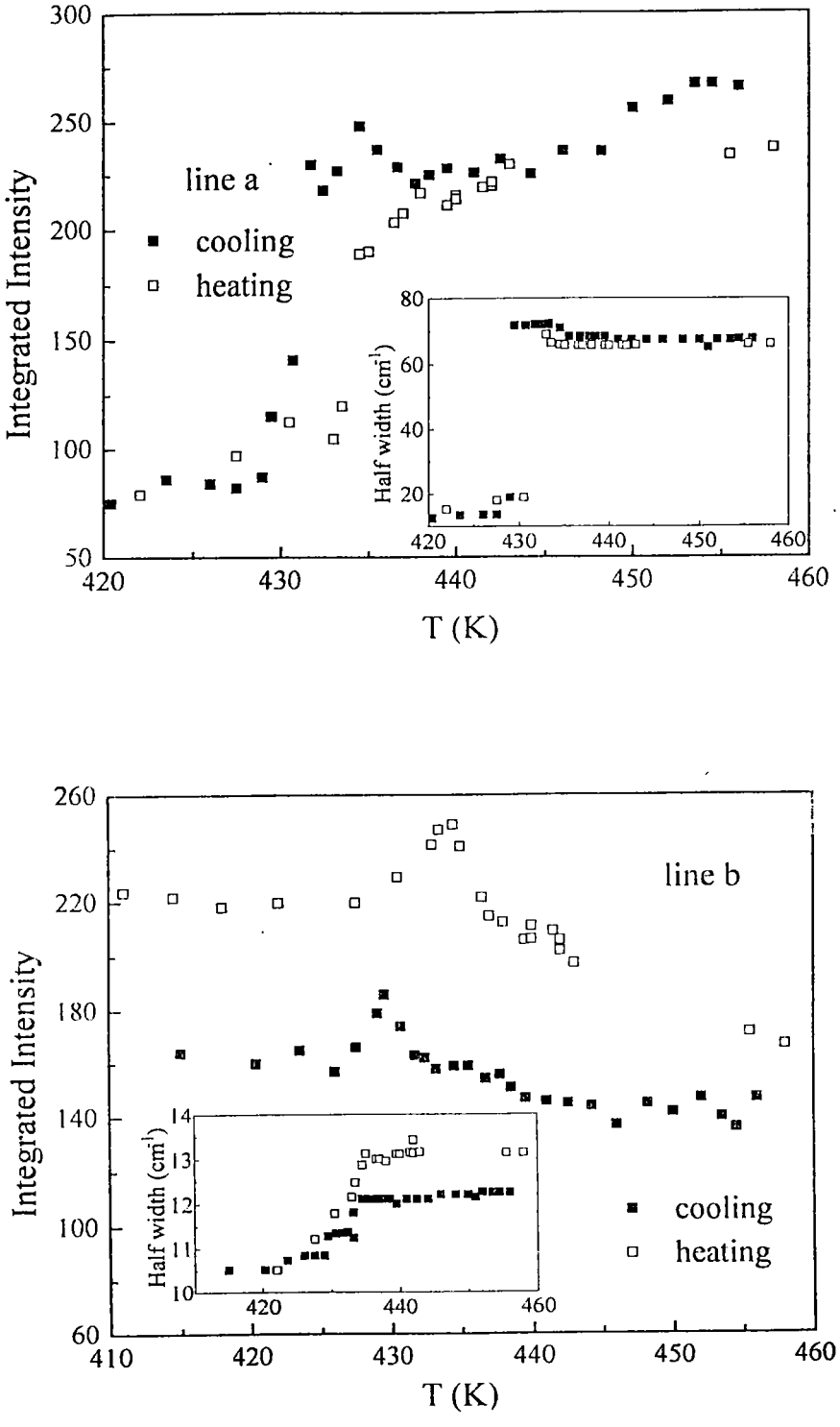


Figure 4.23. Temperature changes of the calculated integrated intensity and half-width (insets) for lines which play the most important role in the $A_1 \rightarrow A_2$ phase transition. (a) line *a* and (b) line *b* in the vicinity of the $A_1 \rightarrow A_2$ phase transition.

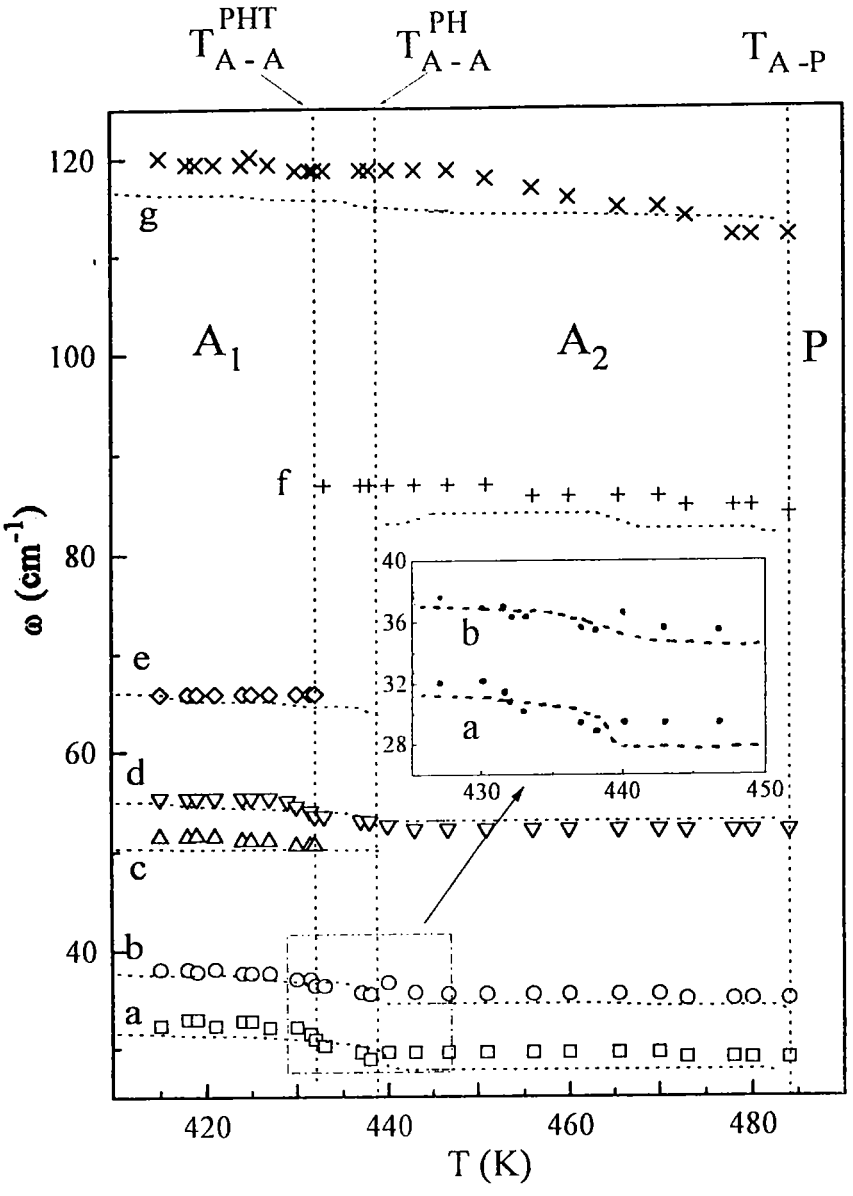


Figure 4.24. Temperature dependence of the Raman lines frequencies from 400 to 485 K for PHT. The broken lines, added for comparison, show the corresponding frequencies obtained for pure $PbHfO_3$ sample.

4.8.5. Influence of low frequency Raman lines on low frequency dielectric response in the vicinity of the A_1 and A_2 phases for $PbHfO_3$ and PHT

As mentioned in par 2.3.3. (Figure. 2.27 - ε(T)), the $A_1 \rightarrow A_2$ transition is accompanied by a significant jump in the low-frequency dielectric constant when going from A_1 (ε~250) to A_2 (ε~600). Since the two phases involved in this phase transition are both known to be

antiferroelectric (using Sawyer-Tower system we observed clearly the double hystheresis loops in both phases), the question of the origin of this dielectric jump is quite interesting. From Figure 4.22, reporting the quasi-elastic light scattering intensity as function of temperature, no high-frequency relaxational process seems to occur at this phase transition $A_1 \rightarrow A_2$. On the other hand, relative modifications in the phonon mode characteristics are noted in Figures 4.21 and 4.24, especially for the lowest-frequency *a* and *b* modes.

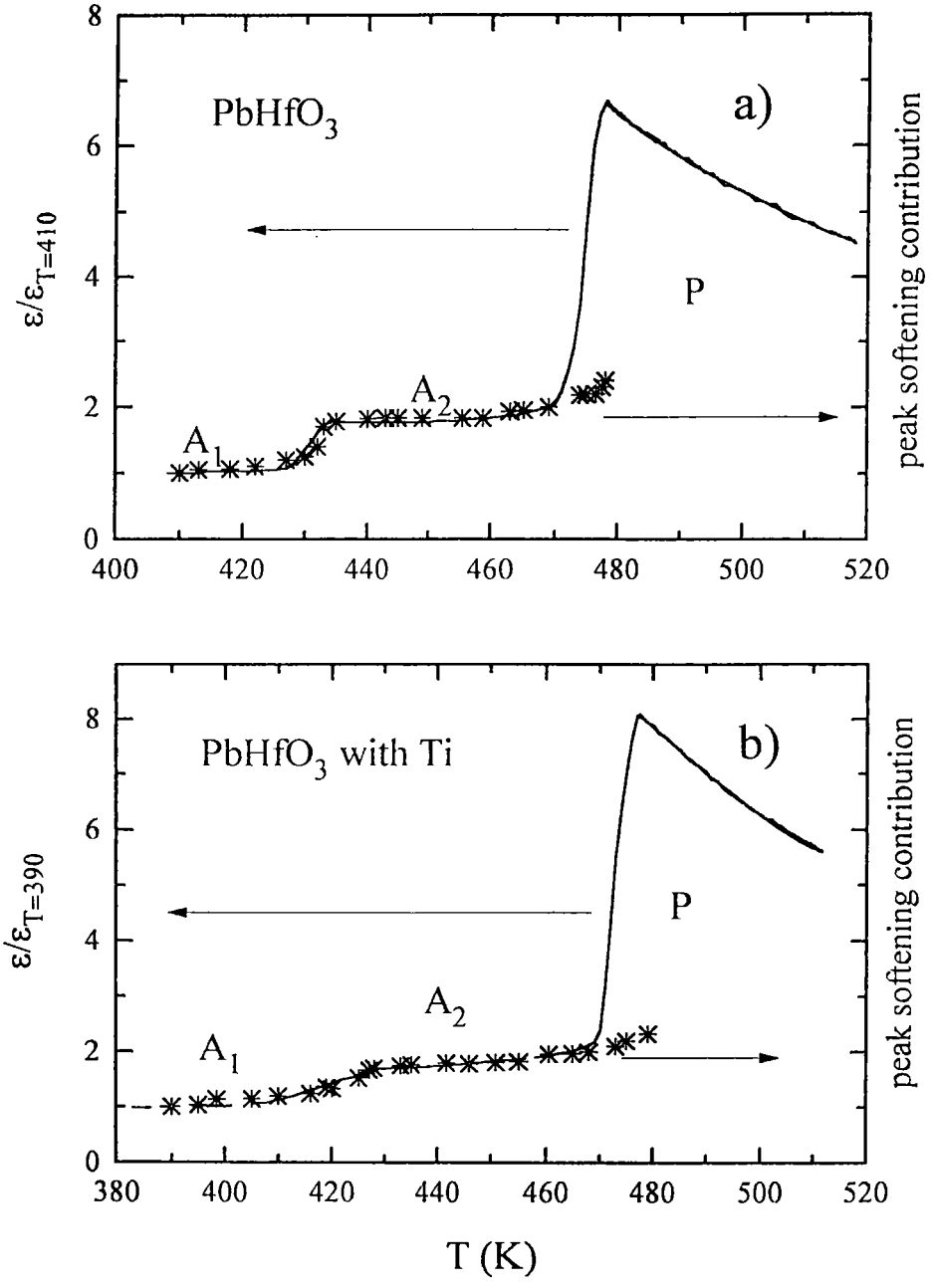


Figure 4.25. Comparison of the experimental dielectric permittivity as a function of temperature (—) with the calculated values from the LST relation (*) in the vicinity of the $A_1 \rightarrow A_2$ and $A_2 \rightarrow P$ phase transitions: (a) for pure $PbHfO_3$ crystal; (b) for $PbHf_{0.96}Ti_{0.04}O_3$.

For this reason we attempt to relate the dielectric jump to the anomalies of the *a* and *b* peaks at the phase transition and on the base of the Lyddane-Sachs-Teller equation. We assumed that except for the *a* and *b* modes considered as TO modes, all the other TO and LO modes are temperature independent. Consequently these modes contribute to the L.S.T. relation as a global constant, and only the modified *a* and *b* play a role in ε(0) jump. In both, pure and Ti doped samples, the down jump of ε(0) from 600 in A_2 to 200 in A_1, can be described by the increase in frequency of the two *a* and *b* modes through this phase transition, all other contributions being considered as constant.

The results - presented in Figure 4.25a. for $PbHfO_3$ and 4.25b. for $PbHfO_3$ with Ti - accord well with the detected dielectric data.

Of course we are aware that this calculation takes into account a strong assumption. Indeed, in the low-temperature phase A_1, all the modes measured by Raman scattering are *g* modes, consequently non-polar and not contributing to the dielectric properties. In the A_2 phase, this objection is removed. In fact, our assumption means that non-active Raman modes of *u* symmetry (predicted by theory as infrared modes which are polar modes) are lying at equivalent frequencies as the visible *a* and *b*, g (gerade) modes. Furthermore all the other modes are stable through the transition. Since about 40 modes are visible in the Raman spectra (instead of 48) and since no additional mode anomaly contributes to the jump appearing in the phase transition $A_1 \rightarrow A_2$, such an assumption can find some justification

4.8.6. Study of the A_2-P transition and Raman light scattering in P phase.

As a continuation of Figure 4.11, which showed the Raman spectra through the $A_2 \rightarrow P$ phase transition, in Figure 4.26 we represent the Raman intensity temperature dependence above $T_{A2\text{-}P}$ for $PbHfO_3$. Since the paraelectric phase, from symmetry considerations is described by the Pm3m space group, there should be no Raman active mode in this phase. Our spectra exhibit, together with strong quasi-elastic diffusion (observed in Figure 4.17) a broad shoulder whose intensity is found to be temperature dependent. Above $T_{A2\text{-}P}$ the global light scattering intensity still increases up to 525 K, then decreases and finally vanishes near 700 K.

The Raman scattering response was fitted with a scattering function involving Debye-like quasi-elastic scattering and a highly overdamped phonon resonator (eq. 4.40). The results of such a fit are shown as an insert in Figure 4.26.

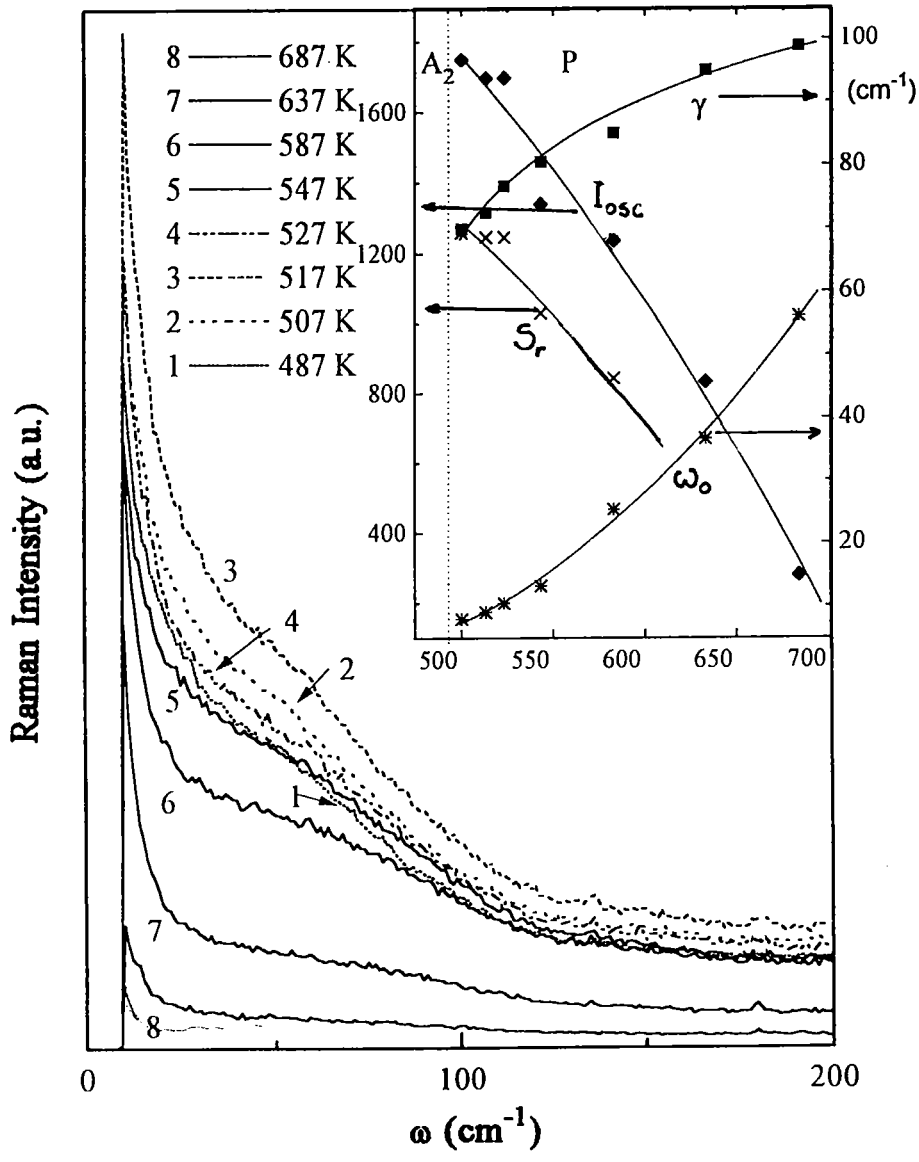


Figure 4.26. Raman spectra recorded for pure $PbHfO_3$ for various temperatures in the paraelecrtic phase. The results of a fit using a response function including an oscillator (ω_o, γ, I_{osc}) and a relaxor (of strength S_r) are shown in the inset.

The appearance of strong quasi-elastic scattering around $T_{A_2\text{-}P}$ and its persistence above the transition temperature is known to be a common feature in many lead perovskite compounds (Roleder et al., 1988; Roleder et al., 1989; Kania et al., 1992; Fontana et al., 1991) and seems to be an indication that this phase transition involves either strong

relaxational motion which is persistent even above T_c or the existence of some kind of disorder (static or dynamic). Disorder of this kind in the Pb sublattice, already reported in X-ray diffraction studies by Kwapulinski et al. (1994) has been shown to vanish near 700 K (as in our case).

This disorder could explain the activation of the lowest frequency phonon modes (or a phonon density of states) which is shown in our case as the broad shoulder. As deduced from our fit in the P phase this band gradually disappears with the disappearance of disorder, and exhibits a frequency which is located in the energy range where the lowest-frequency mode appears in lead perovskites; furthermore a significant softening - but not of type $\omega^2 \sim (T-T_o)$ - is observed when approaching T_{P-A2} (inset in Figure 4.26).

4.9. DISCUSSION - HIGH FREQUENCY DIELECTRIC RESPONSE ABOVE 10^{11} Hz.

Is there a soft mode in $PbZr_{0.99}Ti_{0.01}O_3$?

The Raman scattering investigations for $PbZr_{0.99}Ti_{0.01}O_3$ single crystal showed soft mode behaviour near each phase transition (Figure 4.14 and 4.18). The phase transition between antiferroelectric and ferroelectric phases is accompanied by clear softening of the *a* line. Moreover the line *g* which takes the position 135 cm^{-1} at room temperature, shifts very slowly into lower frequencies with increasing of the temperature up to the A→F phase transition. The softening of these two lines *a* and *g* probably could explain the small jump in the ε(T) dependence in the A↔F phase transition but this softening is accompanied by strong increase of quasielastic scattering. This may indicate that the A↔F phase transition is both of displacive and order-disorder nature. The phase transition F↔P is also accompanied by the softening of the line (*b'*) and jump in the quasielastic scattering intensity. Since the temperature changes of the integrated intensity of the particular Raman line illustrate the contribution of this line to the ε(T) dependence, the line *b(b')* was shown (Fig. 4.16) to play an important role in the increasing of the ε(T) in the intermediate and ferroelectric phases, however the influence of the other relaxational process or modes cannot be omitted. Indeed a weak relaxation process in the range of few kHz was found in the transient phase (see par 2.3.2) which appeared due to Ti introduction. This relaxation was attributed to the motion of domain walls in the complex domain structure existing in PZT. The exact calculations of the contribution of the mentioned lines to the phase

transitions are however very difficult. This is because of strong damping of these lines in the intermediate phase and because there were not detected all Raman lines predicted by the symmetry. Nevetherless the softening of the mentioned lines can play significant role in the ε value especially at lower temperatures.

Special attention was paid to the paraelectric phase where Raman mode in a form of *broad shoulder* normally forbidden by selection rules was observed. This broad shoulder does not disappear even at high temperatures of the P phase and has no features of second order Raman scattering. The question thus arises why this stable *shoulder* appears, and to what extent it can influence the dielectric response in the P phase.

Since Ti ions were introduced into highly polarizable lattice of $PbZrO_3$ they can be treated, because of remarkable difference in ionic radii of Zr and Ti $\left(r_{Ti} / r_{Zr} = 0.74\right)$as a source of both local, mechanical and electric stresses. These stresses acting in general as disturbance of the whole host lattice may lead to activation of low-frequency Raman excitation.

In this approach the fits showed that in the paraelectric phase the mode indicated as α clearly softens when going to the P-F phase transition and plot of the α line frequency squared ω_α^2 well obeys the Curie-Weiss law (Figure 4.18 b). The temperature dependence of ω_α enables us to calculate hypothetically the share of net resonances to the ε'(T) run. As was shown in Figure 4.20 the values of $\varepsilon_{cal}(0)$ in great part but not completely cover the ε'(T) relation measured at the frequency of 1 MHz. The observed strong changes of central peak near $T_{P\text{-}F}$ (Figure 4.15) seem to confirm the existence of a relaxational process which might complete and thus explain run of ε(T) in the paraelectric phase measured at the frequency of 1 MHz.

To answer the question as to why the broad shoulder appears in the P phase we can come back again to the question of defects in the Pb and O sublattices. From this point of view the main role of the defects would be to destroy conservation of wave vector and allow first- and higher-order Raman scattering by phonons more or less throughout the Brillouin zone. Thus the broad shoulder can be composed of scattering by both acoustic and optic phonons. This would well correspond with dispersion curve seen in Figure 4.19. The strong temperature dependence of the shoulder seems to indicate the more important role of optic phonon in its intensity and thus the dependence $\omega_\alpha^2 \sim (T - T_o)$ seems not to be accidental.

On the other hand the dielectric investigations of the same crystal revealed dielectric relaxation in the range of a few kHz just in P phase. This relaxation appears owing to the Ti introduction or existence of defects and is believed to come from the interface dynamics of induced in this way polar regions. Parameters of the process as relaxation time and dielectric strength exhibit a distinct anomaly at T_c showing that this relaxation is clearly related to P→F phase transition (Jankowska-Sumara et al., 1995a). Thus the activation of the first order Raman lines in the P phase is assumed to come from the fluctuations of dipolar moment induced by Ti ions (polar nanoregions). Theoretical support of this kind of activation has been reported for perovskite compounds doped with foreign atoms (ions) like $KTaO_3$:Nb, $KTaO_3$:Li and $SrTiO_3$:Ca, by several authors (Yacoby, 1978; Uwe et al., 1986; DiAntonio et al., 1993; Bianchi et al., 1994) who discussed the Raman spectra as those emerging from isotropic distortion extending over few lattice constants and modifying selection rules so that Raman scattering can be observed. They showed that, due to this effect, low frequency Raman line of large and strongly asymmetric profile occurs with intensity depending essentially on the dimension of the polar nanoregions. In this analysis we tried to use the theory of Uwe et al. (1986) which is, in our opinion, based on the physical phenomena which might correspond to those expected in the investigated crystal. The model of Uwe et al. however gives values of $\varepsilon_{cal}(0)$ equal to about 200 at T_c which can be neglected with respect to the dielectric permittivity measured in paraelectric phase at 1 MHz. Moreover the calculated on the basis of this theory the value of the polar region size R_o does not extend $2 \cdot a$, where a is the lattice constant equal to ~ 4 Å. Such little value of R_o in comparison with the size of the unit cell throw doubt upon the Uwe's model and thus for the explanation that characteristic Raman spectra in the paraelectric phase are solely related to the polar nanoregion existence.

To answer the question posed in the title of this chapter one can state that although existence of a soft phonon near each phase transition was found its share in dielectric response does not fully correspond to $\varepsilon(T)$ function observed and thus indicates that another soft mode(s) should be present.

Displacive A_1-A_2 phase transition and disorder in P phase in $PbHfO_3$ and $PbHf_{0.96}Ti_{0.04}O_3$

The most important conclusion which can be drawn from the measurements done on these materials is that two phase transitions of quite different nature exist in $PbHfO_3$ and PHT crystals. The first, between two antiferroelectric phases, demonstrates a clear softening of the two low-frequency lines. This softening can be used for the explanation of the radio-frequency ε'(T) behaviour at the $A_1 \rightarrow A_2$ phase transition. Since no change in the quasi-elastic scattering near this phase transition can be observed, hence this phase transition may be described as of displacive nature. The partial displacement of Hf ions by Ti does not change the nature of the $A_1 \rightarrow A_2$ phase transition but only widens the intermediate phase and leads to smoother transition. The substitution of heavy Hf by much lighter Ti ions slightly shifts the positions of the lines *a, f, g* by few cm^{-1} to the higher frequencies which may prove that these modes involves motion of B ions.

On the other hand Ti doping does not affect the second $A_2 \rightarrow P$ phase transition and Raman spectra above T_c. Interpretation of the nature of this phase transition is much more complicated. According to the literature data the permittivity maximum at T_c in ABO_3 perovskites may originate either from a relaxational mode or from softening of low-frequency optic mode, or both. This is also the case, as indicated by data presented in this study, for $PbHfO_3$ and $PbHf_{0.96}Ti_{0.04}O_3$. This means that a relaxation mode usually linked with the order-disorder nature of phase transition, may be taken to be responsible for the dielectric response at T_c in these materials.

The Raman broad band independence of Ti ions above T_c and also its temperature dependence corresponding to the behaviour of the disorder in the Pb sublattice found in X-ray investigations by Kwapulinski et al. (1994) tend to support this supposition.

5. CONCLUSIONS

The presented investigations throw a new light on the problem of the phase transition mechanisms in antiferroelectric ABO_3 perovskite compounds and also adds to explaining the origin of the $\varepsilon(T)$ dependence in wide temperature range and its anomalies in the phase transitions.

Two kinds of antiferroelectric materials were described in this work. The first one with one phase transition, was $PbZrO_3$ single crystal and the second one with two phase transitions which was $PbHfO_3$ single crystal. For these crystals the investigations of relaxational behaviour were made in the frequency region from 10 Hz to 10 MHz and in the range of optical frequencies. The main aim of the investigations was the origin and physical mechanisms responsible for the $\varepsilon'(T)$ dependence in the wide temperature region and especially in the vicinity of the phase transition points and in the paraelectric phase. Moreover the influence of the introduction of Ti ions to the $PbZrO_3$ and $PbHfO_3$ on the dielectric properties in these materials was studied.

In all investigated materials several dielectric dispersion phenomena were observed. The phenomenon, common for all samples, was the existence in very low frequencies (below 100 Hz) of relatively strong response visible in real and imaginary parts of dielectric permittivity and giving large contribution to $\varepsilon'(T)$ measured in this frequency region. This effect was related to the electrochemical processes contributing to the dielectric polarization. It was suggested that the strength of this dispersion depended on the degree of defects introduced during the growth process.

In all crystals a nearly monodispersive dipolar relaxation was observed in the range up to several kHz in the paraelectric phase giving a marked contribution to the $\varepsilon'(T)$ dependence. In general, behaviour of this relaxation was related to the presence of mobile defects in the whole volume of the sample.

The other observed relaxations were basically related to individual properties of the crystals. For example, introduction of Ti ions to $PbZrO_3$ developed a weak relaxation in the range of few kHz clearly visible in the transient phase and little above T_c. This relaxation appeared due to Ti introduction and came from the relaxation of polar regions in paraelectric phase and motion of domain walls in the ferroelectric intermediate phase. A defected $PbZrO_3$ crystal possessing the intermediate phase, revealed a similar relaxation.

This fact would prove that $PbZrO_3$ crystal with one phase transition is structurally more perfect than the one possessing the intermediate phase.

Further investigations of electromechanical properties were performed on these crystals in the paraelectric phase. The experiments showed that in the frequency range where the dipolar relaxation exists, the dispersion of the electrostrictive deformation could be also observed. The existence of electrostrictive dispersion could be treated as a modification of elastic properties. The results of electrostrictive properties nicely prove that the dipolar relaxations observed in the investigated crystals are of bulk character and are connected with the presence of defects which act as local dipoles and which can influence the mechanical properties of the lattice.

In the last part of this work, the Raman light scattering investigations were made in a wide temperature region 10 K - 750 K. The purpose of this studies were searching of the so-called „soft mode" behaviour in the antiferroelectric crystals. In all phase transitions clear anomalies of Raman spectra were observed. In the $PbZr_{0.99}Ti_{0.01}O_3$ in all phase transitions the mode softening occurred. Especially, assuming the behaviour of the broad shoulder in the paraelectric phase as a soft mode, its marked influence - although not completely covering the $\varepsilon'(T)$ dependence - was ascertained. In $PbHfO_3$ and $PbHf_{0.96}Ti_{0.04}O_3$ a clear soft mode behaviour was observed in the vicinity of the A_1-A_2 phase transition, which could speak for mostly displacive type of this phase transition.

The provided investigations let us describe the influence of particular relaxational and resonance processes on $\varepsilon(T)$ dielectric response in the temperature range in which investigated materials undergo structural phase transformations. In the used frequency regions, the processes found were not sufficient to explain the $\varepsilon(T)$ dependencies in $PbZrO_3$ and $PbHfO_3$ in particular in the vicinity of phase transition to the cubic paraelectric phase. The lacking part of $\Delta\varepsilon$ values could be connected to the dielectric relaxations existing in the frequency region not investigated in this work.

REFERENCES

Arlt G., U. Bottger and S. Witte, Ann. Physic, **3**, 578 (1994)

Balyunis L.E.,V.Yu. Topolov, A.V. Turik and O.E. Fesenko, Ferroelectrics, **111**, 291 (1990)

Barnett H.M., J. Appl. Phys., **33**, 1606 (1962)

Barsch G.R., B.N.N. Achar and L.E. Cross, Ferroelectrics, **35**, 191, (1981)

Bauerle D. and A. Pinczuk, J. Am. Ceram. Soc., **19**, 1169 (1976)

Bauerle D., Y. Yacoby and W. Richter, Solid State Commun., **14**, 1137 (1974)

Bauerle D., W.B. Holzapfel, A. Pinczuk and Y. Yacoby, Phys. Staus Solidi b, **83**, 99 (1977)

Benguigi L., J. Solid State Chem., **3**, 381 (1971)

Bianchi U. K. Kleeman and J.G. Bednorz, J. Phys.: Condens. Matter, **6** , 1229 (1994)

Bidault O., P. Goux, M. Kchiteh, M. Belkaoumi, M. Maglione, Phys. Rev. B, **49**, 12, 7868 (1994)

Blinc R. and B. Žeks, *„Soft modes in Ferroelectrics and Antiferroelectrics"* , Selected Topics in Solid State Physics (North-Holland, American Elsevier) (1974)

Cieminski J. von, K. Roleder, J. Handerek, Ferroelectrsic Lett., **10**, 9, (1989)

Cochran W., Adv. Phys. **9**, 387 (1960)

Cole K.S., R.H. Cole, J. Chem. Phys., **9**, 341 (1941)

Davidson D.W. and R.H. Cole, J. Chem. Phys., **19**, 1484 (1951)

Debye P., H. Sack, Handb. Radiol., **6/2**, 69 (1934)

Dec J. and J. Kwapulinski, J. Phys.: Condens. Matter, **1**, 3389 (1989a)

Dec J. and J. Kwapulinski, Phase Trans., **18**, 1 (1989b)

DiAntonio P., B.E. Vugmeister, J. Toulouse, L.A. Boatner, Phys. Rev. B, **47**, 10, 5629 (1993)

Fatuzzo E. and W.J. Mertz, *„Ferroelectricity"*, Selected Topics in Solis State Physics (North-Holland Publishing Company - Amsterdam, Oxford) (1974)

Fesenko O.E., Kristallografia, **24**, 826 (1979)

Fesenko O.E. and L.E. Balyunis, Ferroelectrics, **29**, 95 (1980)

Fontana M.D. , H. Idrissi and K. Wójcik, Europhys. Lett., **11**(5), 419 (1990)

Fontana M.D. , H. Idrissi, G.E. Kugel and K. Wójcik, J. Phys.: Condens. Matter, **3**, 8695 (1991)

Fontana M.D., G. Metrat, J.L. Servoin and F Gerwais, J. Phys. C: Solid State, **16**, 483 (1984)

Forker M., A. Hammersfahr, A. Lopez-Garcia and B. Wolbeck, Phys. Rev. B, **7**, 1039 (1973)

Forsbergh P.W., *„Piezoelectricity, Electrostriction and Ferroelectricity"*, Hanbuch der Physik, 17 (Springer-Verlag, Berlin) (1956)

Fuishita H. and S. Hoshino, J. Phys. Soc. Japan, **53**, 226 (1984)

Fuishita H. and E. Sawaguchi, Solid State Phys. Jpn, **16**, 2, (1981)

Fuoss R.M., J.G. Kirkwood J. Amer. Chem. Soc., **63**, 385 (1941)

Glarum S.H., J. Chem. Phys., **33**, 639 (1960)

Glazer A.M., Acta Cryst., **B28**, 3384 (1972)

Glazer A.M., Acta Cryst., **A31**, 756 (1975)

Glazer A.M., K. Roleder, J. Dec, Acta Cryst., **B49**, 846 (1993)

Goulpeau L., Fiz. Tvierd. Tiela, **8**, 2469 (1966)

Hańderek J., J. Kwapuliński, M. Pawełczyk and Z. Ujma, Phase Trans., **6**, 35 (1985)

Hańderek J. and Z. Ujma, Acta. Phys. Pol., **751**, 87 (1977)

Hassan H., M. Maglione, M.D. Fontana and J. Handerek, J. Phys.: Condens. Matter, **7**, 8647 (1995)

Havriliak S. and S. Negami, J. Polymer. Sci., Pt C, **14**, 99 (1966)

Hill R. M., Nature, Lond., **275**, 96 (1978)

Jaffe B., W.R. Cook and H. Jaffe, *Piezoelectric ceramics* (Academic Press, London, 1971)

Jayaraman A., S.K. Sharma, J. Phys. Chem Solids, **55**, 11, 1207 (1994)

Jankowska- Sumara I., K. Roleder, J. Dec, S. Miga, J. Phys.:Condens. Matter, **7**, 395 (1995a)

Jankowska-Sumara I., G.E. Kugel, K.Roleder, J.Dec, J. Phys.:Condens. Matter, **7**, 6137 (1995b)

Jona F and G. Shirane, *Ferroelectric Crystals*, (Oxford: Pergamon) (1962)

Jona F., G. Shirane, F. Mazzi and R. Pepinski, Phys. Rev., **105**, 849 (1957)

Jonscher A.K., *Dielectric relaxation in solids*, (Chelsea, New York) (1983)

Jonscher A.K., Colloid. Polymer. Sci., **253**, 231 (1975)

Joncsher A.K., *Universal relaxation law*, (Chelsea Dielectric Press, London) (1996)

Kania A., K. Roleder, G.E. Kugel and M. Hafid, Ferroelectrics, **135**, 75 (1992)

Känzig W., Solid State Phys., **4**, 1 (1957)

Kittel C., Phys. Rev. **82**, 729 (1951)

Kleemann W., V. Schonknecht, D. Sommer and D. Rytz, Phys. Rev. Lett., **66**, 6, 762 (1991)

Kwapulinski J., M. Pawelczyk, J. Dec, J. Phys.: Condens. Matter, **6**, 4655 (1994)

Lahlou S., *Thesis* (CLOES, Metz) (1990)

Lanagan M.T., J.H. Kim, Sei-Jeo Jang and R.E. Newnham, J. Am. Ceram. Soc, **7[4]**, 311 (1988)

Leontiev, N.G. R.V. Kololesova, V.V. Eremkin, G.E. Fesenko, V.G. Smotriakov, Sov. Phys. Crystallgr., **29**(2), 238 (1984)

Lines M.F. and A.M. Glass, *„Principles and applications of ferroelectrics and related materials"*, (Clarendon, Oxford) (1977)

Lyddane R.H., R.G. Sachs and E. Teller, Phys. Rev , **59**, 673 (1941)

Maglione and Belkaoumi (1992)

Maglione M., R. Bohmer, A. Loidl and U.T. Hochli, Phys. Rev. B, **40**, 11441 (1989)

Megaw H., *„Ferroelectricity in crystals"* (Methuem, London) (1957)

Miga S., J. Dec, Phys. Stat. Solidi (a), **153**, 257 (1996)

Mitsui T., T. Tatsuzaki and E. Nakamura, *„An introduction to the Physics of Ferroelectrics"*, (Englisch translation by Gordon and Breach) (1969)

Morozow E.M., W.P. Smirnow, W.W. Klinow and S.N. Soloviev, Kristallografia, **23**, 119 (1978)

Nomura S., J. Kuwata, S.J. Jang, L.E. Cross and R.E. Newnham, Mat. Res. Bull., **14**, 769 (1979a)

Nomura S., J. Kuwata, S.J. Jang, L.E. Cross and R.E. Newnham, Phys. Status Solidi a, **57**, 317 (1979b)

Pasto A.E. and A.R. Condrate, J. Am. Ceram. Soc., **55**, 331 (1972)

Pasto A.E. and A.R. Condrate, J. Am. Ceram. Soc., **56**, 436 (1973)

Perry C.H., D.J. McCarthy and G. Rupprecht, Phys. Rev. A, **138**, 1537 (1965)

Roleder K., Acta. Phys. Pol. A, **58**, 623 (1980)

Roleder K., J. Phys. E: Sci. Instrum., **16**, 1157 (1983)

Roleder K., Phase Trans., **15**, 7 (1989)

Roleder K., *"Obszary polarne, zjawiska krytyczne i zachowanie ferrolektryczne w kryształach $PbZrO_3$ i $PbZr_{1-x}Ti_xO_3$"*, Habilitation work, Silesian Univ. Katowice (1990)

Roleder K. and J. Dec, J. Phys.: Condens. Matter, **1**, 1503 (1989)

Roleder K., J. Grzywacz and J. Wolak, Ferroelectrics, **124**, 219 (1991)

Roleder K., I. Jankowska, J. Dec, Phase Trans., **42**, 241 (1993)

Roleder K., G.E. Kugel, J. Handerek, M.D. Fontana, C. Carabatos, M. Hafid and A. Kania, Ferroelectrics, **80**, [161]/809 (1988)

Roleder K., G.E. Kugel, M.D. Fontana, J. Handerek, S. Lahlou, C. Carabatos-Nedelec, J. Phys.: Condens. Matter, **1**, 2257 (1989)

Roleder K., M. Maglione, M.D. Fontana and J. Dec, in press (1996)

Samara G.A., Phys. Rev. B, 1, 3777 (1966)

Sawaguchi E. J. Phys. Soc. Japan, 7, 333 (1952)

Sawaguchi E. J. Phys. Soc. Japan, **8**, 615 (1953)

Sawaguchi E., H. Maniwa and S. Hoshino, Phys. Rev., **83**, 1078 (1951)

Sawaguchi E., Y. Shiozaki, H. Fujishita and M. Tanaka, J. Phys. Soc. Japan, **49** (Suppl.), B191 (1980)

Scott B.A. and G. Burns, J. Amer. Ceram. Soc., **55**, 331 (1972a)

Scott B.A. and G. Burns, J. Amer. Ceram. Soc., **55**, 225 (1972b)

Shirane G. and R. Pepinski, Phys. Rev. B, **91**, 812 (1953)

Shirane G., K. Suzuki, A Takeda, J. Phys. Soc. Japan, **1**, 12 (1952)

Shirane G., and A. Takeda, J. Phys. Soc. Japan, **1**, 5 (1952)

Smolenskii G.A., V.A. Bokov, V.A. Isupov, N.N. Krainik, R.E. Pasinkov and M.S. Shur, *„Ferroelectrics and Antiferroelectrics"* (Nauka, Leningrad) (in Russian) (1971)

Sommer D. and W. Kleemann, Ferroelectrics, **124**, 231 (1991)

Szot K., W. Speier, S. Cramm, J. Herion, Ch. Freiburg, R. Waser, M. Pawelczyk, W. Eberhard, J. Phys. Chem. Solids, **57**, 1765 (1996)

Tanaka M., R. Saito, K. Tsuzuki, J. Phys. Soc. Japan, **51**, 8, 2635 (1982a)

Tanaka M., R. Saito, K. Tsuzuki, Jpn. J. Appl. Phys., **21**, 291 (1982b)

Toulouse J., P. DiAntonio, B.E.Vugmeister, X.M.Vang, L.A. Knaus, Phys. Rev. Lett., **68**, 2 (1992)

Topolov V.Yu., L.E. Balyunis, A.V. Turik and O.E. Fesenko, Ferroelectrics, **110**, 41 (1990a)

Topolov V.Yu., L.E. Balyunis, A.V. Turik and O.E. Fesenko, Sov. Phys. Crystallogr., 35(3), (1990b)

Uchino K. and L.E. Cross, Ferroelectrics, **27**, 35 (1980a)

Uchino K., L.E. Cross, R.E. Newnham and S. Nomura, Phase Trans., **1**, 333 (1980b)

Ujma Z. and J. Handerek, Phys. Stat. Sol. (a), **28**, 489 (1975)

Uwe H., K.B. Lyons, H.L. Carter and P. Fleury, Phys. Rev. B, **33**, 9, 6436 (1986)

Whatmore R.W., *Thesis* (Cavendish Laboratory, Cambridge) (1976)

Whatmore R.W. and A.M. Glazer, J. Phys. C: Solid State, **12**, 1505 (1979)

Williams G. and D.C. Watts, Trans. Far. Soc., **66**, 80 (1970)

Yacoby. Y., Z. Phys., B**31**, 275 (1978)

Yamada T., J. Appl. Phys., 43, 2 (1972)

Zaitsev S.M., G.P. Zhavoronko, A.A. Tatarenko, M.F. Kuprianow, W.S. Filipiev and G.E. Fesenko, Sov. Phys. Crystallogr., **24**(4), 474 (1979)